A thesis entitled

The Kinetics of Si and SiGe Growth from Hydrides

by

R.W. Price

Submitted for the

Degree of Doctor of Philosophy
of the
University of London

Imperial College of Science, Technology and Medicine
London

2000

Abstract

In gas source molecular beam epitaxy (GSMBE) gaseous hydrides of silicon and germanium, such as silane, disilane and germane, are used as the growth precursors. The hydrides produce silicon or germanium via a dissociation reaction occurring upon collision with the heated substrate surface. The reaction products are identified by modulated beam mass spectrometry (MBMS) which can be employed during steady state growth. The pyrolysis reaction of disilane is shown to produce gaseous hydrogen and Si on the Si(001) surface. The Si hydrides fragments produced on the Si(001) surface upon adsorption of disilane are investigated by temperature programmed desorption (TPD) experiments. The findings confirm that only the monohydride phase is produced at high temperatures and the resulting hydrogen passivates the surface against further adsorption of disilane, silane or germane. The desorption of hydrogen is observed to have a first order dependence on surface coverage as is reported in the literature. In conjunction with the temperature modulated growth (TMG) technique, the reaction pathway for the pyrolysis reaction of disilane is shown to occur via a sequential loss of hydrogen ending with the monohydride phase and eventual recombinative desorption of molecular hydrogen. The growth rate is examined in detail using in-situ reflection high energy electron diffraction (RHEED) oscillation techniques and ex-situ thickness measurements using x-ray diffraction. The growth rate was found to reduce at high temperatures as well as having a weak flux dependence at low temperatures this has not been reported in the current literature. The growth process is modelled using the rate equation of hydrogen coverage given that hydrogen has been identified to have a passivation effect. The newly observed growth rate behaviour has been incorporated into the model through a limited lifetime at high temperatures and hydrogen abstraction at low temperatures and full coverage. The pyrolysis of monosilane is also investigated. The reaction is shown to occur via similar pathways but with a much reduced sticking coefficient compared to that of disilane. The effect of surface germanium on the growth of SiGe is studied using TPD and RHEED oscillation techniques. A lower energy pathway to hydrogen desorption is identified along with the observation of a lower sticking probability. TPD suggests that desorption can occur from Si-Si dimers or mixed Si-Ge dimers with a lower activation energy. Desorption from a monohydride phase can also occur from Ge-Ge dimers which is characterised by another activation energy.

Contents

List of Figures **5**

List of Tables **11**

1 Introduction **12**
1.1 Diodes and Triodes . . . 12
1.2 Surface Tax . . . 13
1.3 Gas Source Molecular Beam Epitaxy . . . 15
1.4 Outline of Thesis . . . 15

2 The Structure and Growth of Group IV Semiconductors **17**
2.1 Introduction . . . 17
2.2 Group IV Semiconductors . . . 17
2.2.1 Crystal and Band Structure . . . 17
2.2.2 Surface Structure: Reconstruction . . . 20
2.2.3 Growth . . . 23
2.2.4 Bi-Layer Growth . . . 25
2.2.5 Segregation . . . 27
2.3 The Kinetic Theory of Thermal Molecular Beam Epitaxy . . . 29
2.3.1 Introduction: Gases in Equilibrium . . . 29
2.3.2 The Impingement Rate . . . 29
2.3.3 Thermal Molecular Beams . . . 31
2.3.4 Adsorption and Desorption . . . 32
2.3.5 The Kinetics of Chemisorption . . . 35
2.4 Adsorption of Hydrides on the Si(100) Surface . . . 37
2.4.1 Introduction . . . 37
2.4.2 Adsorption Mechanisms . . . 37
2.4.3 Homoepitaxial Growth . . . 44
2.4.4 Heteroepitaxial Growth . . . 49
2.5 Hydrogen on the Si(100) and $Si_{1-x}Ge_x$(100) Surfaces . . . 51
2.5.1 Introduction . . . 51
2.5.2 The Si(100) Surface . . . 52
2.5.3 The $Si_{1-x}Ge_x$ (100) Surface . . . 55
2.6 Summary . . . 58

3 System Description and Experimental Techniques **59**
3.1 Introduction . . . 59
3.2 GSMBE system . . . 59
3.2.1 Vacuum Chamber . . . 59
3.2.2 Substrate Preparation . . . 64
3.3 The Reflection High Energy Diffraction Apparatus . . . 65
3.4 The Quadrupole Mass Spectrometer . . . 66
3.4.1 Introduction . . . 66
3.4.2 Temperature Programmed Desorption . . . 67
3.4.3 Modulated Beam Mass Spectrometry . . . 67
3.5 Summary . . . 69

4 Hydrogen Desorption Kinetics **70**
4.1 Introduction . . . 70
4.2 Practical Considerations . . . 70
4.3 Adsorbed Hydride Species . . . 72
4.4 Molecular Hydrogen Desorption Kinetics . . . 74
4.5 Summary . . . 81

5 Kinetics of Growth from Disilane **82**
5.1 Introduction . . . 82
5.2 Identification of the Desorbing Species During Steady State Growth . . . 83
5.2.1 Silicon Hydride Desorption . . . 83
5.2.2 Hydrogen desorption kinetics during growth . . . 85
5.3 Reaction Pathways of Disilane Dissociation at Elevated Temperatures . . . 86
5.3.1 Temperature Modulated Growth . . . 87
5.4 A Model for the Steady State Growth of Silicon . . . 90
5.4.1 The Established Growth Process . . . 92
5.4.2 Limitations of the Established Model for the Growth Process . . . 93
5.4.3 Establishing the Order of the Adsorption Process . . . 94
5.4.4 Modelling the Growth Phenomenon . . . 98
5.5 Summary . . . 106

6 Kinetics of Growth from Silane **107**
6.1 Introduction . . . 107
6.2 Hydrogen Desorption from a Silane Exposed Surface . . . 107
6.3 Adsorption of Disilane on a Clean Si(001) Surface Studied by TMG . . . 109
6.4 Steady State Growth Rate Measurements . . . 109
6.5 Steady State Growth Rate Modelling . . . 111
6.6 Summary . . . 112

7 Kinetics of Growth from Germane **113**
7.1 Introduction . . . 113
7.2 Hydrogen Passivation Effect on Alloy and Germane Dosed Surfaces . . . 113
7.3 Hydrogen Desorption During Temperature Modulated Growth . . . 116
7.4 Steady State SiGe Growth Rate Measurements . . . 120
7.5 Summary . . . 123

8 Conclusion **124**
8.1 Hydrogen Desorption Studies . . . 124
8.2 Pyrolysis Reaction Pathways . . . 125
8.3 Disilane Adsorption and the Pathway for Dissociation of Silicon Hydride Radicals . . . 125
8.4 Rate Limiting Steps in the Growth of Si from Hydrides . . . 126
8.5 Growth from Silane . . . 126
8.6 The Influence of Germanium on the Growth of Alloys . . . 127
8.7 Future Work . . . 128
8.8 Publications . . . 129

A List of Abbreviations **130**

B The Boltzmann Distribution **132**
B.0.1 The Maxwell Velocity Distribution . . . 133

C Reflection High Energy Electron Diffraction **136**
C.0.2 RHEED Patterns . . . 136
C.0.3 Features of RHEED Patterns . . . 138
C.0.4 RHEED Intensity Oscillations . . . 139

D The Quadrupole Mass Spectrometer **141**

E Growth Rate Modelling Solutions **143**
E.1 Model 1 . . . 143
E.2 Model 2 . . . 143
E.3 Model 3 . . . 144
E.4 Model 4 . . . 144
E.5 Model 5 . . . 145
E.6 Model 6 . . . 145
E.7 Model 7 . . . 146

F Acknowledgements **147**

Bibliography **148**

List of Figures

2.1 The diamond structure 18
2.2 The germanium, silicon and GaAs band structure [94]. For silicon the indirect bandgap is between the Γ point and to just inside the X point of the Brillouin zone boundary. There are therefore six ellipsoids of constant energy along the $\langle 100 \rangle$ axes see Figure 2.3 19
2.3 Constant energy surfaces for germanium, silicon and GaAs [94] For Si there are six ellipsoids along the $\langle 100 \rangle$ axes with the centres of the ellipsoids located $\frac{3}{4}$ of the distance from the Brillouin zone centre. 19
2.4 The monohydride and dihydride surfaces. The monohydride (a) is associated with a 2x1 reconstruction and the dihydride (b) a '1x1'. 21
2.5 Si(001) surface reconstructions observed during GSMBE growth from disilane. Mokler *et al* 1991 22
2.6 Atomic structural models for Si(001) surfaces with (a) disorded (2×1)+(1×2), (b) (2×2), (c) c(4×4) and (d) ordered (2×1)+(1×2) structures, Mokler *et al* , 1991 23
2.7 RHEED intensity oscillations observed in the specularly reflected beam along the [110] azimuth at a substrate temperature of 560 ^{0}C using a disilane flow rate of 0.36 SCCM Ohtani *et al* , 1993 24
2.8 Schematic representations of Si(100) surfaces with monotomic steps (top) and biatomic steps (bottom) 26
2.9 Schematic energy diagram of the two site exchange model of surface segregation. k_- and k_+ denote the rate of exchange where the positive subscript denotes transfer from the subsurface to surface site 27
2.10 A schematic one dimensional potential energy surface 33
2.11 Static SIMS study of silane and disilane adsorption by Gates *et al* at 150 K. m/z = 28 corresponds to Silicon, 29 SiH, 30 SiH_2 and 31 SiH_3 38
2.12 The period of the first half RHEED oscillation versus the inverse disilane flux. The period was used to characterise the adsorption of disilane on clean surface, this period is seen to be almost independent of temperature and shows a similar dependence on flux. The legend gives the sticking coefficients derived from the fit. Werner *et al* [101] 43

2.13 Gates *et al* [24] : Comparison of model prediction (solid lines) and literature growth rate data. Two values of silane reactive sticking probability are used for the two solid lines. One SiH_4 flux is used. Data show epitaxial Si film growth rates: squares from [10] at 0.0006 Torr, dots from [49] at 0.003 Torr, open triangles from [78] at 0.05 Torr, solid triangles from [29] at 0.01 Torr and crosses from Meyerson *et al* at 0.001 Torr 45
2.14 Mokler *et al* [57]: Arrhenius plot of growth rate data from RHEED intensity oscillation frequency in [010] azimuth. A change in the slope near 600 °C is seen. Below this temperature growth rate is limited by Si_2H_6 arrival rate. An activation energy of 1.77 eV is calculated for the low temperature region. Solid and dashed lines are derived from the model in [49] for fluxes (dashed) 2 and (solid) 5×10^{15} molecules cm^2s^{-1}, respectively, and for equation $GR = \alpha J(1-\theta)^2$, where α is a weakly dependent reaction probability, J is the beam flux and θ represents the fraction of surface covered by hydrogen. The inset shows θ values used which were derived from [24] 47
2.15 Mokler *et al* [58]: Arrhenius plots for the growth rate data during Si homoepitaxy and $Si_{1-x}Ge_x$ heteroepitaxy. Addition of GeH_4 to the system lowers the activation energy from 1.77 eV (40.7 kcal/mol) found for Si homoepitaxy to 1.52 eV (35 kcal/mol) for $Si_{1-x}Ge_x$ below 600 °C . The addition of Ge to the surface results in a higher desorption rate of hydrogen desorption and therefore shifts the transition between adsorption/dissociation limited and desorption limited kinetics towards lower temperature 49
2.16 Modelled growth rates of $Si_{1-x}Ge_x$ layers with composition, x produced by Robbins *et al* [79]. The model assumed an increase of the rate of hydrogen desorption and a lower sticking coefficient with increasing x. 50
2.17 Zhang *et al* [112]: Comparison of $Si_{1-x}Ge_x$ layer growth rate as a function of germanium fraction for the growth method using Si_2H_6 and Ge as sources among different substrate orientations. The symbols are experimental data and the solid line is a guide for the eye 51
2.18 Nakazawa *et al* [63]: TPD spectra, the high temperature peak has been attributed to desorption from the monohydride phase, β_1, and the lower temperature peak to desorption from the dihydride phase, β_2. 54
2.19 Kim *et al* [40]: TPD spectra from SiGe with various surface concentrations of germanium. 56
2.20 Ning *et al* [65]: Occupation of desorption sites. The total hydrogen coverage approaches 1.5 ML 57

3.1 Photograph of the GSMBE vacuum system. The rack on the left contains all the hardware required to drive the quadrupole mass spectrometer, multichannel scalar and beam modulator 60
3.2 Schematic illustration of the GSMBE vacuum system. The two deposition chambers are separated by the common preparation/analysis chamber. For simplicity, only one deposition chamber is depicted. The system is constructed from argon-arc welded high purity stainless steel segments, which have a low degassing rate and a low level of magnetic impurities. 60
3.3 Schematic illustration of the gas manifold. 61

3.4 Beam equivalent pressure (BEP) dependence on gas line pressure for a water cooled system for disilane and silane. The silane pressure is modified to take into account the different ionisation cross sections for disilane and silane. Disilane has an ionisation cross section 2.23 times that of silane. The line is the fit BEP = $5\times10^{-5}(P_{source})^{1.3}$ 62
3.5 Disilane beam effective pressure (circles) and background pressure (squares) dependence on gas line pressure for the liquid nitrogen cooled system 63
3.6 Schematic of the complete RHEED system 66
3.7 Schematic illustration of the Modulated Molecular Beam System 68

4.1 TPD spectra from the Si(001) surface previously exposed to disilane from a gas line pressure of 1 Torr. Exposure at temperatures of 430 °C falling to 360°C for the duration of 1 minute produce the β_1 peak only. Exposure at 200 °C for 1 minute produces an additional β_2 peak at lower temperatures. 71
4.2 TPD spectra demonstrating the effect of pre-adsorbed hydrogen on further adsorption. Curve (c) shows a TPD spectra from a surface dosed for 1 minute at 430°C and curve (a) shows one from dosing at 200 °C . Curve (b) is also dosed at 200 °C but has previously been dosed as in curve (c) and the β_2 peak is not observed 73
4.3 A plot of $ln\left(\frac{T_M^2}{\beta}\right)$ against $\frac{1}{T_M}$ will give an intercept and gradient from which E_d and k_{d_0} can be calculated. For the monohydride phase (solid line): activation energy for desorption is 2.48 ±0.4 eV and the pre-exponential is $3.16\times10^{14}s^{-1}$ For the dihydride phase (dotted line): activation energy for desorption is 1.22 ±0.4 eV and the pre-exponential is $4.27\times10^{7}s^{-1}$ 77
4.4 TPD spectra from a Si(001) surface exposed to disilane form a gas line pressure of 1 Torr and at a substrate temperatures 200°C ±5°C . The ramp rates used were 0.5°C per sec, 1°C per sec and 2 deg per sec 78
4.5 TPD spectra from a Si(001) surface exposed to disilane at 200°C for 1 minute (b) and atomic hydrogen for 15 minutes (c). The peak areas are identical and are assumed to be from a full coverage of hydrogen. (a) is from the monohydride surface produced from disilane dosing at 430°C falling for 1 minute. 79
4.6 TPD from a Si(001) surface for various hydrogen coverage. The lack of a variation in the temperature of the peak desorption rate indicates a first order desorption process. A slight movement to higher temperatures for low hydrogen coverages could be due to experimental errors or a change towards second order desorption kinetics. 79

5.1 Modulated Beam Mass Spectrometry (MBMS) study of Silicon Hydride desorption: The temperature dependence of the amplitude of the mass spectrometer signal is calculated at the first harmonic of the modulation frequency (39 Hz) at a mass to charge ratio of 30 corresponding to silicon hydride fragments. 84

5.2 Modulated Beam Mass Spectrometry (MBMS) study of Hydrogen desorption: The temperature dependence of the amplitude of the mass spectrometer signal is calculated at the first harmonic of the modulation frequency (39 Hz) at a mass to charge ratio of 2 corresponding to hydrogen. The signal recorded from the electron multiplier in pulse counting mode is multiplied by the square root of the substrate temperature 85
5.3 Arrhenius Plot of hydrogen desorption measured using MBMS. The activation energy for desorption is 1.8 eV 86
5.4 Temperature Modulated Growth (TMG) sample structure: Layer (a) is a 0.0068 μm SiGe marker layer with a Ge content of 8.5 percent. Layer (b) is a 0.00667 μm Si buffer layer under the TMG Si layer (c). Layer (d) is a another SiGe marker and (e) is 0.000389 μm Si cap. 88
5.5 X-ray diffraction rocking curves recorded from the Temperature Modulated Growth (TMG) samples. The greater spacing of the XRD features indicate a smaller spacing of the diffracting layers. This is then used to calculate the amount of silicon deposited during one cycle in the TMG experiments . . . 88
5.6 RHEED pattern of a clean and hydrogenated Si(001) surface in the [110] azimuth. All patterns show the (2×1)+(1×2) reconstruction indicating the presence of dimers. 91
5.7 Arrhenius plot of the growth rate measured using the period of RHEED intensity oscillations. The lower data is recorded from growth from a flux produced from a gas line pressure of 0.1 Torr which gives a beam equivalent pressure (BEP) of 2.4×10^{-6} mbar. The upper data is from 1.5 Torr (BEP = 6×10^{-5} mbar) and the middle from 0.4 Torr (BEP = 1.5×10^{-5} mbar) . . . 92
5.8 Arrhenius plot of the growth rate measured using ex-situ XRD on samples similar to those used in the TMG study. The three different fluxes are the same as those shown in Figure 5.7. A decrease in growth rate with increasing temperature is clearly present. 94
5.9 Growth rate measured using RHEED intensity oscillations along with fits for first and second order adsorption growth models. Hydrogen desorption is first order for both. It can be seen that there is little difference in the fit from the two models although the second order model fits slightly better. The two models agree at coverages of 1 at low temperatures and 0 at high temperatures 95
5.10 Growth rate measured using RHEED intensity oscillations for various fluxes along with fits for second order adsorption growth models. The model fits the data well with no modifications required to simulate the flux dependence at high temperatures. 97
5.11 The second order adsorption growth model fits the RHEED data well but the growth rate temperature dependence measured at very high temperatures using XRD is not predicted by the standard model 98
5.12 Growth rate dependence on incident flux measured using XRD and RHEED intensity oscillations. The dotted line is given by $GR = 2SJ(1-0.9)^2 = 0.02SJ$. The growth rates were recorded at 462 °C (bottom), 503°C (middle) and 531 °C (top). The solid lines show the growth rate dependence on BEP predicted by the standard second order model. 99

5.13 Growth models 1 and 2: Model 1 (left) is the standard model with second order disilane adsorption and first order hydrogen desorption. Model 2 (right) is the same as model 1 but with a temperature dependent sticking probability 100
5.14 Growth models 3 and 4: Model 3 (left) is the standard model 1 but with a flux dependent abstraction. Model 4 (right) is the same as model 3 but with the flux dependent abstraction thermally activated. 101
5.15 Growth models 5 and 6: Model 5 (left) is the standard model but with the abstraction depending on the flux to the power of $\frac{1}{2}$. Model 6 (right) is the same as model 5 but with the flux dependent abstraction thermally activated 102
5.16 Growth model 7 is a combination of the standard growth model 1 with model 6. The model incorporates a hydrogen abstraction reaction dependent on $J^{\frac{1}{2}}$ and both the abstraction reaction and the trapping probability are temperature dependent. Growth from a BEP = 6×10^{-5} circles, BEP = 1.5×10^{-5} squares and BEP = 2.4×10^{-6} triangles. RHEED data points solid XRD data points open. 103

6.1 Temperature programmed desorption from a Si(001) surface exposed to silane and disilane. The disilane dose was from a 1 Torr gas line (BEP = 5.2×10^{-5} mbar) for 1 minute at 430 °C and the silane dose was from a gas line pressure of 2 Torr (BEP = 0.15×10^{-3} mbar) for 10 minutes at 200°C 108
6.2 Arrhenius plot of the growth rate of silicon from silane (solid circles) and disilane (error bars only) on the Si(001) surface. The dotted line shows the fit for disilane from the standard model 1, see chapter 5 110
6.3 Arrhenius plot of the growth rate of silicon from silane (solid circles) and disilane (error bars only) on the Si(001) surface. The dotted line shows the fit for disilane and the solid line the fit from the silane growth model 111

7.1 RHEED intensity oscillations recorded from growth from disilane. (a) is recorded from growth on a clean silicon surface. (b) is from growth on a surface previously exposed to germane for 1 minute, (c) is from growth on a surface exposed to germane for 3 minutes. No difference in oscillation period is seen between (b) and (c) meaning the same amount of germane was deposited in each case 114
7.2 (a) shows RHEED intensity oscillations recorded from homoepitaxial growth on the Si(001) surface, the remaining curves (b) and (c) are from growth from disilane on a surface previously exposed to disilane followed by exposure to germane. Disilane exposure times are 10 seconds for (b) and 1 minute for (c). The surface produced from disilane exposure prevents germane adsorption. 115
7.3 RHEED intensity oscillations recorded after a form of temperature modulated growth for germane dosing. (a) is from growth from disilane on the clean surface. (b) is from growth from disilane on a surface exposed to germane. (c) is from growth from disilane on a surface exposed to two cycles of germane dosing and annealing 116
7.4 Temperature programmed desorption from a Si(001) surface exposed to disilane from a gas line pressure of 1 torr at 430°C falling for 1 min and germane at 200°C from a gas line pressure of 2 torr for 10 mins. The ramp rate used was 4°C per second. 117

7.5 Temperature programmed desorption from a Si(001) surface repeatedly exposed to germane. The germane dose was at 340°C for 10 minutes from a gas line pressure of 1 torr. The ramp rate used was 4 °C per sec. The numbers in bold refer to the number of exposures to germane. 118
7.6 TPD recorded from temperature modulated growth from germane on a silicon surface after 4 exposure and annealing cycles but with various TPD ramp rates. The ramp rates used are 0.5, 2 and 5 °C per sec. The germane dose was for 10min from a gas line at 2 torr with a substrate temperature of 200°C 119
7.7 RHEED intensity oscillations from SiGe growth on a clean Si(001) surface. After introduction of the gas into the chamber the period of oscillations decreases until a steady state is reached, before the oscillations disappear a transition to bilayer growth is indicated 121
7.8 Arrhenius plot of the growth rate of silicon and SiGe. The silicon was grown from disilane at gas line pressures of 0.1 Torr (solid triangles) and 0.25 Torr (solid squares). The SiGe growth (solid circles)is from gas line pressures of disilane (0.2 Torr) and germane (0.05 Torr). The solid line is produced from a simple SiGe growth model and serves mainly to guide the eye. 122

C.1 The Ewald Sphere construction and reciprocal lattice rods. The bottom eft hand figure illustrates the effect of broad lattice rods and the bottom right hand figure the origin of arrowhead shaped features [64] 137
C.2 RHEED pattern of a clean (2x1)(1x2) reconstructed Silicon(100) surface taken in the [110] direction 138
C.3 RHEED oscillations during growth from a gas line pressure of 10 Torr with a substrate temperature of 550 °C . The growth rate is calculated at 0.027 ML/sec 139

D.1 Cracking pattern of Disilane in a water cooled system at a background pressure of 2.5×10^{-7} mbar. The top trace is from an ion energy of 70 eV and the bottom is 16 eV. ΔM is set at 60% 142

List of Tables

2.1 Hydrogen desorption parameters, activation energy of desorption: E_d (eV) and pre-exponential: $k_{d_0}(s^{-1})$ 52

3.1 Table showing the wet etching methods. The chemical etch involves repeated oxidation and etching of the Si surface (3-6) followed by the removal of organic contamination (7) and finally the production of a hydrogen passivated surface. (9) 64

5.1 Table showing the TMG sample data 89

Chapter 1

Introduction

1.1 Diodes and Triodes

The discovery of some interesting properties of a group of materials which included the most abundant element on the earth, silicon, instigated one of the greatest revolutions mankind has ever witnessed. This group of elements and compounds was found to have electrical properties intermediate to the well established conductors and insulators and were thus termed semiconductors.

Simple conductors introduced electrical circuits which were only useful for power and simple data transmission but in 1890 John Ambrose Fleming discovered the process of rectification and this lead to the invention of the thermionic valve in 1904.

In 1906 the crystal diode was invented by Pickard which was later developed during the second world war as a detector in microwave radar systems. This was not possible before because of the inability to prepare the semiconductor materials needed with adequate purity.

In 1947 Bardeen and Brattain working at the Bell Laboratories in America invented the transistor and this brought about the end of the thermionic valve which had served so well for so long. There were many objections to the use of valves and these were mainly connected with their high power consumption, their fragility and the necessity of using a hot cathode which produced noise, thus limiting the sensitivity of radio receivers and other similar devices.

The transistor was made entirely from solid materials and required no heated parts so avoided most of these difficulties. It also worked at much lower voltages than the valve which was a great safety issue. Initially the transistor was made from germanium but this suffered from high leakage currents, eventually silicon was used as a superior replacement.

The ability to reduce the dimensions of these devices well below that of the valves

made these devices attractive for more complicated electronic devices and marked the beginning of the race to reduce the dimensions of the transistor that is still seen today in one of the most profitable industries in the world.

Silicon is currently still the most popular semiconductor from which devices are manufactured although other semiconductors such as Gallium Arsenide are becoming more popular. At the present it is these manufacturing methods that determine the degree to which transistor dimensions in integrated circuits can be reduced, a thorough understanding of these methods is clearly necessary for further development. Ultimately the minimum feature size of integrated circuits will be governed by quantum effects and this is just beginning to be realised.

1.2 Surface Tax

It is the sensitivity of the semiconductors electrical characteristics on impurity concentration that is both its advantage and its downfall. Development of the transistor was hindered by the need for pure crystals so it is clear before any device can be manufactured a good starting substrate is necessary. Not only does the crystal need to be pure but for good conduction its also needs to be single-crystal so as to reduce defect scattering of the conduction carriers.

The technology of silicon crystal growth is now well developed with crystals grown from molten silicon onto a seed crystal which is then drawn away from the molten material. However a pure silicon crystal is of little use, to manufacture devices it must be cut into thin wafers upon which new layers are deposited. The deposition process has been termed *epitaxy* which comes from the Latin *epi* meaning surface and *taxis* meaning arranged. These layers must be etched into the required pattern before metal contacts are deposited and finally packaged into the large scale device.

Many forms of Epitaxy have been developed, the simplest of these is liquid phase epitaxy (LPE), this involves growth of the crystal on the substrate from a solution well below their melting point. In LPE the solution can be placed onto the wafer by the use of a graphite slider which holds the substrate and this is then drawn through a enclosed slot which includes pockets of the melt.

The same low temperature high purity conditions of LPE can be achieved by crystallisation from the vapour phase instead of the liquid phase, this technique is, of course, called vapour phase epitaxy (VPE) and is performed by evaporating a solid source in a carrier gas which is then passed over the substrate. It is also possible for crystal growth

to occur from the gas phase where a chemical reaction takes place on the surface, when this occurs at high pressures it is termed chemical vapour deposition (CVD) this is currently the most popular method of deposition due to its high growth rates. Versions of VPE include metal-organic vapour phase epitaxy (MOVPE).

As devices reduced in size a more controlled method of epitaxy was required, this means growth rates need to be reduced but purity must remain the same. The reduction of the amount of growth precursor requires a reduction in pressure, when this pressure is reduced significantly below atmospheric pressure ($< 10^{-7}$mbar) the growth precursor can travel freely with few collisions. In this regime the flow of the precursor will flow in straight lines for an appreciable distance from the source. The precursor molecules will remain in a beam until they strike the substrate and hence this technique is called molecular beam epitaxy (MBE).

Gallium Arsenide can be grown from solid sources in high vacuum since GaAs has a relatively low melting temperature, however the melting point of Silicon is extremely high which can lead to complications such as spitting and the need for heat sinks. One way to reduce the temperatures is to use electron beam evaporation but this has other complications such as charging effects. One further technique to grow silicon other than solid source molecular beam epitaxy (SSMBE), is to use gaseous sources and the silicon hydrides silane and disilane are particularly suitable. This technique is called gas source molecular beam epitaxy (GSMBE) and is the topic of interest of this thesis.

Reducing the growth rate allows greater control if the growth rate is known, this can be established by measuring layer thicknesses after a know period of growth. A suitable technique for this is X-ray diffraction which can be performed outside of the growth chamber. However, a slower growth rate is not in itself an advantage since electronic control of shutters can allow very fast termination of molecular beams, [1] the advantage of the use of ultra high vacuum lies in the fact that thermionic emission can be sustained without rapid oxidation of the filament. Thermionic emission is used throughout the high vacuum system to ionise molecules to measure molecule density (hence pressure) and is also used to produce electron beams for diffraction experiments. This is somewhat ironic since it seems the thermionic valve has had the last laugh!

[1] there is of course some limitation of this due to the mechanical nature of the shutters

1.3 Gas Source Molecular Beam Epitaxy

GSMBE has many advantages over solid source MBE one significant advantage is the ability to recharge the sources without opening the growth chamber. A new gas bottle can simply be attached to the gas manifold in place of the old one, this means only the gas lines need to be baked, the vacuum chamber itself can be left at high vacuum. The result is a very high throughput of samples which is advantageous for industry.

Silicon based technology continues to dominate the electronics industry in the form of metal oxide semiconductor (MOS) technology. Devices based on quantum wells, superlattices and heterostructures are just beginning to be realised, however a complete understanding of the growth process at an atomic level is not fully developed. If device technology is to advance this situation must be remedied.

In gas source molecular beam epitaxy (GSMBE) gaseous hydrides of Si and Ge, such as silane, disilane and germane are used as the growth precursors. Doping is achieved using gases such as diborane, arsine and phosphine which can be introduced into the growth chamber in addition to the growth precursor. The hydrides produce crystal growth by dissociating during collisions with the heated substrate. The details of this dissociation and the eventual incorporation into the crystal surface is the topic of this thesis. Several *in situ* techniques, including reflection high energy electron diffraction, are used to measure the growth rate of silicon and silicon germanium, the temperature dependence is then compared to mathematical models. Desorbing Surface species are identified using mass spectrometry during thermal annealing and also during growth using lock in techniques.

The details of the growth of silicon from silane and disilane on the Si(001) surface are discussed along with details for SiGe deposition on the clean Si(001) surface using germane and disilane.

1.4 Outline of Thesis

This thesis consists of 8 chapters the first being this introduction. Chapter 2 is a general introduction to the growth of group IV semiconductors from hydride precursors. The chapter is divided into four, the first section is a review of growth and concentrates on the various different states of the surface during growth, the second section contains a theoretical treatment of gases and their interaction with surfaces. The final two sections review the present understanding of the interaction of silane, germane and disilane with the silicon (001) surface and the Si(111) surface.

Chapter 3 is concerned with the experimental systems and techniques. The experimental techniques can be divided into two main categories, *in situ* and *ex situ*. The *in situ* techniques Mass Spectrometry and Reflection High Energy Electron Diffraction (RHEED) are used to characterise surface states and can also be used to measure growth rate. Mass spectrometry during thermal annealing is termed Temperature Programmed Desorption (TPD) and is used throughout chapter 4. Mass spectrometry is also used with lock in techniques to study the desorbing molecular beam during growth reported in chapter 5. *ex situ* techniques such as X-ray Diffraction (XRD) are used in later chapters to complement the growth rate measurements.

As already mentioned, Chapter 4 is concerned with TPD. This chapter concentrates on the desorption of hydrogen from the Si(001) surface after exposure to disilane. By studying the temperature dependence of the desorption of hydrogen from the surface and its variation depending on the conditions under which the surface is exposed to disilane, a picture of the decomposition of disilane can be gleaned.

The next chapter continues to study the growth of silicon from disilane but reports on studies carried out on the growing surface as opposed to the static surface studied in chapter 4. Chapter 5 introduces the lock in technique of Modulated Beam Mass Spectrometry (MBMS) to study desorption during growth and also reports on a thorough analysis of the temperature and flux dependence of the growth rate. A mathematical model is developed for the growth process.

Chapters 6 and 7 report similar studies to those in earlier chapters but are concerned with the precursors silane and germane respectively. The model for silane growth is developed from the model for disilane growth used in chapter 5. Germane has some interesting effects on growth and in chapter 7 these are studied using both RHEED intensity oscillations and TPD.

Finally Chapter 8 contains a summary of the results and a conclusion and discusses possible routes of investigation for the future

Chapter 2

The Structure and Growth of Group IV Semiconductors

2.1 Introduction

This chapter serves as a general introduction to the growth of group IV semiconductors such as silicon, Si, and germanium, Ge, from hydride precursors. The chapter is divided into four major sections; the first is an overview of growth from non-specific precursors and concentrates on the various different states of the surface during growth, the second is a theoretical treatment of the gas precursors and their interaction with surfaces. The final two sections review the present understanding of the interaction of silane, germane and disilane with the silicon (001) surface and briefly the Si(111) surface.

2.2 Group IV Semiconductors

2.2.1 Crystal and Band Structure

The structure of silicon and germanium are the same as that of diamond with lattice constants of 5.43 and 5.65 Angstroms respectively. The unit cell is shown in Figure 2.1 and is repeated periodically in a perfect crystal.

In a periodic structure, the valence electrons experience a periodic potential and the energy eigenfunctions are Bloch functions with wavevector k as simultaneous eigenvalues. This interaction also leads to forbidden energy gaps in the eigen energy and wavevector relationship E(k) often known as the dispersion relation. Consequently, the allowed energy states form bands which in semiconductors are either full or empty at zero K. The highest

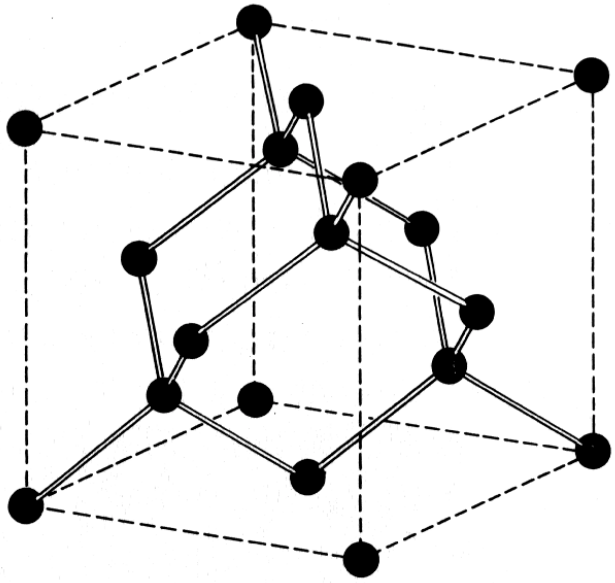


Figure 2.1: The diamond structure

filled band is known as the valence band and the lowest unoccupied band is known as the conduction band. The energy difference between the conduction band minimum and the valance band maximum is the fundamental band gap. The band gap, together with the dispersion relationship determines most of the electronic and optical properties of semiconductors. If the conduction band minimum and valance band maximum is located in the same place in k space, such as it is for GaAs, then the semiconductor is known as a direct gap material. Otherwise, it is known as an indirect gap semiconductor. Si and Ge are examples of indirect gap materials and their band structure along with that for GaAs is shown in figure 2.2.

When Silicon is grown in a SiGe alloy, the resulting strain modifies the band structure [73]. The bandgap of bulk SiGe alloys spans the 0.8 eV to 0.95 eV range. This fact makes alloys extremely attractive for applications involving long wavelength integrated optoelectronics on Si. The strain induced modification to the band structure was modelled by Abstrieter *et al* [1]. Their model, based on experimental data, attempted to describe the band offsets and potential wells in the Si/Si_xGe_{1-x} strained layer superlattices. For $Si_{0.5}Ge_{0.5}$ the band structure is very similar to that of Si. The conduction band minima are found to be along the $\langle 100 \rangle$ directions close to the X point of the Brillouin zone. With applied stress along the $\langle 100 \rangle$ direction, the sixfold degenerate conduction band minima, see Figure 2.3, is split into twofold and fourfold degenerate valleys. For uniaxial compression,

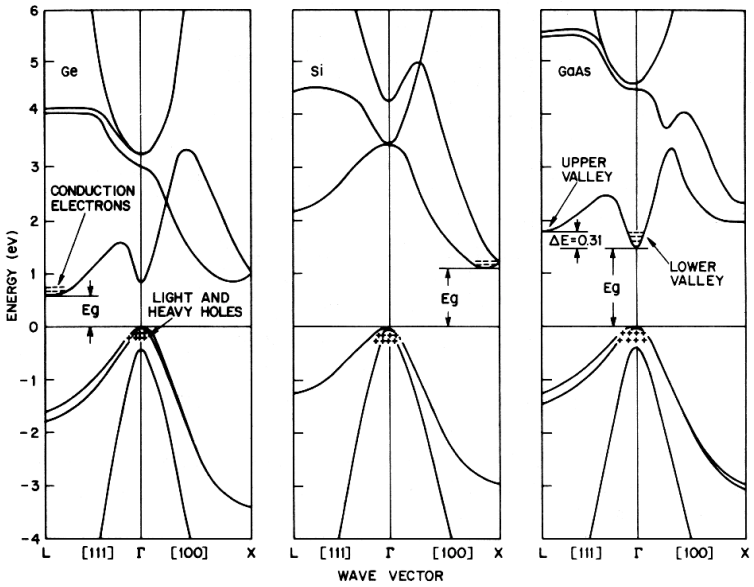


Figure 2.2: The germanium, silicon and GaAs band structure [94]. For silicon the indirect bandgap is between the Γ point and to just inside the X point of the Brillouin zone boundary. There are therefore six ellipsoids of constant energy along the $\langle 100 \rangle$ axes see Figure 2.3

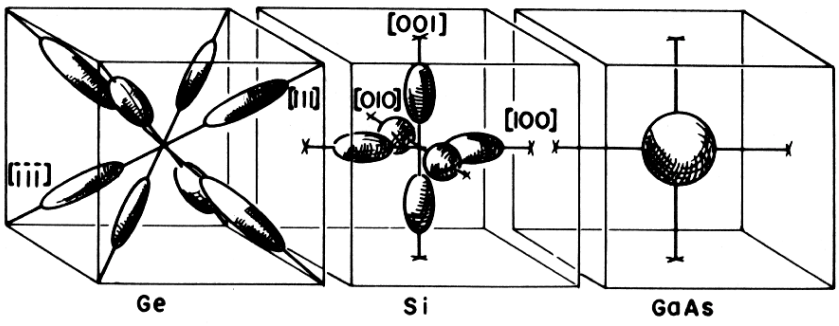


Figure 2.3: Constant energy surfaces for germanium, silicon and GaAs [94] For Si there are six ellipsoids along the $\langle 100 \rangle$ axes with the centres of the ellipsoids located $\frac{3}{4}$ of the distance from the Brillouin zone centre.

two valleys are lowered in energy by 5.8 meV/kbar, the other four valleys are shifted upwards by 2.9 meV/kbar. Abstrieter *et al* [1] obtained a splitting of approximately 150 meV for a stress of about 17 kbar.

Tensile strain exists in Si grown pseudomorphically on strain-relaxed SiGe. This tensile strain induces splittings and shifts in the conduction band which can lead to the situation where the valence band barrier is increased with respect to that in the conduction band. It is, therefore, possible to confine electrons in the Si layer where a quantum well exists. The lifting of the conduction band degeneracy, as the result of strain, also reduces inter-valley scattering and enhances the electron mobility of the confined carriers in the Si layer. It is these type of quantum wells that are used to confine the conduction channel away from the oxide semiconductor interface in modulation doped field effect transistors (MODFETs) and heterojunction metal oxide field effect transistors (HMOSFET)[1]. The band alignment/offset has been studied theoretically by Van de Walle *et al* [96].

Epitaxial growth of pseudomorphic SiGe layers on Si also opens up the possibility of forming hetero-pn-junctions. When employed in the emitter base junction of a bipolar transistor, the barrier for injection of holes from the base to the emitter is raised relative to that for the injection of electrons from emitter to base. Thus the ratio of emitter current due to injection from emitter to the total emitter current (including injection from base to emitter), known as the emitter injection efficiency, becomes less sensitive to the base doping level. Hence the base doping can be increased so as to reduce the base series resistance which is beneficial for high frequency applications, without compromising the emitter injection efficiency and current gain [94].

2.2.2 Surface Structure: Reconstruction

When a bulk crystal of Silicon or Germanium is suddenly terminated, the 'ideal' structure (one identical to the bulk of the crystal) would leave bonds on the surface that are not satisfied, they are said to be 'dangling'. This is energetically unfavourable and results in the dangling bonds combining with their nearest neighbours to form dimers on the (100) surface. These dimers form a new surface with a reduced symmetry/lower energy. The form of the new symmetry depends on the growth conditions and these dimer bonds can be disrupted in the presence of hydrogen.

On the clean Si (100) surface, the dimer consists of a pair of neighbouring Si atoms forming a relatively stable σ bond and a weak π bond. The resulting surface has a 2×1 symmetry. The π bonds are sometimes refered to as dangling bonds due to their unstable

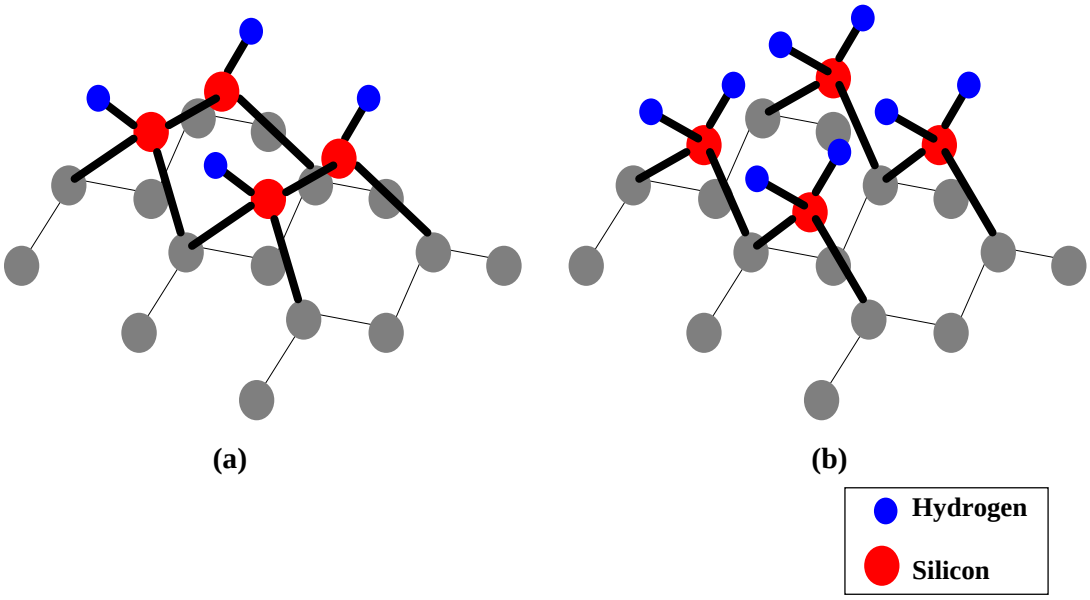


Figure 2.4: The monohydride and dihydride surfaces. The monohydride (a) is associated with a 2x1 reconstruction and the dihydride (b) a '1x1'.

nature. This π bond is easily broken upon the adsorption of atomic hydrogen leading to the formation of a new σ bond between the Si atoms and the adsorbed H atoms. This surface configuration also has a 2×1 symmetry and the surface is known as the mono-hydride phase. Further adsorption of atomic hydrogen can lead to the breakage of the σ bond between the Si dimer atoms with each Si atom bonded to two hydrogen via newly formed σ bonds. This is known as the di-hydride phase and the surface has a 1×1 symmetry. The monohydride and dihydride surface are illustrated in figure 2.4.

In the non-hydrogen terminated, 'clean' surface the dimers are 'tilted' due to an effect termed the 'Jahn-Teller' distortion. This is a consequence of the instability of a single non-bonded electron, this electron will combine with the electron on the other dimer atom creating a completely filled dangling bond. This reduces the symmetry of the surface by tilting the dimer where one silicon atom is depressed and the other is raised. Theoretical energetic calculations have suggested the asymmetric dimer is more favourable than the symmetric dimer [110] [8] [2] [76] . However scanning tunnelling microscopy (STM) studies [95] show predominately symmetrical dimers. This discrepancy has been explained as due to an energy barrier existing between these two coordinations of tilt. At a suitable energy the

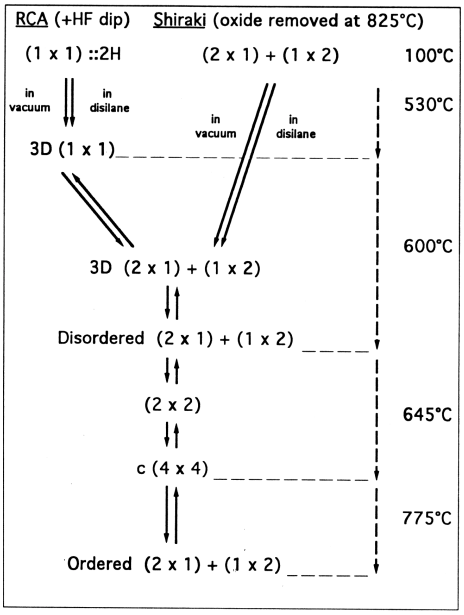


Figure 2.5: Si(001) surface reconstructions observed during GSMBE growth from disilane. Mokler *et al* 1991

tilt direction is thought to oscillate resulting in the STM observations being time-averaged and falsely indicating symmetrical dimers.

These reorganisations of the surface atoms are all examples of reconstruction and, since it is a dynamic process, its development during growth can be monitored using techniques such as RHEED. Sakamoto *et al* [83] were the first to observe layer by layer alternating surface reconstructions of Si(001) 2×1 and 1×2 using RHEED. Later work, [55], studied the evolution of RHEED patterns from growth on Si(001) surfaces from disilane. Their results are summarised in figure 2.5.

The surface was found to undergo a number of reconstruction changes during growth as a function of both substrate temperature and surface coverage. These changes were thought to be related to the gradual desorption of hydrogen adatoms and the simultaneous increase in the coverage of Si dimers. Below 600°C , RHEED patterns displayed features indicative of three dimensional island growth with the {311} faceting planes. At low temperatures where the surface hydrogen is prevalent, growth of Si on the substrate is three dimensional in the areas free of hydrogen. Raising the substrate temperature increases the hydrogen desorption rate and they suggest this also increases the sticking probability of the arriving Si atoms. The surface mobility also increases and the three dimensional islands begin to coalesce resulting in a disorded (2×1)+(1×2) reconstruction. As the temperature is raised further the reconstructions change from the disorded (2×1)+(1×2) to a transitional

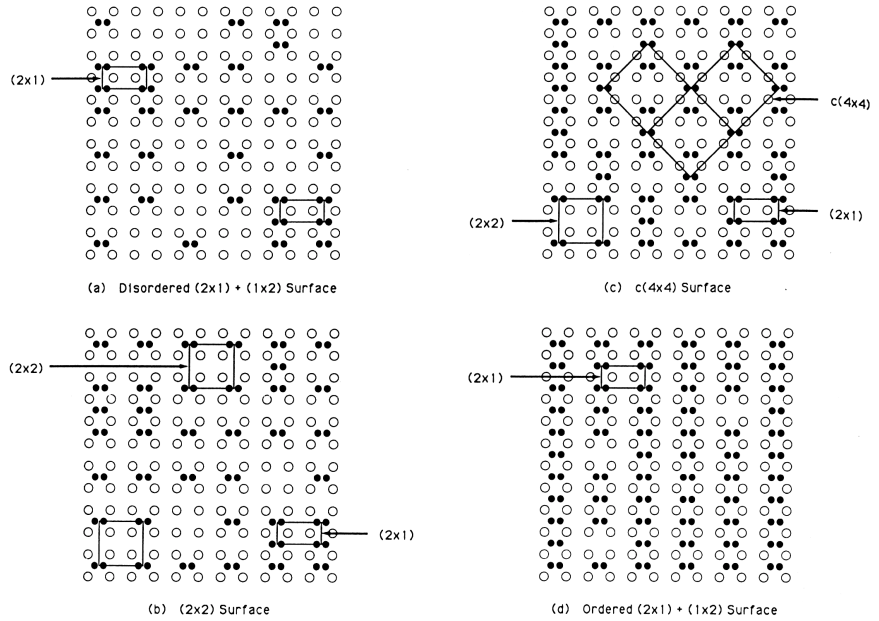


Figure 2.6: Atomic structural models for Si(001) surfaces with (a) disorded (2×1)+(1×2), (b) (2×2), (c) c(4×4) and (d) ordered (2×1)+(1×2) structures, Mokler *et al* , 1991

(2×2) and then a predominately c(4×4) structure, see figure 2.6.

At temperatures above 775 °C the surface concentration of hydrogen adatoms was further reduced and the vacant sites were also completely filled by Si due to an increased surface mobility. Growth thus proceeded two dimensionally giving rise to a well ordered (2×1)+(1×2) reconstruction. Mokler *et al* ,[56] [55], also showed that the initial modes of reconstructions were dependent on the method used to prepare the sample.

Ohtani *et al* , [67] [68] studied RHEED intensity during growth on a double-domain Si(001). They observed a clear transition from monolayer growth to growth by deposition of two layers at a time, bilayer growth, see figure 2.7. This transition occurred after seven or eight periods and was found to be quite reproducible. This phenomenon of bi-layer growth related to anisotropic growth kinetics is described in section 2.2.4:Bi-Layer Growth.

2.2.3 Growth

So far a study of the actual growth process itself has been neglected. While MBE growth often occurs far from thermal equilibrium, we shall initially consider growth processes occurring close to equilibrium conditions.

For the growth of Si on Si there is no mismatch of lattice parameters and the crystal grows uniformly. However if another type of crystal is grown on top, the mismatch in lattice parameter will produce strain in the epitaxial layer, *i.e.* SiGe on Si or *vice versa*.

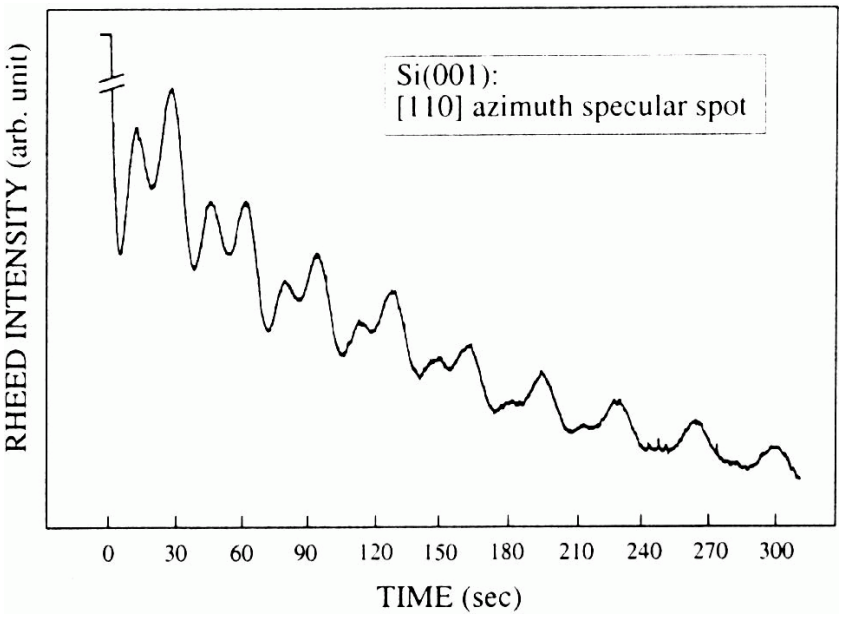


Figure 2.7: RHEED intensity oscillations observed in the specularly reflected beam along the [110] azimuth at a substrate temperature of 560 ^{0}C using a disilane flow rate of 0.36 SCCM Ohtani *et al* , 1993

Energetic calculations have shown that three dimensional growth is favoured when the strain in the island is relaxed [75]. Strain relaxation usually takes place by the creation of misfit dislocations. It has also been shown that lattice mismatched materials can be grown on each other up to a certain critical thickness before misfit dislocations form to reduce the strain. The possibility of metastable layers grown away from equilibrium will be addressed later.

Growth can occur in many different modes since the molecules deposited onto the substrate are subject to many different energy dependent processes. Intuitively, one can expect that the arriving molecules would either deposit one layer at a time, coalesce to form islands, *c.f.* water droplets on a polished surface, or form a mixture of both. This is indeed the case and the mode of growth followed is dictated by the relative formation energy of each mode. Frank and van der Merwe [18] described the two-dimensional growth which proceeds layer by layer and is thus termed the Frank-van der Merwe (FvdM) growth mode. The three dimensional 'droplet' growth mode was considered by Volmer and Weber, [99], and is termed the VW mode. Growth that is initially two-dimensional but then changes to three-dimensional growth is termed the Stranski-Krastanov (SK) growth mode [90]. Both the SK and VW modes can result in the growth of smeared interfaces and undulating growth 'fronts'.

The relative surface energies between the substrate, epilayer, interface and the strain energy are related, in equilibrium, in the following equation [3]

$$\Delta\sigma = \sigma_f + \sigma_i + d(h) - \sigma_s \tag{2.1}$$

where σ_f is the surface energy of the epilayer, σ_i is the energy of the interface, σ_s is the surface energy of the substrate and $d(h)$ is the strain energy due to the lattice mismatch. When $\Delta\sigma < O$ the surface of the substrate is 'wetted' and growth is the layer by layer FW growth. If $\Delta\sigma > O$ the growth mode followed will be the three dimensional VW mode. SK growth is observed when $\Delta\sigma$ is initially negative turning positive as the growth proceeds as $d(h)$ increases with layer thickness, h. Marée *et al* [52] studied the heteroepitaxial growth of Germanium on Silicon. They showed that the growth mode of Ge on Si(111) is of the SK type and after four monolayers island formation takes place. Si on Ge(111) is found to exhibit VW type growth. Ge_xSi_{1-x} alloys grown on a Si substrate are found to follow the SK growth mode [74] but this is strongly dependent on the alloy composition [109].

For heteroepitaxial growth, layers can be grown psuedomorphically up to a critical thickness this was first considered by van der Merwe [97]. As the film thickness increases, the homogeneous strain energy of the two dimensional film becomes large enough to make nucleation of misfit dislocations energetically favourable. The critical thickness is thus defined as the thickness at which an epilayer can be grown where only one misfit dislocation forms. However layers can be grown to thicknesses far greater than the prediction of energetic arguments since the process of MBE growth occurs far from equilibrium and there exists a kinetic energy barrier to the lowest energy state of the growth system.

This transition from two to three dimensional growth has been studied using STM [54] and RHEED [43]. Koide *et al* observed three dimensional islands with {311} facets when Ge is grown on Si(100). Mo *et al* reported a three dimensional cluster phase with a {105} facet structure. It was suggested that these 'hut' clusters define the kinetic path for the formation of the macroscopic Ge islands. Since MBE is a kinetic process, formation of islands can be suppressed by lowering growth temperature [4]. This can be attributed to a lower surface mobility but lowering the temperature results in poor crystal quality.

2.2.4 Bi-Layer Growth

Because Si(001) has twofold symmetry, it is not unreasonable to assume that there will be anisotropy in the surface migration of adatoms. This anisotropy was recorded by Mo *et al* , [53]. As highlighted in section 2.2.2, the Si(001) surface forms a (2×1) reconstruction,

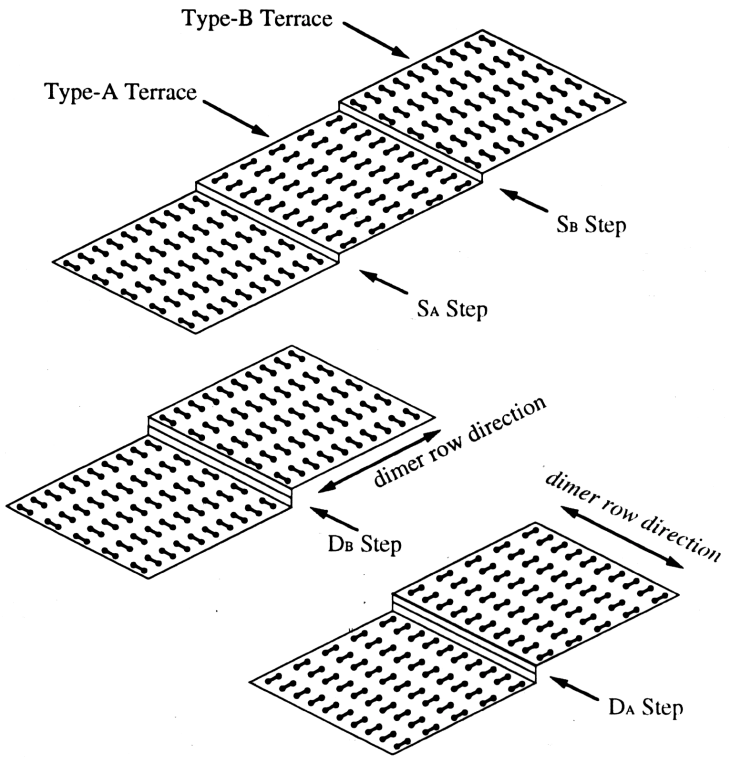


Figure 2.8: Schematic representations of Si(100) surfaces with monotomic steps (top) and biatomic steps (bottom)

with top-layer atoms dimerising to reduce the number of dangling bonds. Thus there are two characteristic directions on the surface, either along or perpendicular to the surface dimer rows. Mo *et al* suggested that the diffusion is at least one thousand times greater along the dimer row direction than perpendicular to it. Since there are two characteristic directions on the surface there will also be two types of steps. The two types of steps S_A and S_B are shown in Figure 2.8 Mo *et al* found the S_B steps are good sinks for Si and Ge adatoms, while S_A steps are not. Furthermore, S_B steps appear to be symmetric sinks for either adatoms coming from either down or up the terraces. There are therefore two factors explaining why the type-B terrace, one with dimers parallel to the step, is more prevalent. The anisotropy in diffusion along the type-A surface towards the steps edges and preferential sticking at the type-B steps.

The relative stabilities of the monolayer and bilayer growth were studied by Chadi [9, 1987]. Chadi calculated the energies of single and double layer steps on Si(001) surfaces and showed that bi-layer steps become energetically more favourable on surfaces misorientated towards [110] or [$\bar{1}$10] The double layer steps are labelled D_A and D_B and these are illustrated in Figure 2.8.

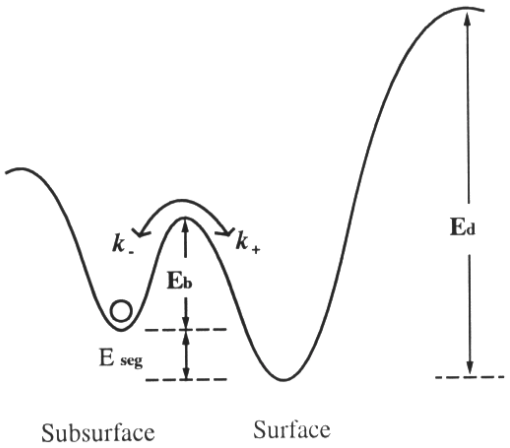


Figure 2.9: Schematic energy diagram of the two site exchange model of surface segregation. k_- and k_+ denote the rate of exchange where the positive subscript denotes transfer from the subsurface to surface site

2.2.5 Segregation

Since MBE is a relatively low temperature process it was originally thought the effects of thermal diffusion and intermixing would be negligible. However dynamic growth studies have hinted at a higher surface germanium concentration than that in the bulk crystal. Studies [37] have shown that Ge moves to the epitaxial surface during the growth of Si/Ge/Si structures and this can inhibit the formation of abrupt heterointerfaces, this phenomenon has been termed segregation. Subsequently there have been many studies on the effects of Ge segregation; Nakagawa and Miyao [62] studied the segregation of Ge on Si(100) and Si(111) using x-ray photoelectron spectroscopy. They discovered a peak temperature at which segregation is prevalent and a decrease in segregation at higher temperatures.

Segregation has also been studied using secondary-ion mass spectroscopy (SIMS), [111]. The process of Ge segregation can be described by a two site exchange model where the energy of a subsurface state is separated from the lower surface energy state by an energy barrier. Figure 2.9 shows the energy of the subsurface, bulk states and the surface states, differing by an amount E_{seg}, the Gibbs free energy of segregation, and separated by an energy barrier E_b. The energy barrier to desorption, E_d, is considered infinitely high in relation to E_{seg} and E_b. The population of these energy states is dependent on the thermal energy of the atoms in these states and the energy barriers between them and, under equilibrium, will be governed by Boltzmann statistics:

$$\frac{n_{surf}}{n_{sub}} = e^{\frac{E_{seg}}{k_B T}} > 1 \tag{2.2}$$

At an infinite temperature the two states will be equally occupied since the energy barrier, E_b, will be infinitesimal. At lower temperatures the lower energy state will have a higher population provided that the rate of exchange between the surface and sub-surface sites is fast compared with the growth rate, *i.e.* the sites are at equilibrium. Therefore, segregation will be more severe at low temperatures if it is in the equilibrium region. In contrast the two sites may not reach equilibrium if the growth rate is fast enough. In growth, the deposition of one monolayer will change the surface site to a subsurface site, if this deposition occurs in a time less than it takes atoms to transfer from site to site, the system will not reach equilibrium. To produce a sharp interface during growth the growth conditions can be varied depending on the energetics of the system. If the system is kinetically limited, E_b is large, the growth rate should be increased to reduce segregation so subsurface atoms do not have time to move to the surface. However, if the system is in equilibrium, E_b is small, the growth temperature should be increased to incorporate the greatest fraction of surface atoms into subsurface sites. This depletes the reserves of the other type of atoms on the surface and creates a sharper interface. Both these conditions assume E_{seg} and E_b are constant.

If a third type of atom is placed on the surface which preferentially segregates compared to Ge it would be reasonable to expect the Ge segregation to be suppressed. This has been reported by Copel *et al* [11] using Arsenic as the third type of atom and Osten *et al* , [70] using Antinomy. These layers of a third type of atom are termed 'surfactants'. Zalm *et al* [111] studied the effect of a Ga surfactant during growth of $Si_{1-x}Ge_x$/Si multilayers, they found that Ge segregation was completely absent. Using RHEED Ohtani *et al* [66] studied the temperature dependence of Ge surface segregation during silicon gas source molecular beam epitaxy (Si-GSMBE) from hydride sources. It was discovered that surface hydrogen, which is produced by the dissociation of Si_2H_6 and GeH_4 on the growing surface, may act as a growth-controlling surfactant.

2.3 The Kinetic Theory of Thermal Molecular Beam Epitaxy

2.3.1 Introduction: Gases in Equilibrium

Since this thesis reports on the studies of growth mechanisms via the investigation of adsorption and desorption of molecules and atoms, an understanding of the properties of thermal molecular beam is required in order to extract information on surface processes/reactions. This basic understanding is founded in the classical kinetic theory of gases and the properties of molecular beams are derived from it.

The classical kinetic theory of gases describes an assembly of non-interacting particles at thermal equilibrium. In a molecular beam formed in moderate vacuum, collisions are rare and chemical reactions are in-frequent as conservation of energy and momentum are difficult to satisfy simultaneously in two body collisions when a change of internal energy occurs. Thus a model of molecular beams derived from a classical gas provides an adequate description of the relationships between flux (I), temperature(T), beam equivalent pressure(P), number density(n) and velocity distribution.

2.3.2 The Impingement Rate

An classical gas has an isotropic velocity distribution. Hence the number density of particles with velocity $\underline{v}$ defined by direction in a solid angle $d\Omega$ defined by polar coordinates (θ, ϕ) is given by

$$n(\underline{v})d\Omega = \frac{n(v)}{4\pi}d\Omega = \frac{n(v)}{4\pi}\sin(\theta)d\theta d\phi \tag{2.3}$$

where $n(v)$ is the density of particles having *speed* v.

Consider a small area A with its normal in the polar axis direction, the flux of particles with velocity $\underline{v}(\theta, \phi)$ passing through it is given by

$$I(\underline{v})d\Omega = \frac{n(v)}{4\pi} \times v \times \cos(\theta)d\Omega \tag{2.4}$$

Hence the flux of particles crossing this area from above can be evaluated by integrating over all possible speeds and solid angles

$$\begin{aligned} I &= \int_0^\infty \int_0^{\frac{\pi}{2}} \int_0^{2\pi} \frac{vn(v)}{4\pi} dv \sin\theta \cos(\theta) d\theta d\phi \\ &= \frac{1}{4}\int_0^\infty vn(v)dv \end{aligned}$$

giving

$$I = \frac{1}{4} n \bar{v} \tag{2.5}$$

where the average speed $\bar{v}$ is given by

$$\bar{v} = \frac{1}{n} \int_0^\infty v n(v) dv \tag{2.6}$$

By integrating Eq 2.4 over speed only, the flux of particles from solid angle $d\Omega$ is given by:

$$I d\Omega = \frac{n\bar{v}}{4\pi} \cos(\theta) d\Omega$$

This is known as the cosine law and shows that the greatest Impingement rate is associated with the element of solid angle normal to the area.

The pressure P exerted by an ideal gas on the surface of the container can be derived using equation 2.4 and Newtons law. At equilibrium, equal numbers of particles are leaving the surface as are arriving. The momentum exchange with impingement of each particle is given by

$$p = m\delta v = 2mv\cos(\theta)$$

where m is the mass of the particle. Hence the pressure exerted by a flux of molecules $I(\underline{v})$ from solid angle $d\Omega$ is given by

$$P(\underline{v}) d\Omega = 2mv\cos(\theta) I(\underline{v}) d\Omega$$

Integrating over all speeds and solid angles, the total pressure is obtained.

$$P = \frac{m}{3} \int_0^\infty v^2 n(v) dv = \frac{1}{3} mn\overline{v^2} \tag{2.7}$$

To obtain further relationship between state variables such as pressure, temperature and flux require additional information in the form of the Boltzmann distribution (see appendix B).

Using the Boltzmann relationship , the average speed $\overline{v}$ and rms speed $\sqrt{\overline{v^2}}$ are related to temperature and molecular weight by:

$$\overline{v} = \frac{2}{\sqrt{\pi}} \sqrt{\frac{2k_B T}{m}}$$

$$\sqrt{\overline{v^2}} = \sqrt{\frac{3k_BT}{m}}$$

From these relations, the impingement rate and pressure are related by:

$$I = \frac{P}{\sqrt{2\pi m k_B T}} \tag{2.8}$$

$$= n\sqrt{\frac{k_BT}{2\pi m}} \tag{2.9}$$

2.3.3 Thermal Molecular Beams

In the previous sections, one of the basic assumptions in deriving the properties of ideal gas at equilibrium is the isotropic velocity distribution. This is clearly violated by a molecular beam where all the atoms/molecules are moving in essentially the same direction. However, such molecular beam may have a speed distribution and temperature characteristic of the source. Thermal molecular beams can be produced by the flow of gas through a small orifice in a wall containing an ideal gas at equilibrium. Provided the equilibrium of the gas is not significantly disturbed by the loss of molecules and the radius r of the orifice is small compared with the mean free path of the molecules, the flux at a distance L away from the orifice is given by:

$$I = \left(\frac{P}{\sqrt{2\pi m k_B T}}\right)(cos\theta)(\frac{r}{L})^2 \tag{2.10}$$

where P and T are the pressure and temperature of the source. Such a molecular beam source is known as Knudsen source and its velocity distribution is given here without derivation [36].

$$Pr(\nu)d\nu = \frac{\nu^3 m^2}{2(k_BT)^2} e^{\frac{-m\nu^2}{2k_BT}} d\nu \tag{2.11}$$

Integrating over the entire energy distribution yields an expression for the mean translational kinetic energy of the beam[1]:

$$\bar{E} = 2k_BT \tag{2.12}$$

Equation 2.10 shows that if the sample is far away from the source the beam intensity will be low, most of the material effusing through the orifice will be wasted. To decrease

[1]For supersonic beams where beams expand into a differentially pumped chamber this is given by $\frac{5}{2}k_BT$ $^\circ C\,f.\ \frac{3}{2}k_BT$ for the static gas

this loss of the beam to the background it can be collimated by using a second orifice or 'skimmer' or, more simply, by using an orifice with some thickness, in this case the cosine distribution is elongated along the orifice axis toward the sample. The total beam intensity can be increased by using many of these tube like orifices.

2.3.4 Adsorption and Desorption

When the molecules in a molecular beam impinge on a surface they can undergo a number of different processes:

1. Reflected from the surface without interaction.
2. Trapped permanently on the surface.
3. Trapped on the surface followed by departure back into the gas phase.

We are primarily concerned with the latter two processes where crystal growth may occur and information about the surface process may be extracted.

The interaction of molecules with the surface can take place in many different forms and this can be illustrated by an energy surface showing the variation of potential energy with distance from the surface, see figure 2.10.

As can be seen in figure 2.10 there may exist many minima in the potential energy surface and these can be attributed to different binding processes. The minimum at the largest molecule-surface separation will normally be shallow and can be attributed to weak Van der Waals forces, binding to this state is called *physisorption*. The behaviour of any adsorbed species will depend on the variation of the surface potential and its magnitude relative to k_BT. For a shallow potential well relative to k_BT the adsorbed molecule will be relatively free to move on the surface, this is termed mobile adsorption. The other extreme, immobile adsorption, is where the potential well depth is much greater than k_BT. In between these two extremes is localised adsorption. Experimental studies of adsorption indicate that all three types of adsorption are observed in practice.

Minima that exist closer to the surface will normally be lower in energy and can be attributed to hydrogen bonds, ionic bonds or strong covalent bonds where electron charge transfer occurs, binding to these states is termed *chemisorption*, see section 2.3.5. The lifetime of the molecule will depend on the depth of the potential well (the mode of adsorption) and temperature.

The time the molecule can spend on the surface is finite and this implies that at some point the molecule will leave the surface and return to the gas phase. This departure

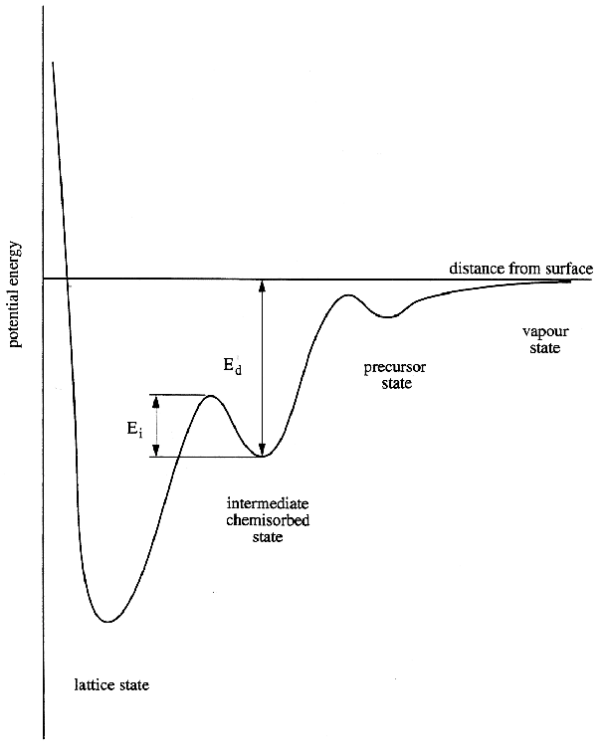


Figure 2.10: A schematic one dimensional potential energy surface

from the surface is termed *desorption* and can be characterised by a probability that the molecule will desorb and a desorption frequency [36]

$$\nu_{des} = \nu_0 \times exp\left(\frac{-\Delta G_{des}}{k_B T}\right) \tag{2.13}$$

ν_{des} is the desorption frequency, ν_0 an attempt frequency and ΔG_{des} is the energy of activation for the escape process. This leads to [36]

$$\nu_{des} = constant \times exp\left(\frac{-\Delta E_{des}}{k_B T}\right) \tag{2.14}$$

where ΔE_{des} is also the energy of activation for the escape process. The reciprocal of ν_{des} is the mean surface lifetime of the molecule, τ,

$$\tau = \tau_0 exp\left(\frac{\Delta E_{des}}{k_B T}\right) \tag{2.15}$$

When the system is in equilibrium between impingement (rate I) and desorption (rate $= \frac{n_a}{\tau_a}$

where n_a is the surface population) we can say

$$\frac{n_a}{\tau_a} = I \tag{2.16}$$

substituting in equations 2.9 and 2.15

$$n_a = I\tau_a = \left[\frac{P}{(2\pi m k_B T)^{\frac{1}{2}}}\right] \tau_0 exp\left(\frac{\Delta H_{des}}{k_B T}\right) \tag{2.17}$$

This equation may only be applied to cases where equilibrium exists and the desorption process is first order. In order to use this equation in any real system we must assume that all molecules adsorb independently of each other (ΔH_{des} is independent of n_a) and that all positions on the surface are equivalent.

If we study the form of equation 2.17 we can see that for constant temperature n_a is directly proportional to pressure, a plot of these curves at constant temperature but varying pressure is called an adsorption isotherm. Plots for constant pressure and surface population are termed adsorption isobars and adsorption isosteres respectively.

A further modification to this is to assume that molecules that strike a site that is already occupied do not adsorb, the complete model is then termed the Langmuir model. For the Langmuir model at equilibrium with n_0 as the surface site density, the surface population becomes

$$n_a = I\left[1 - \frac{n_a}{n_0}\right]\tau_a \tag{2.18}$$

or

$$n_a = I(1-\theta)\tau_a \tag{2.19}$$

it is easy to show

$$\theta = \frac{\frac{I\tau a}{n_0}}{1 + \frac{I\tau_a}{n_0}} \tag{2.20}$$

or substituting in equation 2.9 we get the Langmuir adsorption isotherm:

$$\theta = \frac{P\chi}{1 + P\chi} \tag{2.21}$$

where $\chi = \frac{\tau_a}{n_0} \frac{1}{\sqrt{2\pi m k_B T}}$. This model provides a good description of the adsorption processes in systems where strong chemisorption occurs but is poor in describing other systems involving physisorption since it cannot account for ad layers thicker than one monolayer and neglects lateral interactions, surface mobility and surface heterogeneity.

2.3.5 The Kinetics of Chemisorption

In the previous section chemisorption was discussed as the name for the process of binding due to strong hydrogen bonds, ionic bonds or covalent bonds. Chemisorption will normally be accompanied by a shallow physisorption state situated at a greater distance from the surface atoms. The form of the total potential energy curve will depend on whether the incoming molecule is adsorbed intact, without breaking bonds, or whether the molecule must dissociate in order for its component atoms to reach the chemisorbed state. For the adsorption as a molecule followed by dissociation into the individual atoms, the energy at infinite distance will no longer be zero since work must be done to break the bonds. If the physisorbed state is sufficiently far away from the surface then chemisorption will be activated since an energy barrier will have to be overcome, this topic will be returned to this at the end of this section. For a physisorbed state close to the surface, chemisorption maybe non-activated.

Consider the kinetics of chemisorption of a homonuclear diatomic molecule $(A_2)_g$, if the system is one of precursor mediated adsorption (the adsorbing molecule will pass through a physisorbed state, $(A_2)_p$, before being chemisorbed, $2(A)_a$,) it can be described as follows:

$$(A_2)_g \;\; {}_{k_p} \rightleftharpoons {}^{I\alpha} \;\; (A_2)_p \;\; {}_{k_d} \rightleftharpoons {}^{k_a} \;\; 2(A)_a \tag{2.22}$$

The superscripts to the arrows denote the rate of the reaction going to the right and the subscripts the rate of those passing from right to left. $k_{a/d/p}$ is the rate constant and is given by $k_{a/d/p} = k_{a_0/d_0/p_0} exp(\frac{-E_{a/d/p}}{k_B T})$. If the fractional coverage of $A_{2(p)}$ is given by θ_p and the fractional coverage of $2(A)_a$ is given by θ then the rate of change of θ_p is given by

$$\frac{d\theta_p}{dt} = \frac{I\alpha}{n_0} - k_p\theta_p + k_d\theta^2 + k_a\theta_p(1-\theta)^2 \tag{2.23}$$

where I is the impingement rate from the gas phase and α is the trapping probability. Under equilibrium conditions the above equation can be rearranged to give

$$\theta_p = \frac{\frac{I\alpha}{n_0} + k_d\theta^2}{k_p - k_a(1-\theta)^2} \tag{2.24}$$

The process of activated chemisorption was mentioned earlier, this is where a positive energy barrier exists between the physisorbed state and the chemisorbed state. This can give rise to the desorption of molecules having excess kinetic energy (departure from the cosine distribution) and a dependence of the adsorption rate on the kinetic energy of the incident molecules. Under such conditions the ratio of the rate of desorption from the physisorbed state to adsorption to the chemisorbed state will be given by Boltzmann statistics [36]

$$\frac{k_a}{k_p} = exp\left(\frac{\Delta E_p - \Delta E_a}{k_B T}\right) = \frac{S(\theta)}{1 - S(\theta)} \tag{2.25}$$

where ΔE_p is the energy barrier to the physisorbed state and ΔE_a is the energy barrier to chemisorption. $S(\theta)$ is the sticking coefficient.

2.4 Adsorption of Hydrides on the Si(100) Surface

2.4.1 Introduction

In section 2.2 the structure of the bulk of a semiconductor crystal and the properties of its surface were introduced. The deposition of a crystalline material on another was described macroscopically but no reference was made to the mechanistic details of the growth itself. Section 2.3 was an abstract theoretical description of the properties of gases and introduced the concept of thermal molecular beams and their interaction with a theoretical surface with non-specific active sites for adsorption. In this section all these concepts will be drawn together and related to research into the growth process undertaken on the silicon surface using silane, disilane and germane gas precursors.

2.4.2 Adsorption Mechanisms

The Langmuir model of adsorption was introduced previously where an active site for adsorption becomes inactive once bonded to, it is this form of adsorption that occurs when a clean silicon surface at room temperature is exposed silane, disilane or germane, however, the process is complicated by the fact that two species, hydrogen and silicon or germanium, are deposited on the surface together and it is the hydrogen that deactivates the active sites. At temperatures far above room temperature this hydrogen desorbs readily reactivating the sites for adsorption, it should be noted, however, that other processes to remove hydrogen from the surface may exist but we shall assume here that thermally activated desorption is the most dominant [46] [77] [89] . Hydrogen has also been shown to affect the Si adatom mobility [14] and suppress 3D island growth [12], the hydrogen terminated Si(100) surface is covered in detail in section 2.5. The reactivation of adsorption sites allows the steady state growth of silicon from silicon hydrides and will be dealt with in the following sections. In this section, the study of adsorption process itself will be discussed.

The study of this dissociative chemisorption on a clean surface can be performed at low temperatures by observing the surface after it has become fully passivated or by studying the growth process at temperatures where the steady state hydrogen coverage is low.

Hendersen and Helm [29] and Joyce *et al* [39] believed the cracking of the silane occurred during collision with the crystal surface as in the reaction of alkanes on metals. Hendersen *et al* used a simple model of the cracking of silane where hydrogen gas was

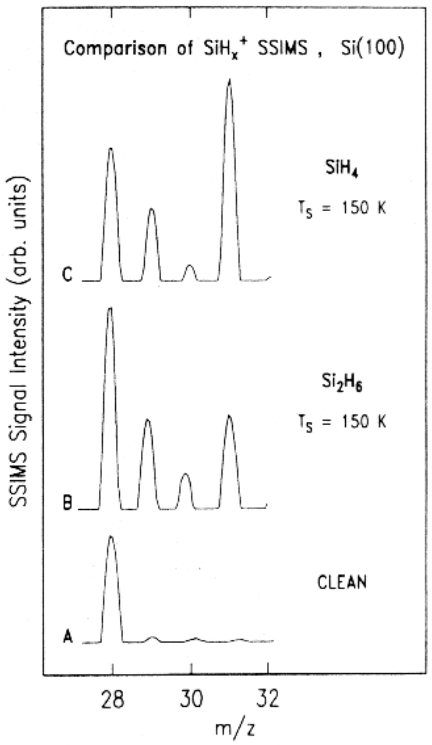


Figure 2.11: Static SIMS study of silane and disilane adsorption by Gates *et al* at 150 K. m/z = 28 corresponds to Silicon, 29 SiH, 30 SiH_2 and 31 SiH_3

released and silicon adatoms were produced, and measured an activation energy of 0.87±0.22 eV. Joyce *et al* used mass spectrometry to study the release of hydrogen into the gas phase at high temperatures to test a model which involved an initial SiH_4 decomposition step which produced SiH_3 and H adsorbed surface species, subsequent surface reactions of these species led to the release of hydrogen gas and silicon adatoms. They measured an activation energy of 0.81±0.09 eV and a reaction order near two. An alternative view was postulated by Farrows et al [16] who believed cracking of the silane followed adsorption to a precursor state on the silicon surface.

More recent studies have used techniques to probe the adsorbed species on the surface which are invasive and significantly disrupt the state of the surface during the measurement. Two of these techniques are temperature programmed desorption (TPD) and secondary ion mass spectrometry (SIMS).

Gates *et al* [23] [21] [22] used static SIMS and TPD to study the SiH_x intermediates during SiH_4 decomposition on atomically clean Si(100)-(2×1) and compared this to that on Si(111)-(7×7). They observed the mass to charge ratio of the secondary ions during ablation by the ion beam after the substrates were exposed to silane at various temperatures. The

samples were then cooled to 50 °C before the SSIMS measurements were taken (except exposure at -123 °C where the data were collected at -123 °C).

Their results can be summarised as follows; for the silicon (100) surfaces after exposure to silane at 50 °C only Si, SiH and SiH_3 were observed. SiH_3 was found to be particularly abundant at low temperatures and concluded that SiH_3 and H are the main products from the initial step of silane adsorption. At higher exposure temperatures only SiH was seen and this provided information on the stability of the SiH_3 fragments. They reported disilane produced less SiH_3 than for silane adsorption and the dihydride population is slightly higher, see Figure 2.11. Gates *et al* also found that the trihydride was stable to much higher temperatures than that produced from silane adsorption and this was interpreted as due to differening local environments of adsorbed species or a site blocking effect by adsorbed undissociated disilane. It was also reported that the decomposition temperature of SiH_3 can vary from 473 °C to 873 °C depending on the dangling bonds coverage and evidence for a coverage dependent decomposition mechanism for SiH_2 is also presented. They conclude that both the mechanism and rate of decomposition of surface SiH_3 and SiH_2 are dependent on the local surface environment near these species. The complete reaction scheme for low surface coverages can be summarised as follows $\underline{Si}-$ denotes a surface silicon dangling bond and $\underline{Si}-X$ denotes an absorbed species X:

$$SiH_4(g) + 2\underline{Si}- \rightarrow \underline{Si}-H + \underline{Si}-SiH_3 \tag{2.26}$$

$$\underline{Si}-SiH_3 + \underline{Si}- \rightarrow \underline{Si}-H + \underline{Si}-SiH_2 \tag{2.27}$$

$$\underline{Si}-SiH_2 + \underline{Si}- \rightarrow \underline{Si}-H + \underline{Si}-SiH \tag{2.28}$$

$$2(\underline{Si}-SiH) \rightarrow H_2(g) + 2(\underline{Si}-Si-) \tag{2.29}$$

and for high surface coverages reaction 2.28 is replaced by 2.30 where the dihydride decays by releasing hydrogen directly into the gas phase.:

$$2(\underline{Si}-SiH_2) \rightarrow H_2(g) + 2(\underline{Si}-SiH) \tag{2.30}$$

Hydrogen desorption will be dealt with in greater depth in section 2.5

For the silicon (111) surfaces after exposure to silane at 50 °C the only significant secondary ions were those found to be associated with Si itself and SiH and SiH_2, no SiH_3 was observed but it is known to be stable at 50 °C from the experiments on the Si(100) surface. Again at higher exposure temperatures only SiH was observed. Direct SiH_2 formation occurs and this is consistent with the results of Farnaam and Orlander [15].

It is therefore evident that two different adsorption mechanisms are observed for Si(111) and Si(100) under these conditions.

Gates *et al* [23] [21] [22] found at zero coverage the two surfaces exhibited a similar adsorption rate of silane, this was attributed to surface impurities or highly reactive defect sites which would be independent of the surface orientation. The silicon (100)-(2×1) surface contains one dangling bond on every surface atom, or 6.8×10^{14} dangling bonds per cm^2. The reconstructed Si(111)-(7×7) surface contains approximately less than half this number 3.0×10^{14}. In the comparison of the two surfaces by Gates *et al* these differences were corrected for. If the single active site on the Si(100) surface is assumed to consist of the two dangling bonds on one dimer there is little correction needed since the densities are 3.0 vs 3.4×10^{14}. Saturation on the (100) surface at 400°C is found to occur as the silane exposure exceeds 10^{20} cm^{-2} and results in approximately 10^{14} silane molecules which have undergone adsorption. This corresponds to four times as many hydrogen atoms and therefore a fractional coverage of $\frac{4\times10^{14}}{6.8\times10^{14}} \approx 0.6$ H/Si, well below one monolayer. It is possible that not all the dangling bonds react with the incoming silane. The requirement of two adjacent dangling bonds for silane adsorption is supported by this saturation well below one monolayer. For adsorption above these coverages silicon must be incorporated through insertion into the Si-H bonds. For the Si(111) surface no saturation behaviour is observed. The corresponding fractional coverage approaches 1 H/Si despite the fact that the density of dangling bonds on the (7×7) surface is 0.39 /Si. Clearly adsorption on the (7×7) surface is not restricted to dangling bonds. The coverages of H from SiH_4 exceed the dangling bond coverage at 300 °C and 400 °C but not at lower temperatures this is consistent with insertion into Si-Si bonds between the first and second layer. This contrasting behaviour between (111) and (100) Si further supports the identification of two different silane adsorption mechanisms with different surface site requirements. Gates *et al* found a weak dependence on surface temperature for the silane adsorption probability on Si(111). The activation barrier derived from the surface temperature dependence is 0.13 eV which has also been used as an estimate of the barrier on Si(100). The low sticking probability of silane was regarded by Gates *et al* as due to the fact that the molecules internal energy is more important than surface structure effects in controlling the adsorption rate. A very small sticking probability is associated with a barrier to adsorption located in the entrance channel of the potential energy surface and hence the rate of chemisorption is dependent on the characteristics of the Boltzmann distribution of the incident gas. A study of the kinetics of silane and disilane with enhanced translational energy was performed by Xia *et al*, see later.

Hirose *et al* [32] [31] studied the adsorption of silane, disilane and also germane on the Si(001)2×1 surface using TPD. For disilane exposure they reported a saturation coverage of hydrogen of 1.6 ML with a plateau at 1 ML for intermediate coverages. Gates *et al* [20] also reported a saturation coverage of 1.6ML and proposed a reaction mechanism where disilane inserts into a surface S-H bond producing silane gas and adsorbed trihydride. For the coverage of 1.6ML the dimer structure was seen to be destroyed by observing the reconstructions using RHEED. At these high coverages the trihydride phase was reported to be stable due to the site blocking effect reported by Gates *et al* [23] [21] [22]. By modelling the hydrogen coverage with exposure Hirose *et al* also suggested the disilane molecule requires two sites to adsorb at low surface coverages, at high coverages the disilane adsorbs by destroying the dimer bond. By simulating the hydrogen coverage for silane and germane exposure they found a fourth order adsorption model best fitted their data and concluded the adsorption process similar for both silane and germane and independent of surface coverage. In the experiments performed with germane a maximum hydrogen coverage of approximately 0.8ML was observed, this is agreement with the experiments of Gates *et al* for silane. Because of differing orders and mechanisms of adsorption from disilane and germane the incorporation of germanium in SiGe growth would be more suppressed by hydrogen than the silicon from disilane. This model could be tested by growing SiGe with silane and disilane where the silane flux is calculated to give the same growth rate as the disilane on clean silicon and measuring the resulting germanium concentration in the SiGe.

To study the state of the surface after adsorption without appreciable destruction of the surface, other techniques utilising the electronic properties of the surface bonds can be used. These are electron energy loss spectroscopy (EELS) , multiple internal refection infra red spectroscopy (MIRIRS), atomic force microscopy (AFM) and scanning tunnelling microscopy (STM). These less destructive techniques allow snapshots of the growth process but are at present difficult to perform during growth itself.

MIRIRS is able to identify species adsorbed on the surface by measuring the transmittance of the surface to infra red radiation, the transmittance is sensitive to the stretching modes of the adsorbate Si-H_x bonds. The MIRIRS study by Wu *et al* [106] of disilane adsorption on the clean Si(100) surface showed that the dominant species after adsorption at 300 K was the dihydride co-existing with a monohydride phase. Some evidence was found for trihydrides but these were completely removed by annealing to 400 K, dihydride was removed by annealing to 450 K (200 °C).

A technique similarly surface sensitive as MRIRS is electron energy loss spectroscopy (EELS). Suda *et al* [91] used EELS and RHEED to study the adsorption of disi-

lane on the Si(100) surface. They concluded that the adsorption of disilane on Si(100)2×1 occurs in two stages. On the clean surface at 300 K and in the low coverage regime disilane dissociatively chemisorbs on dangling bonds and the most likely products are two SiH_3 on adjacent sites. Adsorbed SiH_3 then quickly decomposes to SiH_2 and H.

The imaging of surfaces at low temperatures has been performed using STM and AFM after exposure to group IV hydrides. Wang *et al* [100] also show a temperature dependence on the degree of dissociation of the hydrides, at low temperatures both silane and disilane produce predominately SiH_3 fragments which are randomly distributed on the surface. STM images show that these SiH_3 groups spontaneously dissociate into SiH_2 and H within several minutes of adsorption at room temperature. Thermal annealing leads to diffusion and dissociation of the SiH_2 groups. At low temperatures the monohydride distribution is non-statistical showing a preference for flat terraces over small epitaxial islands. This is in contrast to the findings of Boland [6] and Lin *et al* [50] who suggest that epitaxial islands consisted of monohydride dimers. Confusion can arise in the interpretation of STM images since only differences in fragments can be observed, the actual identification of these species is more difficult. Goldfarb *et al* [25] presented a more recent analysis of island formation using STM images. Again the disilane molecules break up on impact to SiH_3 groups which decay to form SiH_2+H at room temperature, these SiH_2 groups diffuse together to form nonepitaxial monohydride ad-dimers which lose their hydrogen at 150°C . Most of these ad-dimers are found to become mobile at around 200°C and react together to form a square structure which is a nucleus for a string of dimers. Above 200-300°C higher hydrides are rarely seen and virtually all the dimers have formed into rows. This reaction pathway is quite different to that for MBE where adatoms attract each other and form ad-atom-dimer complexes. These are not seen in the gas source experiments and Goldfarb *et al* explained this as due to the fact that a monohydride ad-dimer is not attractive to a SiH_2 group.

Owen *et al* [71] [72] and Goldfarb *et al* [26] also used STM to study silicon growth and observed the SiH_2 groups and hydrogen as a result of disilane decomposition. The SiH_2 decomposed by combining with another SiH_2 on adjacent dimer rows, in full agreement with the study by Wang *et al*. This was also the process suggested by Gates *et al* [21] for high hydrogen coverages where two SiH_2 decay to release hydrogen into the gas phase and produce the monohydride phase. Owen *et al* also concluded that hydrogen played a strong role in the blocking of diffusion along the surface below temperatures of 550K.

Werner *et al* [101] used RHEED oscillations to probe the adsorption of disilane on a clean surface at temperatures where hydrogen desorption is the major limiting factor in

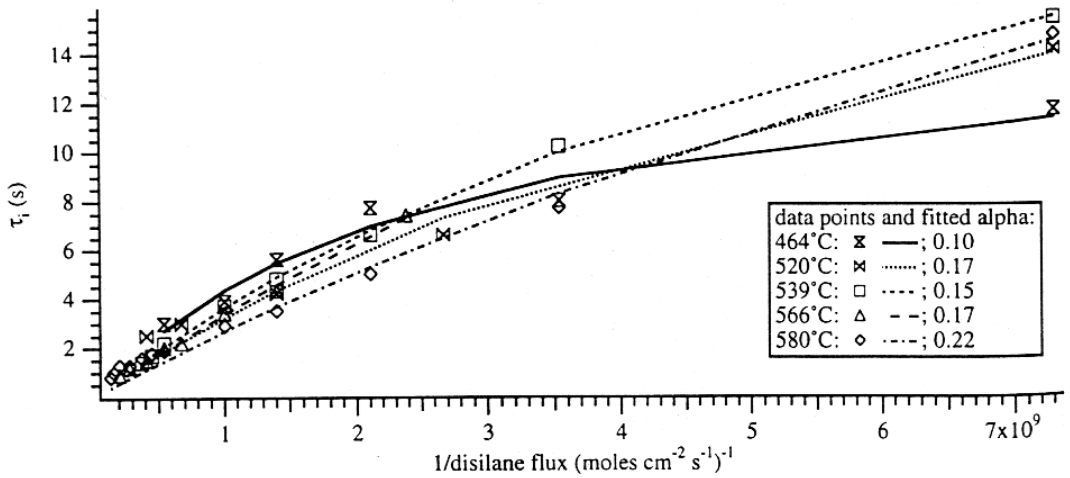


Figure 2.12: The period of the first half RHEED oscillation versus the inverse disilane flux. The period was used to characterise the adsorption of disilane on clean surface, this period is seen to be almost independent of temperature and shows a similar dependence on flux. The legend gives the sticking coefficients derived from the fit. Werner *et al* [101]

the growth process. Although the steady state oscillations are indicative of a considerable steady state hydrogen coverage Werner *et al* used the first oscillation only to study the adsorption onto the clean surface. They related the time taken for the intensity to reach the first minima to the time taken to produce a full layer of hydrogen and fitted the results to a model, the results are shown in Figure 2.12, the curves show that the period of the first half oscillation is independent of temperature. They derived a non temperature dependent sticking coefficient (see Equation 2.25) of 0.15 over the temperature range 464°C to 580°C . They assumed disilane adsorption on the clean surface produced $\frac{1}{2}$ ML silicon. At the temperatures used in their experiments it is more likely the disilane fully dissociated to produce $\frac{1}{3}$ ML silicon before becoming fully passivated. If this was the case their analysis is in doubt since hydrogen desorption becomes significant before the RHEED beam intensity reaches a minima corresponding to $\frac{1}{2}$ ML silicon. Indeed, it is also not clear if the first minima in RHEED oscillations does correspond to $\frac{1}{2}$ ML of silicon.

Hirose *et al* [33] observed a saturation in the amount of hydrogen adsorbing at low

temperatures where hydrogen desorption is negligible using TPD. They presumed all of the hydrogen from the silane molecules remains on the surface along with the adsorbed silicon. By annealing the surface the hydrogen can be desorbed and the process can be repeated, by observing the RHEED pattern change from 2×1 to 1×2 they inferred the completion of 1 ML of Si. From the number of cycles to produce 1ML Si they calculated 0.25-0.33ML Si was deposited per cycle of what is termed temperature modulated growth (TMG). Hirose *et al* [33] suggest a use of this technique is to further control the deposition of silicon for device growth however the technique of TMG can be extended to give many more details of the surface kinetics and this is explored in Chapter 5.

Xia *et al* [107] [108] have measured the sticking coefficient for disilane on clean Si(100) using supersonic molecular beams[2]. They measured the sticking coefficient for disilane over a wide range of translational energies, incident angles and substrate temperatures and found that it increases with substrate temperature and nearly linearly with increasing beam energy. Xia *et al* reported that at these elevated beam energies, disilane adsorbs directly with no evidence for a precursor state. The substrate temperatures employed were of a magnitude where the rate hydrogen desorption was appreciable ensuring a low steady state hydrogen coverage. However these experiments do not reflect the conditions under which conventional gas source silicon epitaxy is performed. This thesis is concerned solely with the interaction of thermal gas source molecular beams with the Si(100) surface for which a unified picture of the growth process does not exist despite the enormous amount of work performed.

As in the Xia *et al* experiments, at very high substrate temperatures and low incoming flux where the rate of desorption of the hydrogen is faster than the rate of adsorption, the surface can be considered to be clean. In this regime the growth rate from thermal beams can give information on the adsorption process on a clean surface. Growth rate measurements can be performed by recording the period of the intensity oscillations of a specularly reflected electron beam since one period of oscillation has been shown to be equivalent to one monolayer of growth [64]. Information on sticking coefficients can be gained by modelling the steady state growth rate and this is the topic of the next section.

2.4.3 Homoepitaxial Growth

Epitaxial growth of silicon must occur via the cracking of the silicon hydride to release the silicon and hydrogen. The silicon is then incorporated into the epitaxial layers

[2] A supersonic beam is produced by the expansion of a thermal beam (see section 2.3.3) into a differentially pumped chamber

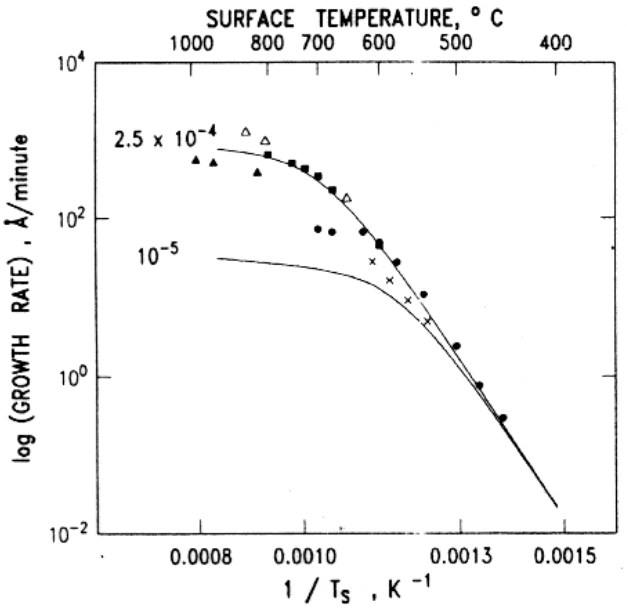


Figure 2.13: Gates *et al* [24] : Comparison of model prediction (solid lines) and literature growth rate data. Two values of silane reactive sticking probability are used for the two solid lines. One SiH_4 flux is used. Data show epitaxial Si film growth rates: squares from [10] at 0.0006 Torr, dots from [49] at 0.003 Torr, open triangles from [78] at 0.05 Torr, solid triangles from [29] at 0.01 Torr and crosses from Meyerson *et al* at 0.001 Torr

and the hydrogen may form surface hydrides or be released into the gas phase. In the case of growth of silicon from silane the overall reaction will be given by: $SiH_4(g) \rightarrow Si + 2H_2(g)$. This reaction can be divided into two sub-processes; the surface decomposition of the silicon hydride to produce adsorbed silicon atoms, and the incorporation of the silicon adatoms into the epitaxial layer, this later process is more important for growth from elemental sources. It is the former of these two processes that is of the most interest in growth studies since it is found to be the rate determining step.

Gates *et al* [24] collated several groups measurements of growth rate from silane on Si(100) and the results of modelling are given in Figure 2.13. The dependence of growth rate on temperature falls into three regimes and these are linked to the steady state hydrogen coverage during growth although in Figure 2.13 only two are shown. At low temperatures, where the flux is great enough to ensure the presence of a silane molecule as soon as an adsorption site becomes active due to hydrogen desorption, the rate of adsorption of hydrogen is equal to the rate of desorption. However, since the hydrogen is associated with silicon, the growth rate is always equal to the rate of hydrogen desorption. The growth rate at low temperatures is seen to be thermally activated and the energy of activation being found to be approximately 2.0 eV. The growth rate has no dependence on the silane flux.

In the second regime the steady state hydrogen coverage will vary from 1 ML at the low temperature boundary to approximately 0 ML at the high temperature boundary. In the third regime the steady state hydrogen coverage can be considered to be negligible and the growth rate is limited by the rate of arrival of a proportion of the silane flux, this proportion is governed by the sticking coefficient. In this regime the rate limiting process is probably the rate of adsorption and decomposition of the adsorbed silane fragments. No evidence has been reported for thermally activated growth rate at high temperatures. RHEED growth rate measurements are not possible in this regime since the growth mode is likely to be that of step flow. RHEED intensity oscillations rely on spontaneous nucleation growth for the 'reflectivity' of the surface to vary periodically.

For the model of Gates *et al* the calculated growth rate at low temperature agrees with the data regardless of the sticking coefficient used for modelling while at high temperatures the best fit is for a sticking coefficient of $2.5\times\ 10^{-4}$ The results were modelled assuming the silane requires two sites to adsorb.

As mentioned previously Hirose *et al* proposed a model where four sites are required by silane to adsorb on the Si(100) surface. However a later study by Suemitsu *et al* [92] suggested the silane adsorption mode changes from two site adsorption to four site adsorption at around 600 °C and interpreted this as due to the presence of a SiH_3 adsorption precursor which can undergo thermally activated desorption from the surface. At high temperatures SiH_3 is able to desorb from the surface so growth cannot proceed through the normal process of SiH_3 decomposition, instead silane adsorbs directly onto the silicon surface using four dangling bonds. There is no evidence that SiH_3 desorption plays a part in the observed effect and the fourth order reaction was derived from a gradient susceptible to large errors.

Mokler *et al* [56] [57] measured the temperature dependence of the steady state growth rate of silicon from disilane using the period of intensity of a specularly reflected electron beam and this is shown in figure 2.14. The dependence of growth rate on temperature and flux is very similar to that for silane. In this figure only the two lower temperature regimes of growth are obvious, since the data were recorded purely by RHEED intensity oscillations, high temperature measurements were not possible. Mokler *et al* also report that RHEED intensity oscillations are not observed at very low fluxes since the rate of formation of silicon from disilane is too low for 2D nucleation. It is likely that at these very low fluxes there is sufficient time for adatoms to migrate to step edges and the growth mode to become step flow.

Suemitsu [93] performed a similar growth study for disilane precursors as they did

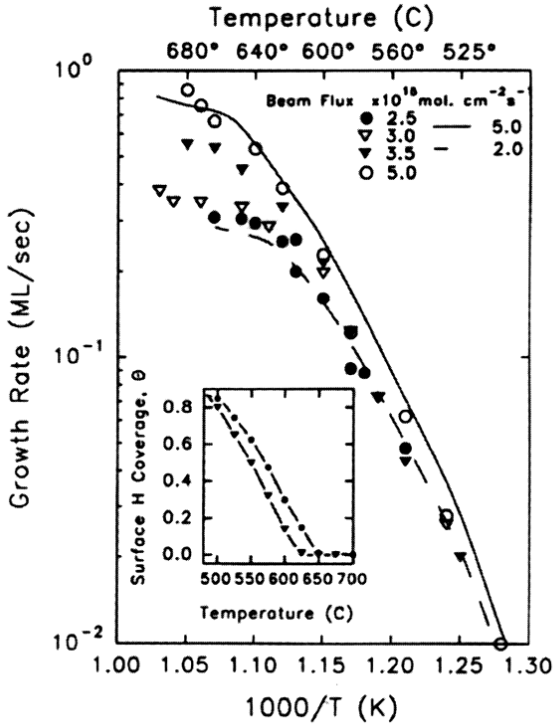


Figure 2.14: Mokler *et al* [57]: Arrhenius plot of growth rate data from RHEED intensity oscillation frequency in [010] azimuth. A change in the slope near 600 °C is seen. Below this temperature growth rate is limited by Si_2H_6 arrival rate. An activation energy of 1.77 eV is calculated for the low temperature region. Solid and dashed lines are derived from the model in [49] for fluxes (dashed) 2 and (solid) 5×10^{15} molecules cm^2s^{-1}, respectively, and for equation $GR = \alpha J(1-\theta)^2$, where α is a weakly dependent reaction probability, J is the beam flux and θ represents the fraction of surface covered by hydrogen. The inset shows θ values used which were derived from [24]

for silane and again reported various reaction orders which were dependent on hydrogen coverage or temperature. The two could not be distinguished since they performed no flux dependent study. The reaction order varied from $\frac{1}{2}$ for high hydrogen coverages to 2 and finally 4 at very low hydrogen coverages. The fractional order was justified by adsorption to a physisorbed state before finally being chemisorbed when they migrate to a suitable site. The integer orders were simply the number of sites required for adsorption

Hirose [30] managed to model the growth rate from disilane using a second order adsorption model and first order hydrogen desorption. The rate of change of surface coverage of hydrogen was given as follows

$$N_0\frac{d\theta}{dt} = 6JSk_aN_0(1-\theta)^2 - 2k_dN_0\theta \tag{2.31}$$

N_0 is the active site surface density, θ is the fractional surface site occupancy, J is the incident flux in ML per second, S is the sticking coefficient and k_a and k_d are the adsorption rate constant and desorption rate constant respectively. The rate constants are given by the relation $k_a = k_{a_0} exp(-\frac{E}{k_B T})$ where k_{a_0} is the pre-exponential, E the activation energy, k_B is Boltzmann's constant and T is the temperature in Kelvin. The factor 6 relates to the six hydrogen atoms released from the disilane molecule and the factor 2 to the production of molecular hydrogen. Equation 2.31 can be solved for θ under steady state ($N_0 \frac{d\theta}{dt} = 0$):

$$\theta = \frac{6k_aJS + k_d - \sqrt{12k_ak_dJS + k_d^2}}{6k_aJS} \tag{2.32}$$

and the silicon growth rate is given by

$$GR = 2k_aJS(1-\theta)^2 \tag{2.33}$$

They produced good fits for their limited range of data using an activation energy of 2.13 eV for hydrogen desorption. Temperatures where they reported a hydrogen coverage of 1.6 ML the extrapolated growth rate would be 0.0001 Angstroms per minute assuming hydrogen desorption remains the rate limiting step. This is five orders of magnitude less than that at high temperatures, clearly growth is negligible for this hydrogen coverage. The growth rate is still appreciable where the steady state hydrogen coverage is 1 ML. Hirose *et al* assumed the sticking coefficient was 1 but Bramblett *et al* [7], using the same model derived a value of 0.036 for the zero steady state surface site occupancy regime of growth.

Gates *et al* [19] [20] observed a slight flux dependence at low temperatures and hydrogen coverages of close to 1 ML and this was accounted for by the reaction of disilane with an adsorbed hydrogen to produce silane in the gas phase and an adsorbed trihydride. The production of silane has been observed in the modulated beam mass spectrometry measurements of Kulkarni *et al* [47] for growth on the Si(111) surface. Werner *et al* [102] suggested the flux dependence at low temperature could be explained without the need for a silane producing reaction pathway and suggested that if the maximum surface coverage was assumed to be greater than 1ML the flux dependence could be accounted for as sites were still available for adsorption. Gates *et al* suggested that modulation of the desorbing product flux and phase sensitive detection with a mass spectrometer would allow confirmation of a silane reaction product.

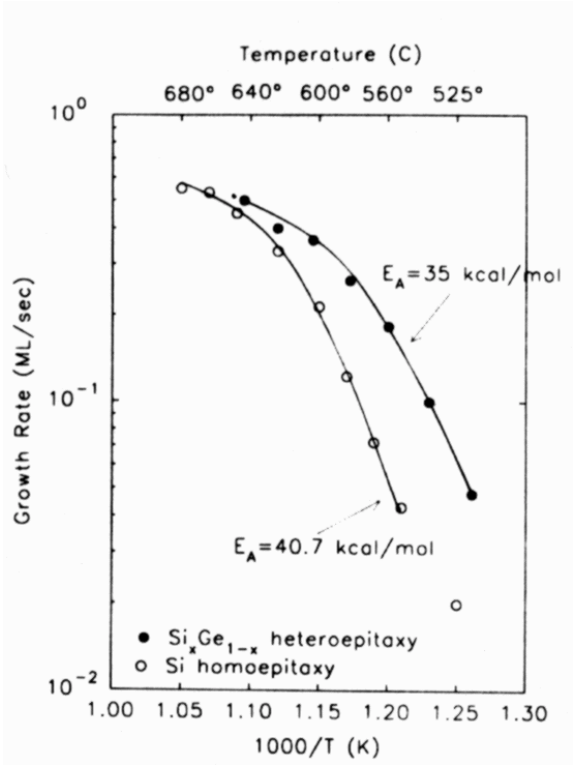


Figure 2.15: Mokler *et al* [58]: Arrhenius plots for the growth rate data during Si homoepitaxy and $Si_{1-x}Ge_x$ heteroepitaxy. Addition of GeH_4 to the system lowers the activation energy from 1.77 eV (40.7 kcal/mol) found for Si homoepitaxy to 1.52 eV (35 kcal/mol) for $Si_{1-x}Ge_x$ below 600 °C . The addition of Ge to the surface results in a higher desorption rate of hydrogen desorption and therefore shifts the transition between adsorption/dissociation limited and desorption limited kinetics towards lower temperature

Optical second harmonic generation (SHG) is surface species sensitive since the non-linear response required to generate light at twice the frequency of the illumination is forbidden from the bulk but not the surface. Hu *et al* [35] used SHG to measure the steady state hydrogen coverage on the Si(100) surface during growth from from a disilane precursor. By modelling their results they produced a temperature independent sticking coefficient of $0.04^{\pm}0.01$ between 740 K and 920 K in good agreement with Bramblett *et al* [7].

2.4.4 Heteroepitaxial Growth

Figure 2.15 shows another Arrhenius plot for homoepitaxial and also $Si_{1-x}Ge_x$ heteroepitaxial growth on the Si(100) surface produced by Mokler *et al* [58] [59] [60]. It is clear from the low temperature regimes, growth for $Si_{1-x}Ge_x$ has a lower activation energy for the rate limiting step which is in this case hydrogen desorption. This has been

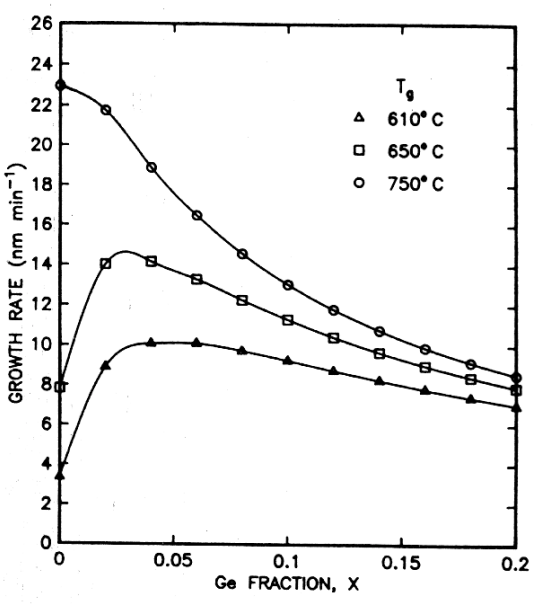


Figure 2.16: Modelled growth rates of $Si_{1-x}Ge_x$ layers with composition, x produced by Robbins *et al* [79]. The model assumed an increase of the rate of hydrogen desorption and a lower sticking coefficient with increasing x.

interpreted as due to a lower energy pathway for desorption from germanium on the surface.

Mokler *et al* speculated that the growth rate at low surface coverages is the same for homoepitaxial growth as it is for heteroepitaxial growth (assuming equivalent fluxes) however studies by Robbins *et al* [79] and later by Zhang *et al* [112] showed that germanium on the surface actually inhibited the rate of adsorption of disilane and germane on clean surfaces. Russell and Breiland [80] successfully modelled the growth rate from silane and germane by using four parallel adsorption processes that of silane on silicon, germane on germanium and the additional two cross terms.

The study of Robbins *et al* used silane and germane and derived growth rates as a function of germanium fraction x at different temperatures using transmission electron microscopy (TEM), Rutherford back scattering (RBS) and SIMS. The modelled results are shown in figure 2.16. The alloy growth rates at 610 °C are greatly enhanced compared with pure silicon but show a peak rather than a monotonic increase with x. Growth rates at 750 °C decrease monotonically with increasing x, and the behaviour at 650 °C lies between these. The modelled assumed an increase of the rate of hydrogen desorption and a lower sticking coefficient with increasing x.

Zhang *et al* [112] performed a similar study to Robbins *et al* but used disilane inplace of silane and varied the germanium composition x from 0 to 0.8 using an atomic

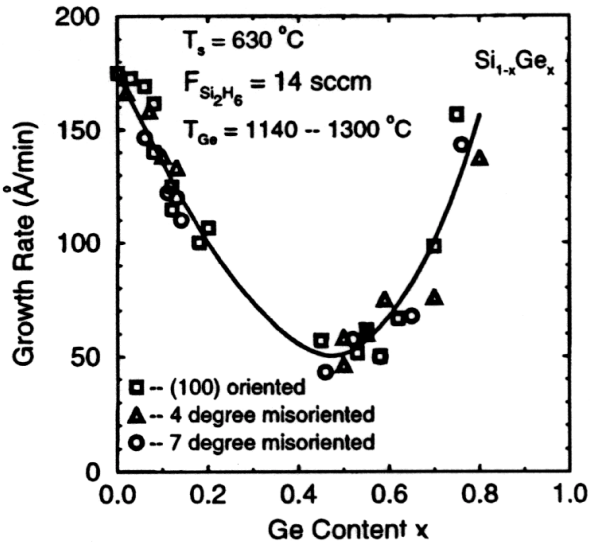


Figure 2.17: Zhang *et al* [112]: Comparison of $Si_{1-x}Ge_x$ layer growth rate as a function of germanium fraction for the growth method using Si_2H_6 and Ge as sources among different substrate orientations. The symbols are experimental data and the solid line is a guide for the eye

Ge flux. The results are shown in figure 2.17. The results are in agreement to those of Robbins *et al* and the increase in growth rate with composition is due to the fact that the composition was varied by increasing the germanium flux. The explanation for the decrease sticking coefficient with increasing germanium content provided by Zhang *et al* assumes that disilane adsorbs at kink sites whereas germanium can adsorb at all surface sites. Germanium will migrate rapidly on the surface and can occupy the kink sites required for disilane adsorption. The use of various misorientated substrates should highlight the effect of surface migration and site blocking but figure 2.17 shows no variation in growth rate with misorientation, Zhang *et al* concluded that the rate of migration is so high no effect is observed.

2.5 Hydrogen on the Si(100) and $Si_{1-x}Ge_x$(100) Surfaces

2.5.1 Introduction

The importance of surface hydrogen has been highlighted in the previous sections. It is clear the presence of hydrogen on the surface prevents the adsorption of disilane and hence stops further growth. In this section the details of the reactivation of adsorption

Hydrogen Desorption Parameters			
Reference	Method	E_d (eV)	$k_{d_0}(s^{-1})$
Sinniah *et al* [87]	LITD	2.03	7.90×10^{11}
Sinniah *et al* [88]	LITD	1.96	2.20×10^{11}
Wise *et al* [103]	TPD	2.52	5.50×10^{15}
Hofer *et al* [34]	SHG	2.48	2.00×10^{15}
Greenlief *et al* [28] [27]	TPD	2.13	8.00×10^{13}
Flowers *et al* [17]	TPD	2.48	2.00×10^{15}
Sakamoto *et al* [82]	RHEED	1.84	-
Okada *et al* [69]	LITD	2.36	2.32×10^{14}
Sharp *et al* [86]	RAS	2.25	6.00×10^{13}
Hu *et al* [35]	SHG	2.26	3.70×10^{13}

Table 2.1: Hydrogen desorption parameters, activation energy of desorption: E_d (eV) and pre-exponential: $k_{d_0}(s^{-1})$

sites by the removal of hydrogen are discussed and the most dominant process of removal is found to be thermally activated desorption.

2.5.2 The Si(100) Surface

Four major techniques are employed to study the thermal desorption of hydrogen; by using a mass spectrometer to measure the species desorbing from the surface as a function of substrate temperature or laser illumination (TPD and LITD respectively) or by using SHG or reflectance anisotropy spectroscopy (RAS) which are both sensitive to the surface hydrogen coverage. The results of studies performed using these techniques are summarised in Table 2.1, it is clear that the variation in pre-exponentials is vast but the derived activation energies are slightly more consistent producing a value around 2.2 eV. To draw a more useful conclusion we must examine these studies on an individual basis.

One of the earliest studies of thermal desorption was performed by Sinniah *et al* [87] [88] who used LITD and reported first order kinetics in the coverage range 0.006-1.0ML and an activation energy of approximately 2 eV. A first order rate law is inconsistent with conventional hopping models that describe the recombinative desorption of hydrogen from the surface of metals which is found to be second order since the reaction depends on the probability of one desorption site to be doubly occupied. Sinniah *et al* proposed a model for desorption where an atom of hydrogen is irreversibly excited into a freely translating state before recombination with a normally bound atom and departure as molecular hydrogen from the surface. However this was dismissed by Kolasinski [44] as unsatisfactory.

TPD studies show two peaks in the spectrum, Figure 2.18 shows some typical spectra recorded by Nakazawa *et al* [63], the high temperature peak has been attributed to desorption from the monohydride phase, β_1, and the lower temperature peak to desorption from the dihydride phase, β_2.

For the TPD studies performed on surfaces exposed to disilane at high temperatures only the β_1 peak is observed, for adsorption at room temperatures the subsequent TPD spectra show both the β_1 and β_2 peaks. For adsorption at the higher temperatures there is sufficient energy present to convert the dihydride phase to the monohydride phase at a rate much greater than that of adsorption. Nakazawa *et al* reported no shift in peak position with coverage for adsorption at high temperatures this is indicative of a first order desorption process. However, for a surface annealed after adsorption, a shift is observed indicating a process of higher order.

Wise *et al* [103] confirmed first order desorption kinetics from the Si(100) surface but reported second order desorption from Si(111). The fact that desorption was surface structure sensitive dismissed the model of Sinniah *et al* since structure would not affect the delocalised hydrogen state proposed. Wise *et al* suggested a pairing model in which recombination occurs across a Si-Si dimer which was supported by the theoretical work of D'Evelyn *et al* [13]. Calculations by Vittadini *et al* [98] proposed two distinct mechanisms for desorption from the monohydride surface, either recombination of two H atoms siting on the same dimer or from adjacent dimers along a row. For the dihydride surface the preferred pathway involves the desorption of two H atoms belonging to the same SiH_2 unit however this was dismissed by Gates et al [21] as the size of the β_2 peak didn't increase without an increase in the β_1 peak. They concluded decay of the dihydride phase produces the monohydride. Deviations from first order kinetics were observed by Hofer *et al* [34] at low coverages using SHG. They reported a desorption rate which was seen to decrease more rapidly than a linear dependence on coverage. This decrease was interpreted as due to singly occupied isolated dimers unable to take part in the pairing mechanism before desorption.

Kolasinski *et al* [45] performed measurements of the internal state of the desorbed molecular hydrogen. Vibrational and rotational state distributions were measured for H_2, D_2 and HD using resonance enhanced multiphonon ionisation (REMPI) and the $\nu = 1$ to $\nu = 0$ population ratio is roughly 20 times higher than that predicted by Boltzmann statistics at the surface temperature of 500 °C . In contrast, the average rotational energies of the desorbed molecules are significantly lower than k_BT. The degree of vibrational excitation suggested that the H-H interatomic distance in the transition state is elongated with respect to that in the gas phase. The low rotational energy rules out recombination

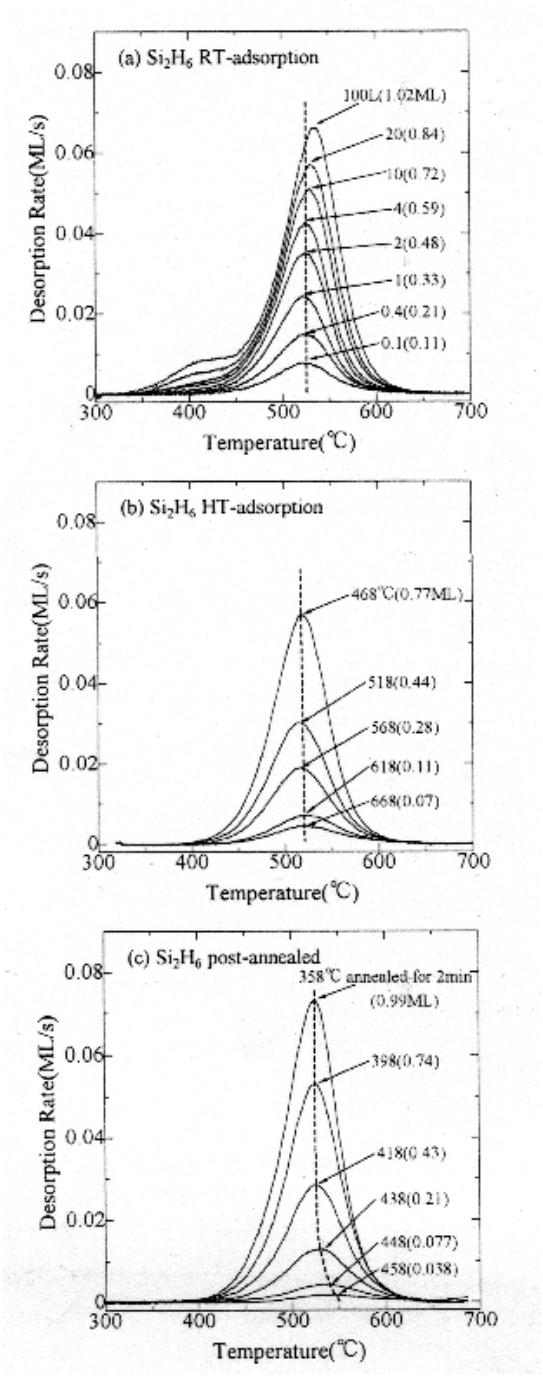


Figure 2.18: Nakazawa *et al* [63]: TPD spectra, the high temperature peak has been attributed to desorption from the monohydride phase, β_1, and the lower temperature peak to desorption from the dihydride phase, β_2.

from a highly asymmetric transition state or recombination from high impact collisions. Shane *et al* [84] performed similar studies on the Si(111) surface and found little differences to those on the Si(100) surface. This suggests that the desorbing molecules from the two different surfaces must pass through almost identical transition states. Kolasinski, Shane and Zare suggested the reaction paths of hydrogen from the two surfaces pass through a 3-centre transition state and was first raised by Nachtigall *et al* [61]. On the Si(100) surface the desorption process starts from a paired set of hydrogen atoms on one dimer unit. One of the hydrogen atoms migrates to the other side of the dimer to desorb passing through a symmetric transition state. A similar transition state is also formed on Si(111). In such a transition state only one Si atom contributes significantly to the forces upon the departing H_2, the long range order of the surface is unimportant and should lead to no changes in the internal state distributions upon change of the surface structure.

It is possible the rate limiting process in the desorption of hydrogen is not the recombination process itself but it is the surface diffusion of hydrogen to the recombination centres which governs the desorption kinetics. Several groups have attempted to calculate the activation energies for the surface diffusion, Vittadini *et al* [98] calculated 1.4eV for diffusion along the dimer rows and 1.9eV for diffusion perpendicular to the dimer rows.Wu *et al* [104] calculated 2.6 eV but Nachtigall *et al* [61] pointed out that these energies could be lowered once surface relaxations were taken into account.

The effect of growth precursors on hydrogen desorption was studied by Okada *et al* [69] and Greenlief *et al* [28] [27]. Okada *et al* reported no difference but Greenlief *et al* found a difference for surfaces prepared by silane in CVD. Greenlief *et al* postulated that monoatomic steps created during silane growth could play a role in the reduction of the desorption activation energy.

2.5.3 The $Si_{1-x}Ge_x$ (100) Surface

A good demonstration of the effect of germanium atoms on hydrogen desorption from the silicon surface is TPD spectra. The studies of Kim *et al* [40] [41] [42] show TPD spectra for increasing concentrations of germanium and are shown in Figure 2.19.

For a surface $Si_{1-x}Ge_x$ composition where $x = 0.03$ the spectra still looks similar to that from pure silicon but a small shoulder on the low temperature side of the β_2 can just be seen. For larger germanium concentrations another peak at even lower temperatures can be seen, this has been associated with desorption from germanium sites and is termed the α peak. Kim *et al* also have introduced a β_1^* peak to fit the results better, they postulated

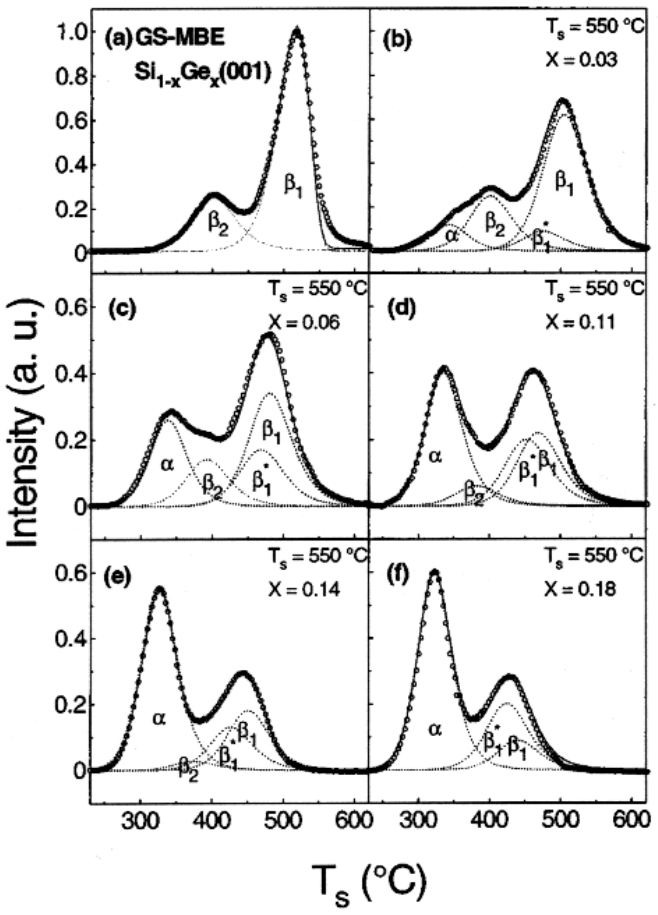


Figure 2.19: Kim *et al* [40]: TPD spectra from SiGe with various surface concentrations of germanium.

this could be due to desorption from mixed dimers. An additional effect is the shift of the β peaks to lower temperature and this has been explained as due to the surface germanium weakening the silicon hydrogen bonds. Wu *et al* [106] also recorded the presence of a more facile route for monohydride decomposition and hydrogen desorption in the presence of surface germanium using MIRIRS.

Sharp *et al* [85] used differential reflection to measure the surface hydrogen concentration as a function of time during isothermal desorption, the desorption rate in the presence of surface germanium is clearly increased. Joyce *et al* [38] used a more advanced technique Reflectance Anisotropy spectroscopy (RAS) and studied the oscillations observed during growth to measure the growth rate which increased with germanium composition and this was explained by an increased rate of hydrogen desorption.

Boishin *et al* [5] reported a similar effect of surface germanium on hydrogen desorption, however, the shift in peak position was accounted for by varied occupation of five

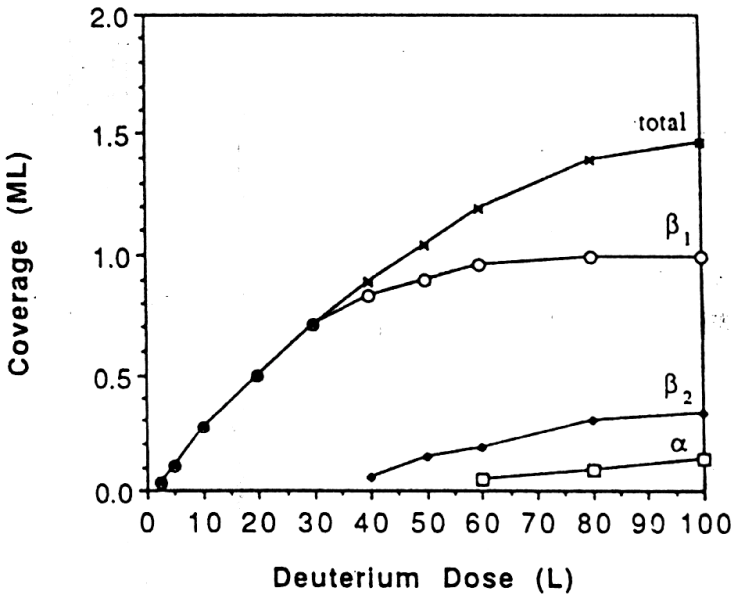


Figure 2.20: Ning *et al* [65]: Occupation of desorption sites. The total hydrogen coverage approaches 1.5 ML

desorption states. They also reported the diffusion of hydrogen from Ge to Si sites during a post dose annealing by measuring a change in work function. Ning *et al* [65] suggested that strain or step edges may be the cause of the decrease in the temperature of the peak in desorption rate. The general consensus [65] [81] [105] is that desorption occurs predominately from three sites, β_1 β_2 and α with varying occupations. Ning *et al* [65] produced a graph from integrated TPD peak areas showing coverage against deuterium dosing, see Figure 2.20, the graph shows that the monohydride β_1 occupation saturates at 1 ML but the dihydride β_2 and germanium monohydride α increase steadily. The total hydrogen coverage approaches 1.5 ML.

The issue of occupation of these desorption sites raises a question on the effect of surface diffusion on the desorption spectra, it is possible hydrogen is able to diffuse to other sites during the temperature ramp. Ning *et al* [65] observed that the silicon monohydride state was the only one observed during varied but low dosing of a SiGe surface using deuterium. This could be explained by the migration of deuterium (hydrogen) from germanium sites to those of silicon during adsorption or the temperature ramp, this is in agreement with the observations of Boishin *et al* [5] . Ning *et al* [65] concluded that the migration could only occur at high temperatures so would most likely occur during the temperature ramp for low deuterium coverages.

Russel *et al* [81] concluded that although Ge may modify the energetics of the

interaction of silicon and hydrogen such an effect alone is not enough to describe the shift and broadening of the β_1 feature. Their model assumed the existence of an alternate pathway to depopulate the silicon monohydride phase in which hydrogen diffuses from the silicon to germanium and desorbs from a short-lived GeH intermediate. For the observations of Ning *et al*, where only one desorption peak is seen for varying hydrogen coverages, to agree with the model of Russel *et al* all the hydrogen in the β_1 state must diffuse to this GeH intermediate before desorption.

Finally it must be highlighted that there are other phenomenon that are possibly of importance in the growth process, one of these is the phenomenon of hydrogen abstraction, this has been studied by many groups Srinvasen *et al* [89], Koleske *et al* [46] Ramalingam *et al* [77] but is normally observed with exposure of the surface to atomic hydrogen. Obviously if hydrogen can be removed by processes other than thermal desorption, the model used to explain growth must be further revised.

2.6 Summary

This chapter has given a brief overview of the enormous and ever expanding subject of the growth of silicon and germanium from hydride precursors. It is clear the hydrogen produced by the decomposition of the hydrides on the surface plays a major role in the overall growth process. The growth rate is governed by a balance between the rate of incoming hydrides and the rate of adsorption site reactivation. The various hydrides exhibit different properties and some dependence on surface orientation has been observed. Although this chapter has tried to summarise the results of research by many groups it is clear no overall model is forthcoming as every experiment has a subtle difference. The variation in results highlights the obvious complexities in the growth process. The remainder of this thesis attempts to produce an overall picture of the growth process for the gas source MBE machine present at Imperial College and this system is described in detail in the next chapter.

Chapter 3

System Description and Experimental Techniques

3.1 Introduction

In addition to the vacuum system itself, consisting of the chamber and substrate manipulator/heater, chamber pumping system and gas manifold (see Section 3.2.1) there were four extra ancillary experimental apparatus; A reflection high energy electron diffraction (RHEED) system consisting of an electron gun a phosphorescent screen, a quadrupole mass spectrometer (QMS) and a molecular beam modulator. These are all described in detail in the following sections.

3.2 GSMBE system

3.2.1 Vacuum Chamber

The vacuum system used for Gas Source Molecular Beam Epitaxy (GSMBE) is similar to that used for conventional solid source MBE but differs in that a pumping system used must be appropriate for a large gas throughput. The system is a modified VG Semicon MBE system which consists of two deposition chambers, dep-A and dep-B, at either end of a central chamber which houses a parking stage, an outgasing stage, a load lock and an Auger electron spectrometer and is pumped by a sputtering ion pump. In dep-A a turbomolecular drag pump backed by an Edwards rotary pump is used while in dep-B a turbopump / rotary pump and cryopump combination are used. Base pressures below 10^{-10} mbar can be achieved after a 50 hour bake at 180 ^{0}C in both chambers. The bake serves



Figure 3.1: Photograph of the GSMBE vacuum system. The rack on the left contains all the hardware required to drive the quadrupole mass spectrometer, multichannel scalar and beam modulator

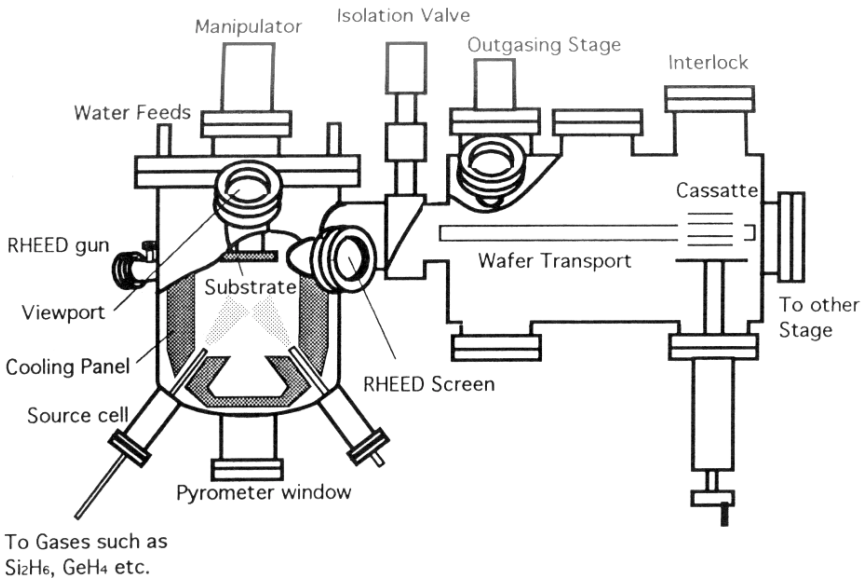


Figure 3.2: Schematic illustration of the GSMBE vacuum system. The two deposition chambers are separated by the common preparation/analysis chamber. For simplicity, only one deposition chamber is depicted. The system is constructed from argon-arc welded high purity stainless steel segments, which have a low degassing rate and a low level of magnetic impurities.

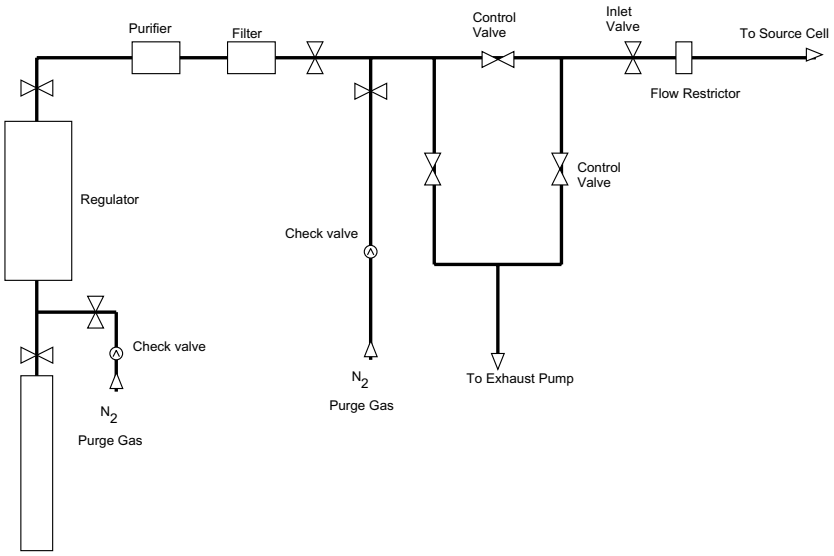


Figure 3.3: Schematic illustration of the gas manifold.

to accelerate desorption of residual materials from the chamber walls which are accrued during system maintenance at atmospheric pressure. It is also possible to outgass the gas lines using permanently installed heater tape. Leak checking can be performed by using the in-situ mass spectrometers to look for helium which is delivered externally from a bottle around the suspect components. Gas lines are tested in a similar fashion using a portable leak tester connected to the exhaust line.

The two deposition chambers and the load lock are connected to the backing line which is initially pumped down by use of a venturi pump followed by sorption pumps to bring the pressure into the turbomolecular pumps operating range. The load lock is pumped by a separate turbomolecular pump which is backed by a rotary pump. The apparatus is shown in the photograph of figure 3.1 and is shown schematically without chamber Dep B in figure 3.2. Both deposition chambers contain cooled panels capable of using liquid nitrogen, however water is normally used to prevent condensation of the precursors which may act as secondary uncontrolled sources and is still effective enough to prevent over heating. In some of the experiments a liquid nitrogen cooled surround was used in vacuum this served as an additional pump and increased the beam to background ratio. This allowed a more detailed study of the effect of beam fluxes since the sensitivity of the detector could be increased without the risk of serious damage.

During growth the substrates, contained in either machined polysilicon or molyb-

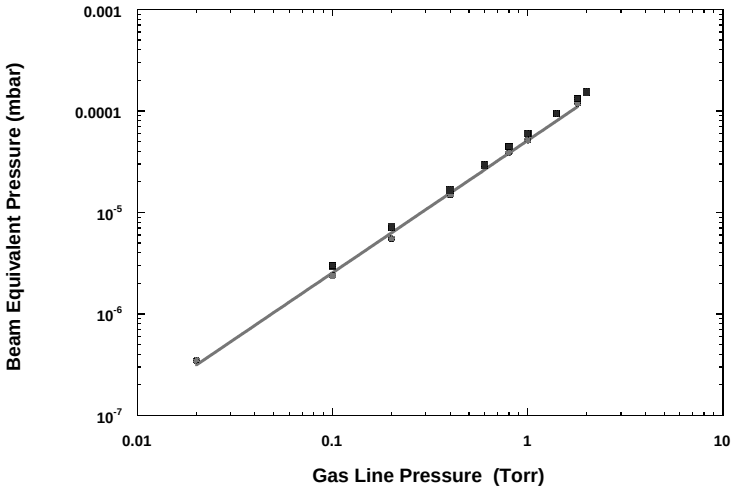


Figure 3.4: Beam equivalent pressure (BEP) dependence on gas line pressure for a water cooled system for disilane and silane. The silane pressure is modified to take into account the different ionisation cross sections for disilane and silane. Disilane has an ionisation cross section 2.23 times that of silane. The line is the fit BEP = $5\times10^{-5}(P_{source})^{1.3}$

denum holders, are heated and rotated using a custom built manipulator in dep-A and a VSW manipulator in dep-B. These consist of a linear stage for the vertical movement of the substrate, a magnetically coupled rotation stage and a stage for the vertical movement of the graphite heater. The temperature of the substrate is measured using a combination of a thermocouple and optical pyrometer. The temperature is controlled with a Eurotherm 825 PID controller and heater power supply.

The gases are introduced into the deposition chamber through a 'shower head' nozzle which is situated 268 mm from the substrate. The flow of gas precursors is controlled by regulating the gas pressure behind a small orifice. A control circuit senses the gas pressure in the line and controls the pressure via solenoid valves. The pressures are measured by Baratron 122a absolute pressure gauges (MKS Instruments Inc). The gas manifold is illustrated schematically in figure 3.3. The precursors used are silane (SiH_4 Union Carbide 99.999% purity), disilane (Si_2H_6 Voltaix 99.999% purity)) and germane (Ge_4 Voltaix 99.999% purity)) and are kept at room temperature. The gas cylinders are housed inside a gas safety cabinet for safe storage and are attached to one of four gas lines. The Si gas line is arranged so that both silane and disilane cylinders can be attached simultaneously and an isolation valve is used to switch operation between the two. The gases are regulated and pass through a catalytic purifier which removes any residual contamination such as water

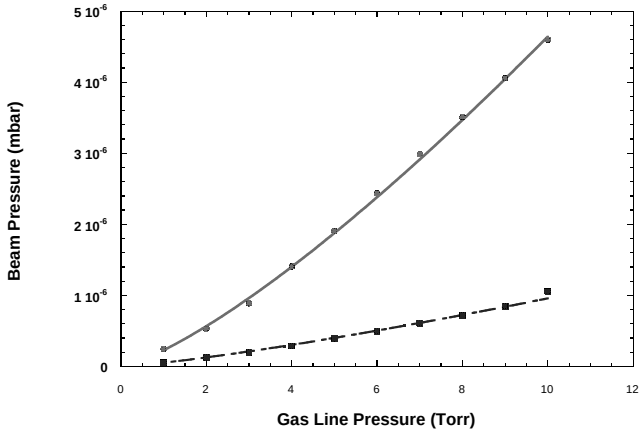


Figure 3.5: Disilane beam effective pressure (circles) and background pressure (squares) dependence on gas line pressure for the liquid nitrogen cooled system

vapour. When the system is idle and when excess gas needs to be evacuated from the lines following growth termination, the gas is pumped through an exhaust line by a turbomolecular pump. The gases are diluted in Nitrogen gas, and pass through a heated gas reactor column where they are cracked into harmless solids. The gas delivery system and substrate stage are monitored and controlled by a PC through the PC3000 process controller making automated growth runs possible. This is particularly useful for the temperature modulated growth experiments where growth run times can reach 24 hrs.

Figure 3.4 shows the beam equivalent pressure (BEP) for disilane and silane in a water cooled system as a function of the gas line pressure. The pressures recorded by the ion gauges for silane were corrected to account for the differences in ionisation cross-section for silane and disilane. Disilane has an ionisation cross-section 2.23 times that of silane, when this modification is performed it is clear the BEP is independent of the gas used and is given by the empirical relation BEP $= 5\times10^{-5}(P_{Source})^{1.3}$ where P_{Source} is the pressure in the gas lines or source pressure in Torr. The BEP dependence on gas line pressure in a chamber with liquid nitrogen cooled panels is shown in Figure 3.5. The beam to background ratio is found to be approximately 4.5 and it is clear the liquid nitrogen cooled panels greatly enhance the pumping of the chamber. At the end of a few days of experiments the cryopanels must be allowed to return to room temperature to prevent a dangerous amount of disilane, silane or germane from building up on the walls. This outgassing is performed very slowly so as not to overload the turbomolecular pump and backing system.

Wet Chemical Etch	
1. HF(5 percent) dip	20 secs
2. Deionised water rinse	2 min
Silicon Oxide etching. Repeat steps 3-6 three times	
3. Nitric Acid 80°C	5 min
4. Deionised water rinse	2 min
5. HF(5 percent) dip	20 secs
6. D/I water rinse	2 min
Organic contamination removal	
7. NH_4OH:H_2O_2:H_2O = 1:4:20 (40°C)	5 min
8. D/I water rinse	2 min
9. HF(5 percent) dip	20 secs
10. Dry by N_2 jet or spinning	

Table 3.1: Table showing the wet etching methods. The chemical etch involves repeated oxidation and etching of the Si surface (3-6) followed by the removal of organic contamination (7) and finally the production of a hydrogen passivated surface. (9)

3.2.2 Substrate Preparation

The quality of the grown epitaxial layers is strongly dependent on the initial morphology and cleanliness of the starting surface. Ionic and neutral molecular residues act as nucleation centres and can initiate defect formation such as stacking faults and dislocations which can then propagate through the epitaxial layers and result in an electronic device with significant degradation of the electrical properties. To ensure good quality of the grown material, the starting substrate should be as free from contaminants as possible. This can be achieved by using in-situ techniques such as ion sputtering or chlorine gas etching or ex-situ, wet chemical methods. In the studies reported here the cleaning process consisted of an ex-situ wet chemical etch shown in table 3.1 followed by in-situ heating and growth procedures. The chemical etch involves repeated oxidation and etching of the Si surface followed by the removal of organic contamination and finally the production of a hydrogen passivated surface.

Once the wafers are loaded into the prep chamber they are placed in the outgassing stage for the minimum period of 1 hour. After transfer into the deposition chamber the samples are gradually heated in a very low flux of disilane to 850°C or until RHEED patterns indicated carbon contamination. The temperature is then dropped to 500°C and a buffer grown for 30 mins, finally a buffer is grown at 700°C . The buffer at 500°C serves to bury contaminates and the buffer at 700°C ensures two dimensional growth.

The resulting surface can be checked in the system using RHEED and a repeat

distance of twice that of the bulk structure indicated by half order streaks in the ⟨110⟩ azimuth is due to the (2x1)(1x2) reconstruction on the surface. This can be enhanced by increasing the order of the surface by the growth of a buffer layer at 700 °C

The wafers used for the growth experiments were 2 inch nominally singular Si(001) with a resistivity of 10-100Ωcm and were held in metal holders. For the temperature programmed desorption (TPD), modulated beam and RHEED oscillation experiments the wafers used were 4 inch and held in molybdenum or polysilicon holders. The TPD wafers required a low resistivity, 0.01-1Ωcm, to ensure enough carriers to absorb radiation from the heater. Since temperatures were recorded using an optical pyrometer if the wafer is of low doping and allows infra-red radiation to pass through, the temperature recorded will be that of the heater and not the wafer itself.

3.3 The Reflection High Energy Diffraction Apparatus

Reflection high energy diffraction (RHEED) has been demonstrated to be a very powerful technique gleaning useful information on the processes occurring on semiconductor surfaces *during* growth. Not only can RHEED give information on the periodicity of surface features but diffraction pattern intensity measured as a function of time can indicate the growth rate [64].

The surface sensitivity of RHEED can be attributed to the geometry of the electron gun and phosphorescent screen. The grazing incidence of the electron beam on the surface ensures the component of momentum perpendicular to the surface is small and hence penetration is minimal. RHEED is possible during growth since the gun and screen can be situated far from the substrate and molecular beams however at high pressures care must be taken to not burn-out the electron gun filament.

RHEED can be used to probe surface reconstructions on the silicon surface and to detect the presence of other impurities such as germanium or carbon. These impurities produce diffraction features indicative of a surface periodicity different to that of the substrate. By careful use of RHEED it is possible to gain precise control of parameters such as growth rate, and hence film thickness, surface quality (growth mode 3D or step flow) and surface purity or alloy composition. The limitations of RHEED are highlighted in a brief theoretical treatment along with some example patterns and oscillations in Appendix C

The RHEED system utilises a 15KeV VG LEG110 electron gun and CCD camera interfaced to a computer. The electron gun is mounted on a moveable stage which allows movement about the centre of the substrate, the angle of incidence can be adjusted between

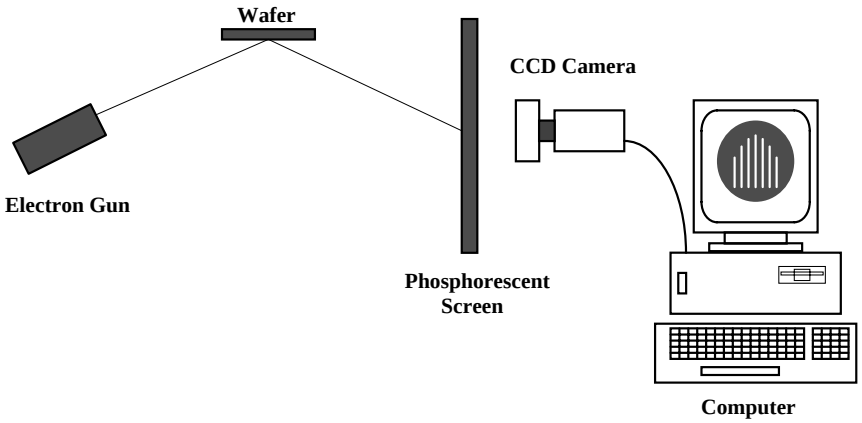


Figure 3.6: Schematic of the complete RHEED system

0^0 and 4^0. The computer software is able to record the changes in intensity of eight different user defined areas of the CCD meaning RHEED feature intensity oscillations can be easily studied. A schematic of the RHEED apparatus is given in Figure 3.6.

3.4 The Quadrupole Mass Spectrometer

3.4.1 Introduction

The quadrupole Mass Spectrometer (QMS) consists of three major components. The first is an electron impact ioniser which creates charged ions from the neutral species. These charged ions are electrically accelerated and then pass through the quadrupole mass filter. This consists of four conducting bars and are arranged to form a square in cross-section. The bars are then connected to the controller which provides a radio frequency (RF) voltage over a DC bias. The electric field acts as a charge to mass ratio filter and will only allow certain ratios to reach the detector itself. This consists of a trumpet shaped electrode which acts as an electron multiplier. The signal is then fed through a pre-amplifier stage and then into the counting electronics.

The QMS signal bears no relation to the velocity, and hence flux, of the detected species and is infact a density detector. The signal must be corrected to give a signal proportional to flux which is in turn proportional to the product of density and mean

velocity, see Equation 2.5. This correction assumes the desorbed species to have been thermally accommodated by the substrate, that is to say the maxwell velocity distribution of the desorbed molecules is governed by the substrate temperature where the mean velocity is proportional to the square root of that temperature, see Equation 2.8. The quadrupole mass spectrometer is explained in more detail in Appendix D.

3.4.2 Temperature Programmed Desorption

Temperature Programmed Desorption TPD involves heating the substrate and observing the desorbing products using a quadrupole mass spectrometer (QMS). TPD experiments are useful in that they are able to distinguish between different species on the surface due to the different energies associated with each different adatom-substrate bond. A adatom with a low activation energy associated with a weak adatom-substrate bond will desorb earlier during the temperature ramp than an adatom with a higher activation energy. This assumes the pre-exponentials are identical as this will also affect the desorption kinetics. Additionally to the temperature of maximum desorption, the area of the desorption features is also useful since this area is proportional to the coverage of these adatom species.

The desorbing species are analysed with a quadrupole mass spectrometer operating in pulse counting mode. The same electronics and Multi Channel Scalar (MCS) as used in the MBMS studies are used in the TDS studies performed here and the scan of the MCS synchronised with the temperature ramp. The apparatus is rudimentary and far from ideal since the QMS ioniser is a relatively large distance from the sample and this can cause confusion with desorption from surfaces other than the sample. If the QMS is placed close to the sample and away from other surfaces the reduction of flux with distance serves to suppress this background signal.

3.4.3 Modulated Beam Mass Spectrometry

TPD measures desorbing species from a surface and from this the state of the surface is inferred, however this bears no relation to the growing surface. To study the Silane/Disilane decomposition during steady state growth a modulated beam technique with multi channel data acquisition is used. In principle multi channel techniques allow measurements at all odd harmonics if a rectangular pulse driving function is used. It also allows averaging over long time periods (up to several hours with a maximum of four to forty days, depending on the modulation frequency used).

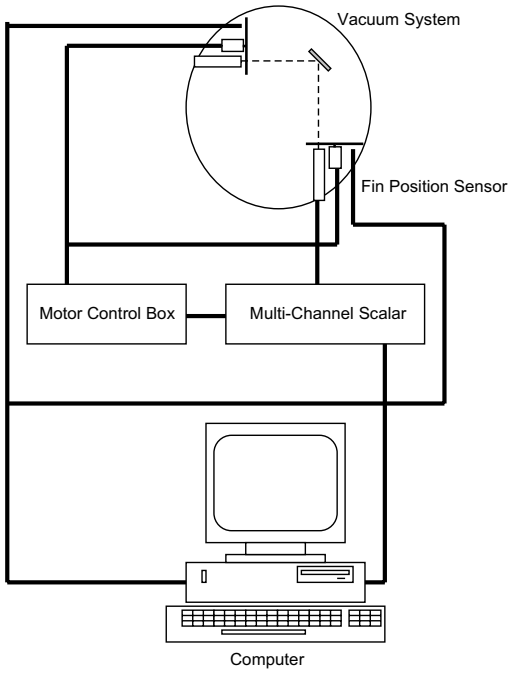


Figure 3.7: Schematic illustration of the Modulated Molecular Beam System

The complete system is shown schematically in Figure 3.7. The QMS was described in section 3.4 and Appendix D, this section will described how all the various components are inter-connected and explain how the data were recorded and analysed.

The multi-channel scalar is allowed to run freely, incrementing channel number at a user programmed rate and counting the number of events detected by the mass spectrometer (QMS) for every channel. The MCS also controls the beam modulation by controlling the motor speed via the phase-locking control box. The function of the phase locking motor control box is to keep the chopping fins in sync with the MCS.

The signal from the multiplier of the QMS operating in pulse counting mode was fed via a charge sensitive pre-amplifier, timing amplifier and discriminator into a multichannel scalar (MCS) as described previously. The MCS was programmed with a channel dwell time of $25\mu s$ and a pass length of 1024 channels to aid Fourier analysis, this produced a corresponding chopping frequency of 39 Hz.

Once the data are recorded and time averaged by the computer a fast Fourier transform (FFT) is performed on the resulting signal to produce a value proportional to the background count at the zeroth harmonic of the chopping frequency and the magnitude

of the modulated signal at the first harmonic. The signal is also modified to take into account the temperature of the desorbing flux.

3.5 Summary

This thesis concentrates on the study of the growth of Si and SiGe using three main techniques described in this chapter. These are: RHEED used to study the surface reconstructions and the growth rate when RHEED feature intensity variations are recorded. TPD is used to study the surface species desorbing as a function of temperature and MBMS is used to record the desorbing species during growth.

Chapter 4

Hydrogen Desorption Kinetics

4.1 Introduction

In the growth of silicon from hydride precursors two atomic species are involved in the overall growth process. Since growth is actually observed it is obvious that a significant proportion of the silicon chemisorbs to the surface, however, the precise involvement of the associated hydrogen is less clear. This chapter reports on a study of the behaviour of hydrogen on the Si(001) surface using a technique termed temperature programmed desorption (TPD) which can be used to give information on:

- The identity of hydride species on the surface by observing the various temperatures of the peak desorption rate of hydrogen.
- The kinetics of hydrogen desorption can be derived by fitting a model to the TPD data where the fitting parameters are the desorption activation energy and the pre-exponential.
- The effect of adsorbed hydrogen on further adsorption can be observed by observing changes in TPD spectra after different exposure conditions.

4.2 Practical Considerations

Standard TPD experiments [17] use a thermocouple bonded to the back of the wafer to measure the temperature. However due to the nature of the vacuum chamber used, one which is for designed for sample throughput, it was not possible to connect up a thermocouple. Alternatively an optical pyrometer is used which is placed outside the chamber and aimed at the growing surface of the wafer. This has the disadvantage in that

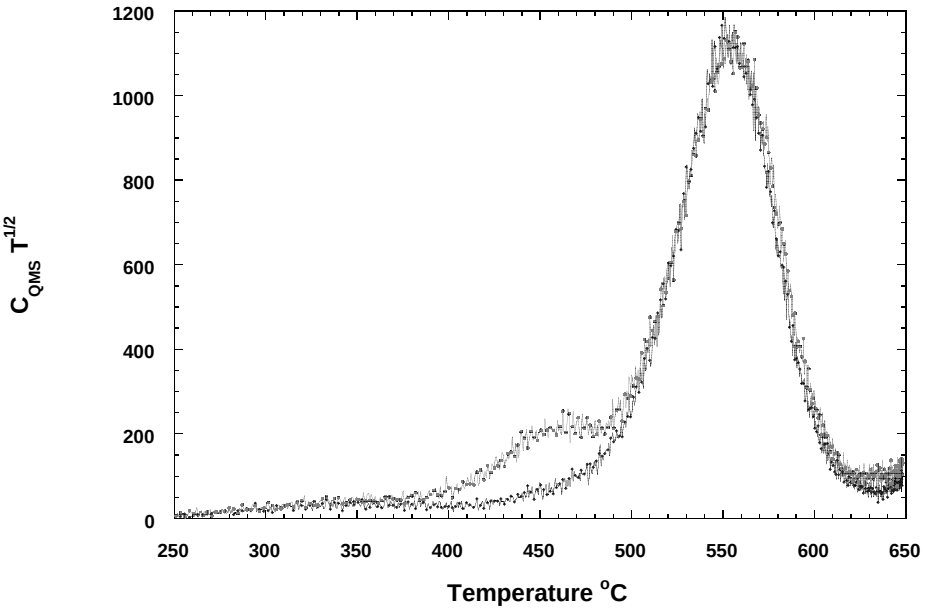


Figure 4.1: TPD spectra from the Si(001) surface previously exposed to disilane from a gas line pressure of 1 Torr. Exposure at temperatures of 430 °C falling to 360°C for the duration of 1 minute produce the β_1 peak only. Exposure at 200 °C for 1 minute produces an additional β_2 peak at lower temperatures.

temperatures cannot be measured to an accuracy of less than ±2°C but does allow easy transfer of the wafer in and out of the chamber aiding outgassing of the chamber after dosing. In conventional TPD the QMS ioniser is placed behind some form of skimmer and the mass filter chamber is pumped additionally to the deposition chamber. In the experiments performed here the skimmer was created by the modulator used in the Modulated Beam Mass Spectrometry (MBMS) experiments.

In all the TPD experiments the wafers used had a diameter of 4 inches to ensure a desorbing flux as large as possible and were held in machined polysilicon holders. Since the wafers were heated radiatively, wafers with high doping levels were used to ensure a good coupling to the infra red radiation. The wafers used typically had a resistivity of 0.01 Ωcm.

Since the TPD experiments are performed in a system far from the ideal, care must be used in analysing the data. At the start of each set of data a TPD run was performed with a wafer that had not been exposed to disilane. This was used for subtracting the background from each TPD run. This background will predominately be due to desorption

from the wafer holder since before every run and after dosing, the wafer is removed from the chamber and the heater ramped up to 800°C for 15 minutes to outgas the chamber and heater.

4.3 Adsorbed Hydride Species

A study was performed on the effect of the substrate temperature during exposure to disilane on the desorption characteristics. The Si(001) surface was exposed to disilane from a gas line pressure of 1 Torr at temperatures of 430 °C falling to 360 °C for the duration of 1 minute and also at 200 °C for 1 minute. The resulting desorption spectra are shown in Figure 4.1. The ramp rate used was 5°C per second.

The TPD spectrum for desorption from the surface after exposure to disilane at 430 °C falling to 360 °C shows a single peak. This peak is not seen in the background scans which are performed after no initial dosing and has been attributed to hydrogen desorption from the monohydride phase and is termed the β_1 peak [28]. For dosing at a lower temperature of 200°C another peak at lower temperatures is seen and has been attributed to desorption from the dihydride phase and is termed the β_2 peak [17].

A study into the conditions required to form these differing hydrogen phases was performed where a monohydride surface was further exposed to disilane at 200°C to ascertain if the dihydride phase is still formed, Figure 4.2 shows the result of such a study. Curve (c) shows a TPD spectra from a surface dosed for 1 minute at 430°C and curve (a) shows one from dosing at 200 °C . As in Figure 4.1 the β_1 peak is seen exclusively for dosing at 430°C but at lower dosing temperatures the dihydride β_2 peak is observed in addition to the β_1 peak. Curve (B) is recorded from a monohydride surface produced from identical conditions to (A) further exposed to disilane at 200°C , it is clear only the monohydride phase is present. The brief dose at 430°C prevents any further adsorption at the lower dosing temperature which would be indicated by desorption from a dihydride phase, a β_2 peak. Clearly the hydrogen prevents further adsorption and this effect has been called hydrogen passivation. Assuming passivation is complete there still exists a pathway to produce the dihydride phase and this would have had to have been through hydrogen desorption followed by disilane adsorption. The effect of desorption between doses was found to be negligible during a TPD study using differing periods between dosing. The area of the monohydride peak was seen to be unchanged. Clearly the monohydride phase is unreactive to incoming disilane.

The presence of the differing hydrogen phases for dosing at different temperatures

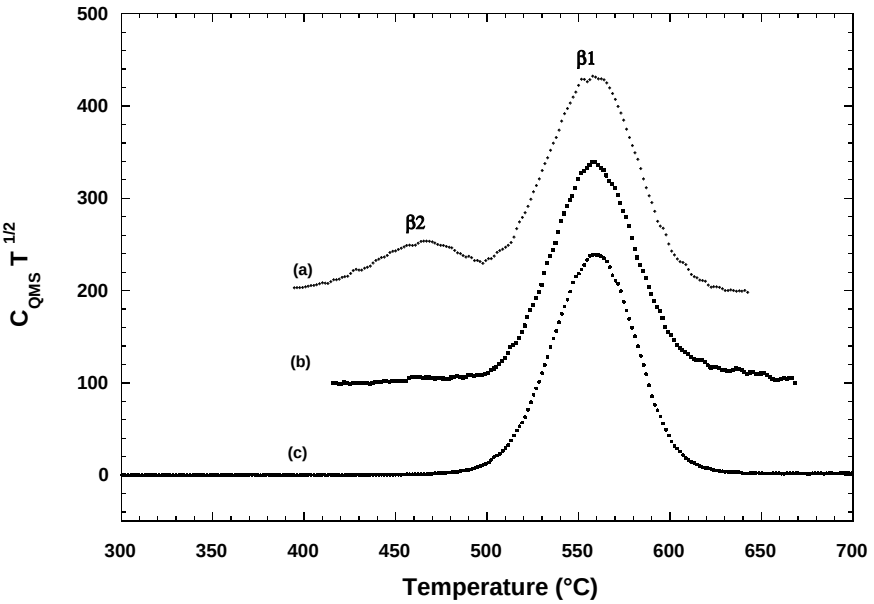


Figure 4.2: TPD spectra demonstrating the effect of pre-adsorbed hydrogen on further adsorption. Curve (c) shows a TPD spectra from a surface dosed for 1 minute at 430°C and curve (a) shows one from dosing at 200 °C . Curve (b) is also dosed at 200 °C but has previously been dosed as in curve (c) and the β_2 peak is not observed

is interpreted as due to the balance between the rate of decomposition of the adsorbed disilane fragments producing passivated sites and the rate of adsorption. At low temperatures the rate of decomposition is slow in relation to the initial adsorption therefore a larger preportion of the surface coverage will consist of large disilane fragments. At high temperatures the rate of decomposition is greater and the surface becomes fully passivated in the vicinity of the initial adsorption site before another disilane molecule can adsorb. For higher temperatures and lower disilane fluxes the surface hydrogen will be more free to migrate over the surface and passivation will not be limited to the area around the initial adsorption site. At even lower dosing temperature a third peak has been reported and this is attributed to desorption from a trihydride phase.

4.4 Molecular Hydrogen Desorption Kinetics

To gain more quantitative information from the TPD spectra a mathematical model must be developed. A connection between the count rate recorded by the QMS and the actual desorbing flux must also be established. In Chapter 2 the impingement rate, I, on a surface from a gas at pressure, P, was shown to be given by:

$$I = \frac{P}{\sqrt{2\pi m k_B T_G}} \tag{4.1}$$

using the ideal gas relation $PV = Nk_BT_G$ gives an impingement rate:

$$I = \frac{Nk_BT_G}{V\sqrt{2\pi m k_B T_G}} = \frac{N}{V}\sqrt{\frac{k_B}{2\pi m}}\sqrt{T_G} \tag{4.2}$$

The quadrapole mass spectrometer (QMS) measures the density of the molecules at the ioniser and bears no relation to the speed at which the molecules are travelling. The count rate C_{QMS} is therefore related to the number of molecules per volume $\frac{N}{V}$

$$I = \frac{N}{V}\sqrt{\frac{k_B}{2\pi m}}\sqrt{T_G} = Constant \times C_{QMS}\sqrt{T_G} \tag{4.3}$$

During the annealing of a surface the flux produced from desorbing molecules is related to the rate of change of the surface coverage θ by:

$$I \propto \frac{-d\theta}{dt} \tag{4.4}$$

using $T_S = T_{S_0} + \beta t$ where β is the ramp rate and $dT_S = \beta dt$ gives:

$$C_{QMS}\sqrt{T_G} \propto \frac{-d\theta}{dt} = \frac{-d\theta}{dT_S}\beta \tag{4.5}$$

and finally:

$$\frac{-d\theta}{dT_S} \propto \frac{C_{QMS}\sqrt{T_G}}{\beta} \tag{4.6}$$

therefore the count rate recorded during the TPD annealing must be modified to relate it to the change of surface coverage as a function of temperature. The desorbing molecules are

assumed to have been thermally accommodated to the substrate therefore the temperature of the gas is assumed to be that of the substrate $T_G = T_S = T$.

Now the surface coverage can be related to an experimental observable, a model for the desorption process can be created. Initially to model the desorption rate it will be assumed the rate of change of surface coverage is given by a first order relation with respect to the surface coverage. The rate is governed by the usual desorption rate constant k_d which is given by $k_{d_0} exp(-E_d/k_B T)$

$$\frac{d\theta}{dt} = -k_d\theta = -k_{d_0}\theta exp\left(\frac{-E_d}{k_B T}\right) \tag{4.7}$$

using $T = T_0 + \beta t$ and $dT = \beta dt$:

$$\frac{d\theta}{dT} = \frac{-k_{d_0}\theta}{\beta} exp\left(\frac{-E_d}{k_B T}\right) \tag{4.8}$$

and solving

$$\int_{\theta_0}^{\theta(T)} \frac{d\theta}{\theta} = \frac{-k_{d_0}}{\beta} \int_{T_0}^{T} exp\left(\frac{-E_d}{k_B T}\right) dT \tag{4.9}$$

gives

$$ln\left(\frac{\theta(T)}{\theta_0}\right) = \frac{-k_{d_0}}{\beta} S(T) \tag{4.10}$$

where $S(T)$ is the value of the integral with respect to substrate temperature given by the relation [51]:

$$S(T) = \frac{E_d}{N_A k_B} \left| \frac{exp(-\epsilon)}{\epsilon^2} \sum_{n=1}^{\infty} \frac{(-1)^{n+1} n!}{\epsilon^{n-1}} \right|_{T_0}^{T} \tag{4.11}$$

in the numerical simulations the sum was taken of the first 15 terms only and $\epsilon = \frac{E_d}{k_B T}$.

The variation of θ with temperature is thus given as follows:

$$\theta(T) = \theta_0 exp\left(\frac{-k_{d_0}}{\beta} S(T)\right) \tag{4.12}$$

and this can be related to the count rate from the QMS:

$$\frac{-d\theta}{dT} \propto \frac{C_{QMS}\sqrt{T}}{\beta} \propto \frac{-d}{dT}\left(\theta_0 exp\left(\frac{-k_{d_0}}{\beta} S(T)\right)\right) \tag{4.13}$$

The above derivation can be performed for nth order kinetics. For a desorption rate which is second order with respect to coverage [51]:

$$\theta(T) = \frac{\theta_0}{1 + \frac{\theta_0 k_{d_0}}{\beta} S(T)} \tag{4.14}$$

The temperature at which the desorption rate is greatest is dependent on ramp rate. By modelling this behaviour an activation energy for desorption, E_d, and pre-exponential, k_{d_0}, can be calculated, this is particularly useful since the area of the TPD peaks was not considered to be a reliable experimental observable due to QMS multiplier degradation.

$$-C_{QMS}\sqrt{T} \propto \frac{d\theta}{dt} = -k_{d_0}\theta exp\left(\frac{-E_d}{k_B T}\right) \tag{4.15}$$

if this equation is solved at the peak desorption rate where $\frac{-d}{dT} C_{QMS}\sqrt{T} = 0$ and the temperature is T_M

$$\frac{-d}{dT} C_{QMS}\sqrt{T_M} = 0 = -\frac{d\theta}{dT} k_{d_0} exp\left(\frac{-E_d}{k_B T_M}\right) \tag{4.16}$$

substituting in equation 4.8 and solving gives:

$$ln\left(\frac{T_M^2}{\beta}\right) = \frac{E_d}{k_B T_M} + ln\left(\frac{E_d}{k_{d_0} k_B}\right) \tag{4.17}$$

therefore by plotting $ln\left(\frac{T_M^2}{\beta}\right)$ against $\frac{1}{T_M}$ will give an intercept and gradient from which E_d and k_{d_0} can be calculated. One such plot is given in Figure 4.3 for the β_1 and β_2 peak. The activation energy for desorption is calculated at 2.48 $\pm$0.4 eV, in excellent agreement with the literature (Kim et al 2.52 eV, $1\times10^{15}s^{-1}$ Greenlief et al 2.33 eV, $1\times10^{14}s^{-1}$ see table 2.1). The pre-exponential is calculated as $3.16\times10^{14}s^{-1}$ this is also in fairly good agreement with the literature.

An activation energy for the β_2 peak was calculated as 1.22 $\pm$0.4 eV with a pre-exponential of $4.27\times10^{7}s^{-1}$. This energy is in fairly good agreement with Kim et al (1.8 eV) but their pre-exponential of $1\times10^{13}s^{-1}$ is in poor agreement. This could indicate a desorption process that is not dependent solely on an energy barrier but may depend on another process such as diffusion on the surface before desorption.

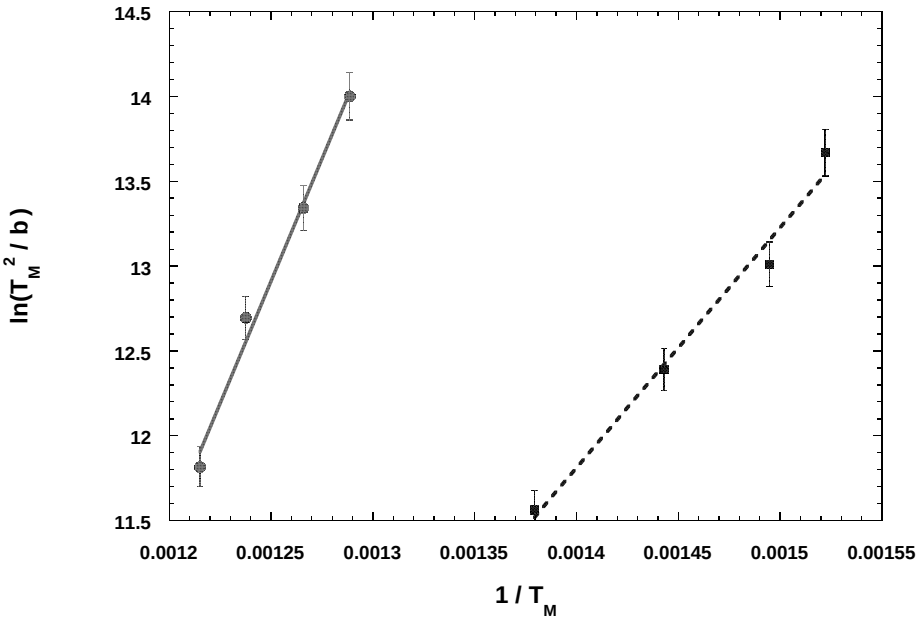


Figure 4.3: A plot of $ln\left(\frac{T_M^2}{\beta}\right)$ against $\frac{1}{T_M}$ will give an intercept and gradient from which E_d and k_{d_0} can be calculated. For the monohydride phase (solid line): activation energy for desorption is 2.48 $\pm$0.4 eV and the pre-exponential is $3.16\times10^{14}s^{-1}$ For the dihydride phase (dotted line): activation energy for desorption is 1.22 $\pm$0.4 eV and the pre-exponential is $4.27\times10^{7}s^{-1}$

The fact that at low temperatures the dihydride phase is formed but is not seen from dosing at higher substrate temperatures suggests the complete monohydride phase can be formed from a dihydride phase with the existence of dangling bonds. This means that this conversion from the dihydride to the monohydride phase could occur during the TPD ramp itself after some initial desorption. An alternative possibility is that the hydrogen can diffuse from the monohydride desorption sites to the dihydride desorption sites during the ramp. To test for any change in the hydrogen phases during the temperature ramp, spectra were recorded using various ramp rates. Any conversion between phases followed by desorption should show as a differing β_2 peak area to β_1 peak area ratio. The established model could then be tested to see if it could predict all the observed changes.

A study of the effect of ramp rate on the TPD spectra was performed and Figure 4.4 shows the TPD spectra for three different ramp rates, 0.5, 1 and 2°C per second. The surface was exposed to disilane from a gas line pressure of 1 Torr and at a substrate

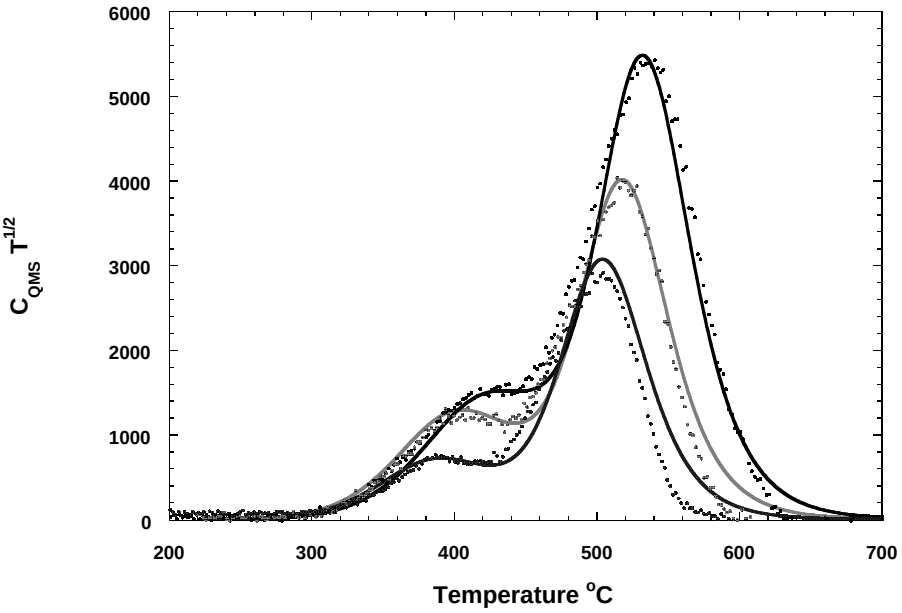


Figure 4.4: TPD spectra from a Si(001) surface exposed to disilane form a gas line pressure of 1 Torr and at a substrate temperatures 200°C ±5°C . The ramp rates used were 0.5°C per sec, 1°C per sec and 2 deg per sec

temperature of 200°C for 1 minute. The data has not been modified for the ramp rate to aid clarity in presentation since the modification is only a division of the count rate by the ramp rate.

The ratio of the peak areas shows no dependence on ramp rate and is relatively constant with $\frac{\beta_1}{\beta_2} = 2.5$. The peak shift with ramp rate is clearly modelled accurately. It can be concluded that interconversion between the hydrogen phases does not occur significantly during the temperature ramp.

Using a first order desorption model it is difficult to fit the TPD spectra exactly. This was not considered further since the important phenomenon is the peak position variation with ramp rate and this does not depend strongly on the order of the desorption process [51]. However information on the order can be gleaned by measuring the peak position but not as a function of ramp rate, instead it should be measured as a function of coverage [63].

The temperature for the peak desorption rate in previous TPD scans was measured from surface coverages assumed to be close to unity. This could be assumed since a long exposure to atomic hydrogen produced a similar area peak to the disilane dose see Figure 4.5.

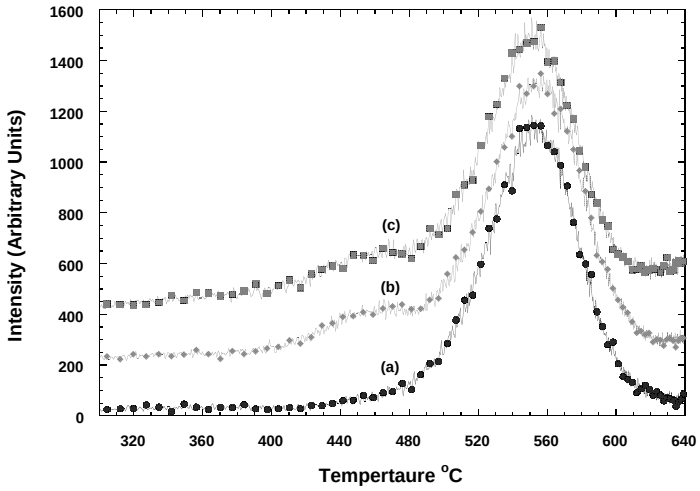


Figure 4.5: TPD spectra from a Si(001) surface exposed to disilane at 200°C for 1 minute (b) and atomic hydrogen for 15 minutes (c). The peak areas are identical and are assumed to be from a full coverage of hydrogen. (a) is from the monohydride surface produced from disilane dosing at 430°C falling for 1 minute.

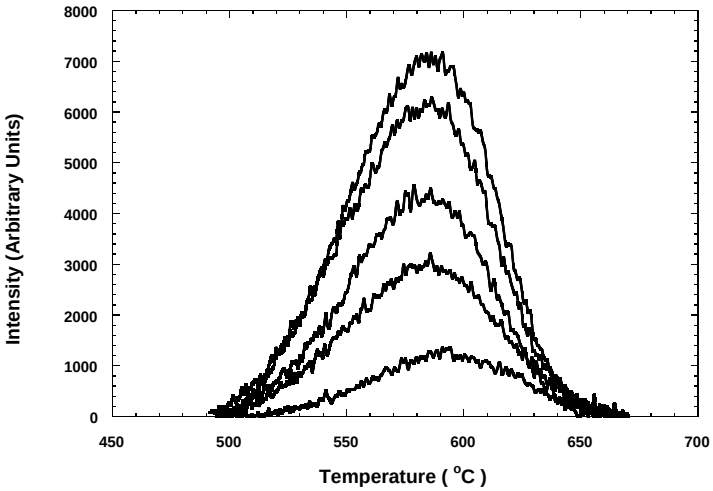


Figure 4.6: TPD from a Si(001) surface for various hydrogen coverage. The lack of a variation in the temperature of the peak desorption rate indicates a first order desorption process. A slight movement to higher temperatures for low hydrogen coverages could be due to experimental errors or a change towards second order desorption kinetics.

However the peak position can change with coverage depending on the governing kinetics [51]. Several TPD scans were performed from a surface dosed under conditions known to produce an almost complete surface coverage but to attain various surface coverages the temperature ramp was delayed for various periods of time after dosing . During these delays the hydrogen was able to desorb resulting in the different hydrogen coverage, no attempt was made to quantify the total coverage. The results are given in figure 4.6

For first order desorption the temperature of the peak desorption rate is independent of total hydrogen coverage and this is clearly the case for the Si(001) surface Figure 4.5. However at very low coverages there is a movement of the peak desorption rate towards higher temperatures, this is indicative of a desorption process of higher order. It is not clear if this phenomenon is the result of errors in background subtraction or really the result of the desorption kinetics becoming higher order in character for very low hydrogen coverages. The departure of the desorption kinetics from first order to second order for low coverages has been reported by Boland *et al* [6] and Hofer *et al* [34]. They assumed as the hydrogen coverage approached zero the mechanism that ensures first order kinetics no longer dominates. This mechanism was suggested by Boland *et al* to be due to the attraction of dangling bonds, this ensured doubly occupied dimers. At low coverages lone dangling bonds would be common and hydrogen would need to diffuse on the surface and combine with other hydrogen atoms prior to desorption as molecular hydrogen. However Nagazawa *et al* [63] dismissed this process as a post dose anneal, produced desorption for high hydrogen coverages that was more second order in nature.

4.5 Summary

Several important phenomena relating the hydrogen desorption from the Si(001) surface have been identified in this chapter and can be summarised as follows:

- The monohydride surface prevents further adsorption of disilane. The competition between the rate of adsorption and the rate of dissociation of SiH_3 and SiH_2, and hence passivation, determines the resulting surface hydrogen phase.

- Modelling predicts the shift of peak rate with ramp rate giving the activation energy for β_1 desorption is calculated at 2.48 $\pm$0.4 eV, in excellent agreement with the literature. The pre-exponential is calculated as $3.16\times10^{14}s^{-1}$. An activation energy for the β_2 peak was calculated as 1.22 $\pm$0.4 eV with a pre-exponential of $4.27\times10^{7}s^{-1}$. This energy is in fairly good agreement with Kim et al (1.8 eV) but the pre-exponential of $1\times10^{13}s^{-1}$ is in poor agreement.

- The ratio of peak areas is insensitive to ramp rate therefore any interconversion between phases is insignificant at these ramp rates. This is probably due decomposition of the dihydride requiring dangling bonds which are not present in any great number until the monohydride phase desorbs.

- The peak shift with coverage indicates first order adsorption for all but very low coverages.

Chapter 5

Kinetics of Growth from Disilane

5.1 Introduction

Chapter 4 identified the role of hydrogen in the growth of silicon from hydride precursors. Hydrogen is found to passivate the surface against further disilane adsorption at temperatures where the hydrogen is not significantly desorbing. However during constant growth, the hydrogen coverage will reach a steady state value ranging from close to 1 for low temperatures/high fluxes to approximately 0 at high temperatures/low fluxes. It is clear hydrogen will desorb during steady state growth, however it is also possible for other species desorb and in the next section, a report of a technique to identify the desorbing species is given. Once the desorbing species are identified a model for the reaction on the surface can be postulated since the incoming and outgoing species from the surface are known. This chapter will concentrate on the following areas

- The identification of the desorbing species at elevated temperatures during growth and the associated energetics.
- The identification of the reaction pathways for disilane pyrolysis reaction once adsorbed on the surface.
- Establishing a model for the growth process

5.2 Identification of the Desorbing Species During Steady State Growth

Distinguishing species desorbing from the substrate to those from the background is problematic and can only be achieved if the desorbing beam is somehow encoded to differentiate it from the background. This is done by interrupting the line of sight from the silicon wafer to the ioniser of the quadrapole mass spectrometer (QMS). A modulation is then created by a rotating circular chopper. The signal from the electron multiplier of the QMS is recorded using a multichannel scalar which is in the free running mode and its end of pass signal is used as a reference for driving the chopper. This technique is termed Modulated Beam Mass Spectrometry (MBMS) and has been used to identify the desorbing pyrolysis reaction products and also to measure the temperature dependence of H_2 desorption under steady state growth conditions. While this may be sufficient to identify that the detected species are from the direction of substrate, it still cannot distinguish this from the reflected incident beam. For this reason the measurement of the temperature dependence of an MBMS signal is performed which may serve to identify the underlying reaction and also confirm that the signal is produced by a reaction product.

5.2.1 Silicon Hydride Desorption

The literature review of Chapter 2 reported that when disilane, Si_2H_6, adsorbs on the clean surface of Si(001) the decomposition of disilane results in the deposition of silicon and hydrogen. The resulting growth kinetics are dominated by the rate of reactivation of adsorption sites relative to the rate of adsorbing disilane. Adsorbed hydrogen is assumed to block the active sites for adsorption and removal of this hydrogen will reactivate the sites.

There are many possible reaction pathways for the initial adsorption and these can be summarised as follows: Disilane can decompose releasing silane and one adsorbed silicon atom

$$Si_2H_6 + \underline{Si}- \rightarrow \underline{Si} - SiH_2 + SiH_4 \tag{5.1}$$

or disilane can completely decompose producing two adsorbed silicon atoms

$$Si_2H_6 + 2\underline{Si}- \rightarrow 2\underline{Si} - SiH_3 \tag{5.2}$$

The role of the adsorbed hydrogen will be discussed in the next section. These two reactions can be distinguished by looking for any desorbing silane and the technique of MBMS is ideal for this purpose.

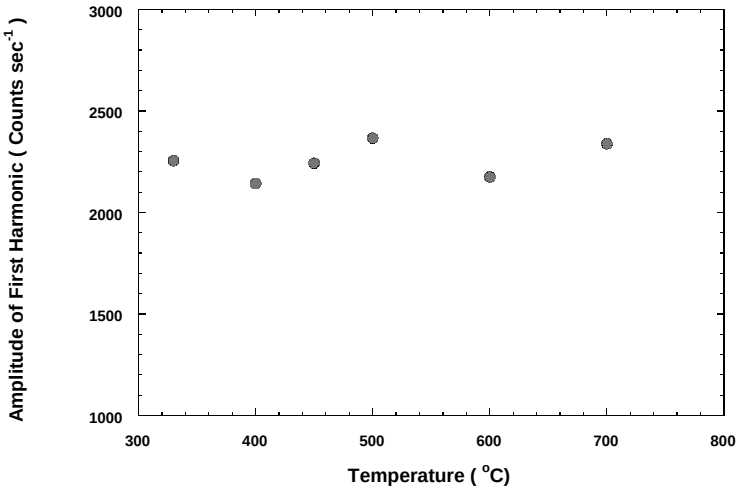


Figure 5.1: Modulated Beam Mass Spectrometry (MBMS) study of Silicon Hydride desorption: The temperature dependence of the amplitude of the mass spectrometer signal is calculated at the first harmonic of the modulation frequency (39 Hz) at a mass to charge ratio of 30 corresponding to silicon hydride fragments.

To measure the signal from the QMS multiplier relating to silicon hydrides, including silane, the mass filter was set to a mass charge ratio of 30, however, the cracking of disilane also produces a signal at this mass/charge ratio. The mass filter was fully deresolved to ensure the transmission remained constant so the QMS was an ideal density detector. Growth was allowed to reach a steady state on the Si(001) 4" wafer at the selected temperature and growth precursor flux before the QMS signal was recorded. The signal was sampled over a period typically of one hour and a fast Fourier transform (FFT) performed to measure the amplitude of the signal at the first harmonic of the modulation frequency.

For the TPD experiments reported in chapter 4 it was discussed how the QMS signal should be modified to relate it to the desorbing flux. In the TPD experiments the signal is probably not due to desorption direct from the surface. However for modulated beam experiments the background signal is removed and the remaining signal relates to desorption *directly* from the surface. Therefore for the MBMS experiments the QMS signal is multiplied by $\sqrt{T}$ where T is the substrate temperature. This assumes the desorbing gas has been thermally accommodated on the substrate.

The amplitude of the first harmonic is plotted against temperature in figure 5.1. In this case the signal is found to be constant over the temperature range studied. This signal has little to do with the pyrolysis reaction but arises from the fragmentation of reflected

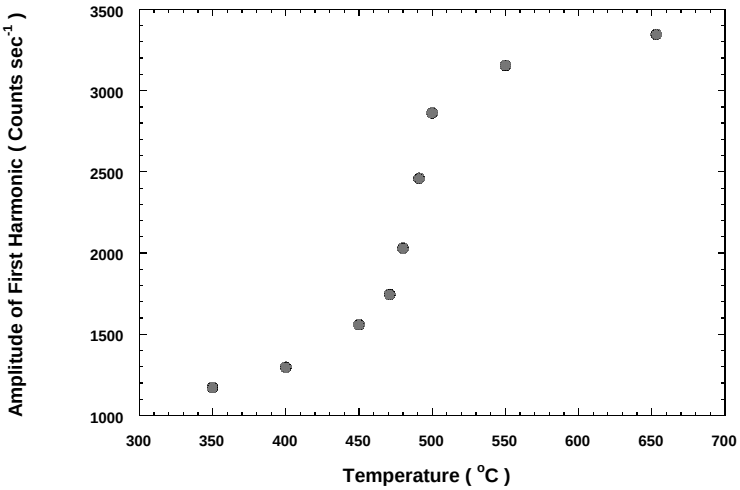


Figure 5.2: Modulated Beam Mass Spectrometry (MBMS) study of Hydrogen desorption: The temperature dependence of the amplitude of the mass spectrometer signal is calculated at the first harmonic of the modulation frequency (39 Hz) at a mass to charge ratio of 2 corresponding to hydrogen. The signal recorded from the electron multiplier in pulse counting mode is multiplied by the square root of the substrate temperature

disilane. The desorption of SiH_x radicals or silane is below the detection limits of MBMS despite the use of long acquisition times.

5.2.2 Hydrogen desorption kinetics during growth

A similar study to that for silane desorption was performed for hydrogen desorption during growth at a mass/charge ratio of 2. The signal as a function of temperature is shown in Figure 5.2 and it is clear the signal is thermally activated at low temperatures. At higher temperatures the signal is independent of temperature. The energy of activation is found to be 1.8 eV $\pm$0.4 eV which is illustrated in the Arrhenius plot of figure 5.3. This is in agreement with the literature reviewed in table 2.1 of section 2.5 and the data of chapter 4 (2.48eV) based on TPD measurements. This study confirms that hydrogen is the only reaction product leaving the surface over the temperature range studied and its desorption is the rate limiting step of growth at low temperatures. At higher temperatures the rate of hydrogen desorption no longer depends on temperature but is a function of the incoming flux of disilane.

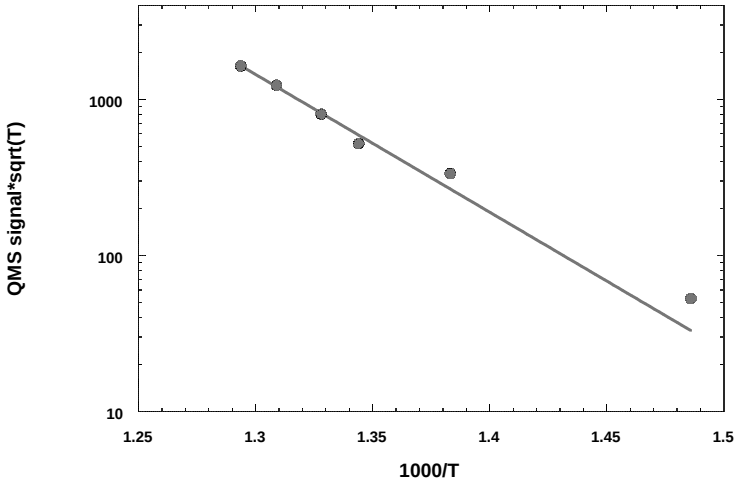


Figure 5.3: Arrhenius Plot of hydrogen desorption measured using MBMS. The activation energy for desorption is 1.8 eV

5.3 Reaction Pathways of Disilane Dissociation at Elevated Temperatures

The thermal activation of the hydrogen desorption during growth demonstrated that the *overall* growth reaction is given by

$$Si_2H_6 + 2\underline{Si} - \rightarrow 2(\underline{Si} - Si) + 3H_2 \tag{5.3}$$

and since no silane production was observed the initial adsorption reaction is given by

$$Si_2H_6 + 2\underline{Si} - \rightarrow 2\underline{Si} - SiH_3 \tag{5.4}$$

The reactions after the initial adsorption 5.4 must therefore consist of the following:

$$\underline{Si} - SiH_3 + \underline{Si} - \rightarrow \underline{Si} - SiH_2 + \underline{Si} - H \tag{5.5}$$

$$\underline{Si} - SiH_2 + \underline{Si} - \rightarrow \underline{Si} - SiH + \underline{Si} - H \tag{5.6}$$

However, the dihydride phase may decompose to release hydrogen:

$$2\underline{Si} - SiH_2 \rightarrow 2\underline{Si} - SiH + H_2(g) \tag{5.7}$$

The two reaction pathways differ in the amount of hydrogen for each adsorbed silicon atom that remains on the surface to achieve a fully passivated surface. The following study serves to clarify the *precise* reaction pathway of disilane decomposition.

For adsorption on a clean surface at a temperature which is well below the β_1 peak at 550°C , see chapter 4, hydrogen desorption will be negligible, therefore the amount of silicon deposited during saturation adsorption will depend on the amount of hydrogen on the surface passivating the adsorption sites. As the decomposition of hydride radicals also requires active sites the surface may be passivated by higher hydrides ($\underline{Si} - SiH_2$) as well as by the lower hydrides ($\underline{Si} - SiH$ and $\underline{Si} - H$).

As thermal desorption is thought to be the most dominant process of adsorption site reactivation a saturation exposure of the clean Si(001) surface to a disilane flux at a temperature below that of the β_1 peak followed by annealing should produce a surface in a similar state to the original clean surface but with a certain coverage of silicon. This Si coverage, or amount of Si deposited, is then dependent on the amount of hydrogen required to passivate the surface and hence the reaction pathways. If this cycle is repeated many times it should be possible to measure the amount of silicon deposited by ex-situ layer thickness measurements such as X-ray diffraction (XRD). The total layer thickness should give the amount of silicon deposited per cycle of dosing and annealing, and in this way be able to probe the degree of disilane decomposition as a function of substrate temperature and incoming flux. This technique has been termed Temperature Modulated Growth (TMG) and a study of disilane on Si(001) is the topic of the next section.

5.3.1 Temperature Modulated Growth

X-ray diffraction rocking curve measurements record the diffracted beam intensity as a function of the incident beam angle. For a complicated structure the resulting XRD spectra show features additional to the diffraction peaks associated with diffraction from planes in the pure crystal lattice. This diffraction can be modelled by Bragg's law $n\lambda = 2d\sin\theta$ where d is the interplanar distance. However, to determine the structure of the sample the experimentally observed rocking curves must be fitted using computer simulations based on the dynamic theory of diffraction with the sample structure as the fitting parameters.

The samples grown utilised SiGe layers to act as markers at either end of the test layer. The layer structures are illustrated in Figure 5.4 with the control sample and the test sample differing only by the TMG layer. In both samples and after an initial buffer layer to

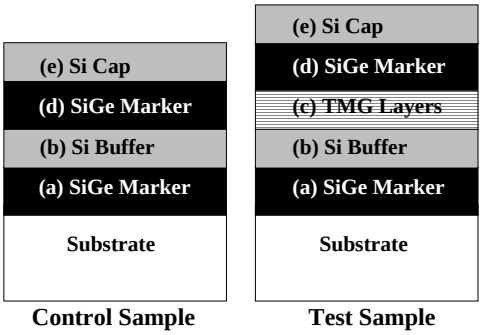


Figure 5.4: Temperature Modulated Growth (TMG) sample structure: Layer (a) is a 0.0068 μm SiGe marker layer with a Ge content of 8.5 percent. Layer (b) is a 0.00667 μm Si buffer layer under the TMG Si layer (c). Layer (d) is a another SiGe marker and (e) is 0.000389 μm Si cap.

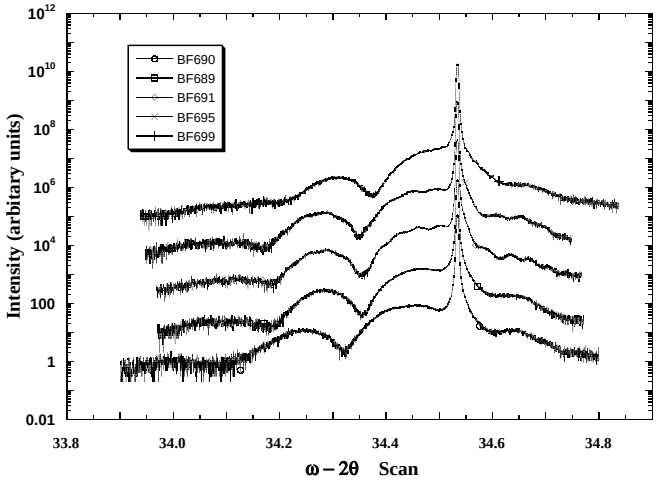


Figure 5.5: X-ray diffraction rocking curves recorded from the Temperature Modulated Growth (TMG) samples. The greater spacing of the XRD features indicate a smaller spacing of the diffracting layers. This is then used to calculate the amount of silicon deposited during one cycle in the TMG experiments

Sample Information				
Sample Number	Dose Temp (°C)	Dose Pressure (mbar)	Dose Time (s)	TMG layer thickness (ML)
BF689	430	1×10^{-5}	20	33
BF690	NA	NA	NA	0
BF691	320	1×10^{-5}	60	39
BF695	430,320	1×10^{-5}	10,60	33
BF699	250-300	8×10^{-5}	60	49

Table 5.1: Table showing the TMG sample data

ensure a good starting surface, a SiGe layer is grown using a disilane/germane flux ratio that has a known growth rate to ensure the thickness is established to ease simulations. A further layer of Si is grown to ensure the surface is entirely Si, this is because of the possibility of Ge surface segregation and its subsequent effect on hydrogen desorption. Once the SiGe layer and Si buffer layer are grown, the 100 cycles of dosing and annealing (TMG) can be performed in the case of the test sample but this step was omitted for the control sample. After this another SiGe marker layer was grown for both the control and the test sample and this was followed by a silicon layer to avoid oxidation of the marker layer.

The measured XRD diffraction rocking curves are shown in Figure 5.5. Once the rocking curves for the control wafer had been successfully simulated, fitting the rocking curves to the test samples only required the alteration of the thickness of the TMG layers, layer (c) in Figure 5.4. The resulting thicknesses are summarised in Table 5.1 .

The table gives the total thickness of the TMG layers in Monolayers (ML) and for the control sample (BF690) this is obviously 0. For sample BF689 the exposure to disilane was performed at 430 °C and the total thickness was 33ML for 100 cycles therefore for every dose 1/3 ML of silicon was deposited. The XRD rocking curves may still be simulated satisfactorily with layer thicknesses varying ±5 Angstroms which is equivalent to ±4 monolayers. The number of monolayers per cycle can therefore be measured to an accuracy of ±0.04 ML per cycle. In the dosing of sample BF695 a brief dose was performed at 430 °C followed by a longer dose at 320 °C . The same amount of silicon was deposited in each cycle as sample BF689. This further confirms that the surface in each case was fully passivated within 10 seconds of the initiation of exposure to the disilane and in each case 1/3ML of silicon was deposited per TMG cycle. The proportion of silicon to hydrogen in the disilane molecule is also 1/3 and it can be postulated that for dosing at 430 °C at 1×10^{-5} mbar the disilane fully dissociates sequentially producing a predominately monohydride

surface without losing molecular hydrogen to the gas phase during its decomposition to the monohydride stage. This is also confirmed by the RHEED patterns which maintain the form indicative of the (2×1)+(1×2) reconstruction throughout the 100 cycles. The adsorption of disilane at these temperatures and pressures does not release hydrogen directly into the gas phase and the decomposition is complete, the reaction is that given by equations 5.4, 5.5 and 5.6.

For exposure at a lower temperature of 320°C (BF691) the amount of silicon deposited per cycle was found to be greater. This can be interpreted as due to the thermal activation of the decomposition process, therefore at the lower temperatures the rate of decomposition is lower in comparison to the rate of adsorption of disilane. The decomposition process requires dangling bonds on neighbouring sites and the surface becomes fully passivated before the higher silicon hydride units are able to decompose. In fact for a much higher pressure exposure at 275°C the amount of silicon deposited per cycle was found to be almost 1/2ML, this is consistent with the disilane dissociating into two dihydride units and two chemisorbed hydrogen atoms given by equations 5.4 and 5.5 only. In all cases the trihydride decomposition given by 5.5 is assumed to be fast and not rate limiting.

In addition to the TMG measurements RHEED patterns were also recorded, Figure 5.6, from surfaces dosed at 430°C , 325°C and room temperature. All the patterns indicate the presence of dimers although the half order diffraction features have a lower intensity compared with the clean surface as the temperature was decreased. The fact that dimers are present even at dosing at room temperatures where the surface contains a considerable dihydride phase means that the dihydride phase co-exists with the monohydride phase since the production of 0.5ML of Si produces 0.5ML of monohydride and 0.5ML of dihydride giving a 1.5ML coverage of hydrogen. No hydrogen is released into the gas phase.

5.4 A Model for the Steady State Growth of Silicon

TMG combined with MBMS has identified the reaction pathways that occur during the steady state growth of silicon from disilane and these are summarised in equations 5.4, 5.5 and 5.6. It was also seen how effective chemisorbed hydrogen is in suppressing the adsorption and dissociation of disilane. However, a detailed study of growth rate is necessary to establish the kinetics and rate limiting steps of the pyrolysis reaction under steady state growth conditions in GSMBE. From the previous studies, the disilane pyrolysis reaction occurs mostly via dissociative chemisorption and subsequent sequential loss of hydrogen until the monohydride phase is reached. The hydrogen on the surface then leaves via

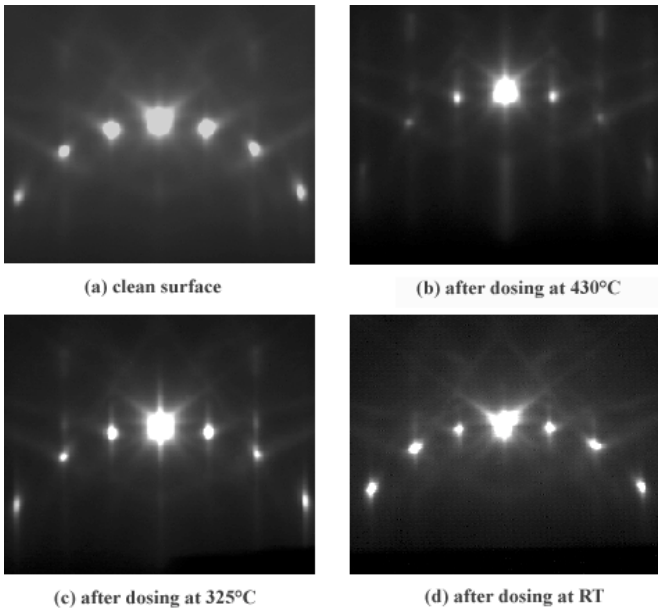


Figure 5.6: RHEED pattern of a clean and hydrogenated Si(001) surface in the [110] azimuth. All patterns show the (2×1)+(1×2) reconstruction indicating the presence of dimers.

recombinative desorption into the gas phase. The steady state active site coverage governs the characteristics of the adsorption of precursors during growth while the surface hydrogen coverage controls the desorption of H_2. At elevated temperatures, the loss of hydrogen from $SiH_2 and SiH_3$ radicals to dangling bonds is fast and this is not the rate limiting step in the pyrolysis reaction or growth rate. An experiment studying the precise role of hydrogen desorption during growth was reported in section 5.2 which demonstrated that hydrogen does indeed block the active sites and desorption reactivates them. For low steady state hydrogen coverages the growth rate becomes limited by the incoming flux, for high steady state coverages the growth is limited by the rate of hydrogen desorption which is found to be thermally activated.

The pyrolysis reaction rate is proportional to the growth rate given that no Si or Si containing species has been observed leaving as a reaction product. During steady state growth, the intensity of a specularly reflected electron beam is seen to oscillate readily and the period of this oscillation has been associated with layer by layer growth [64]. The next section reports on RHEED intensity oscillations during growth on the Si(001) surface using disilane as the growth precursor. The subsequent section measures the steady state growth rate by measuring the thickness of a grown layer using XRD as in the TMG studies.

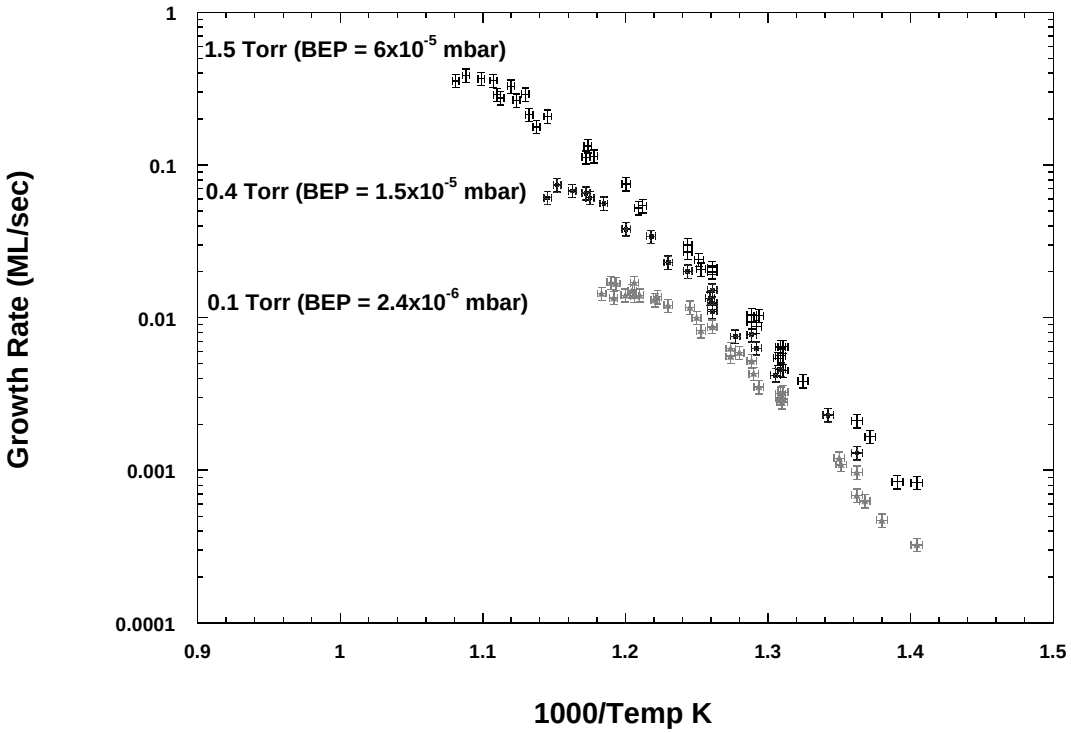


Figure 5.7: Arrhenius plot of the growth rate measured using the period of RHEED intensity oscillations. The lower data is recorded from growth from a flux produced from a gas line pressure of 0.1 Torr which gives a beam equivalent pressure (BEP) of 2.4×10^{-6} mbar. The upper data is from 1.5 Torr (BEP = 6×10^{-5} mbar) and the middle from 0.4 Torr (BEP = 1.5×10^{-5} mbar)

5.4.1 The Established Growth Process

RHEED oscillations were recorded during the growth from three different fluxes over the maximum possible temperature range. The maximum temperature range lies between where the growth begins to proceed by stepflow at high temperatures and at low temperatures where the growth rate becomes laboriously slow and impractical to measure. Here the period of oscillation can approach half an hour where noise, such as movement of the electron beam, can become appreciable. Figure 5.7 shows an Arrhenius plot of the growth rate measured using RHEED oscillations. The details of RHEED and some examples of the form of the oscillations recorded are shown in Appendix C.

Figure 5.7 shows a similar form to the results of Mokler *et al.* [57](see Figure 2.14).

The study was performed over the temperature range 450 °C to 650°C , Mokler *et al* used the range 500 °C to 700°C and used higher fluxes but over a smaller range.

There are many sources of errors in using the RHEED intensity oscillations to measure growth rate. The growth rate is derived from the period of oscillations which is usually measured from an average of many oscillations. It should be possible to measure the period to an accuracy better than 10%. It is also difficult to compare one set of oscillations to another, even from the same surface, since different areas of the surface may grow at different rates. In Figure 5.7 the growth rate error is set at $\pm\frac{0.1}{t}$ where t is the period of oscillation. The other source of error in these data lie in the temperature measurement, this is thought to be possible to an accuracy better than ±2°C , the error on the x-axis is given by $\frac{2000}{T^2}$ where T is the substrate temperature in Kelvin.

The results clearly show the effect of the steady state hydrogen coverage on the temperature that separates the flux limited growth from the hydrogen desorption limited growth. We can define this turn over point as the point where the steady state hydrogen coverage falls to zero. For higher fluxes this point moves to higher temperatures since a higher rate of desorption is needed to remove the hydrogen which is produced by the pyrolysis of the adsorbing disilane and reduce the hydrogen coverage closer to zero.

The hydrogen desorption limited regime of growth shows a similar gradient for all fluxes and it may therefore be inferred the energy of activation is constant, however an unexpected flux dependence at low temperatures was observed.

5.4.2 Limitations of the Established Model for the Growth Process

The growth rate was also measured as a function of temperature and flux by measuring the thickness of a grown layer in a set time. This was performed by growing samples similar to those used in the TMG study, see Figure 5.4, but instead of modulating the temperature and flux both were held constant at the chosen values.

Figure 5.8 shows the results in an Arrhenius plot and the flux dependent regime and hydrogen desorption limited regime are clear. Once again a flux dependence is observed in the low temperature regime and there is also a hint of a temperature dependence in the so called flux dependent regime. In this regime the growth rate is actually lower at 822 °C than at 500 °C .

As for the TMG samples the perceived error in the measured layer thicknesses is 5 Angstroms and growth times were chosen to give total layer thicknesses around 50 Angstroms. The error in growth rate is therefore less than 10%. The x-axis error is again

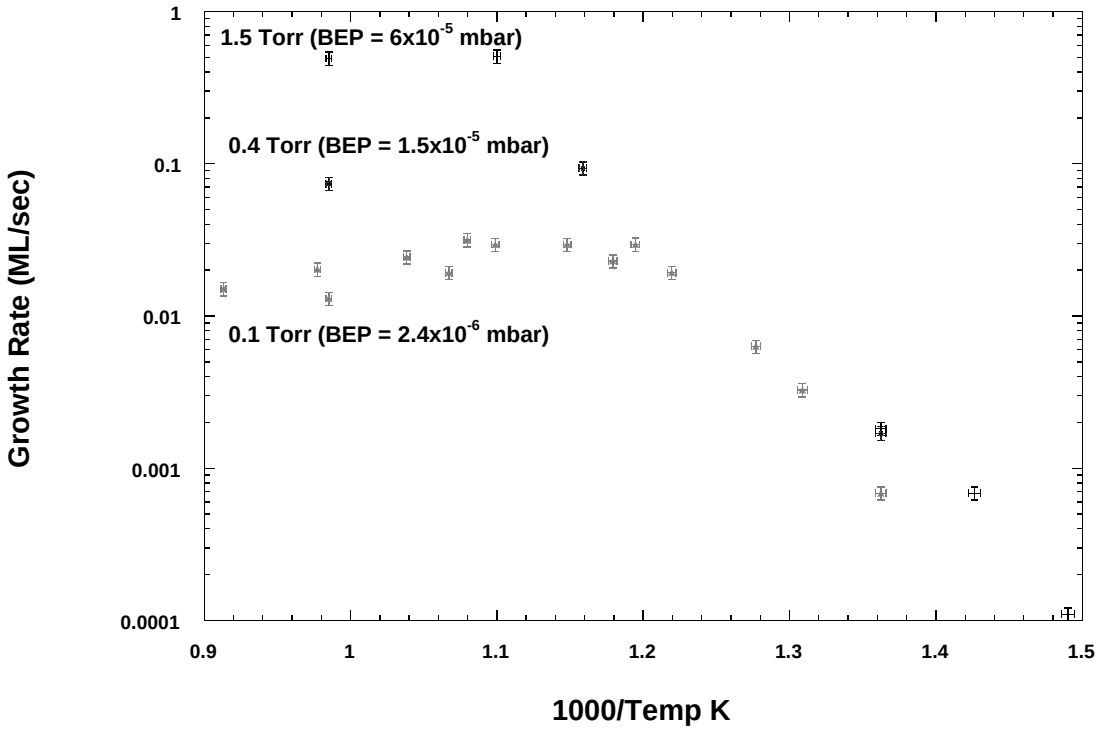


Figure 5.8: Arrhenius plot of the growth rate measured using ex-situ XRD on samples similar to those used in the TMG study. The three different fluxes are the same as those shown in Figure 5.7. A decrease in growth rate with increasing temperature is clearly present.

$\frac{2000}{T^2}$.

The flux dependence at low temperatures observed in both the RHEED and XRD studies points to a process of reactivating adsorption centres other than that by thermal desorption. This will be discussed further in the following section where a mathematical model is developed to explain these various phenomena.

5.4.3 Establishing the Order of the Adsorption Process

The growth rate has been measured by two methods, RHEED and ex-situ XRD, and a general picture of the growth process has been established. At low temperatures and high incident flux, the steady state hydrogen coverage is close to unity and the growth is governed by the hydrogen desorption rate constant. At high temperatures and low incident

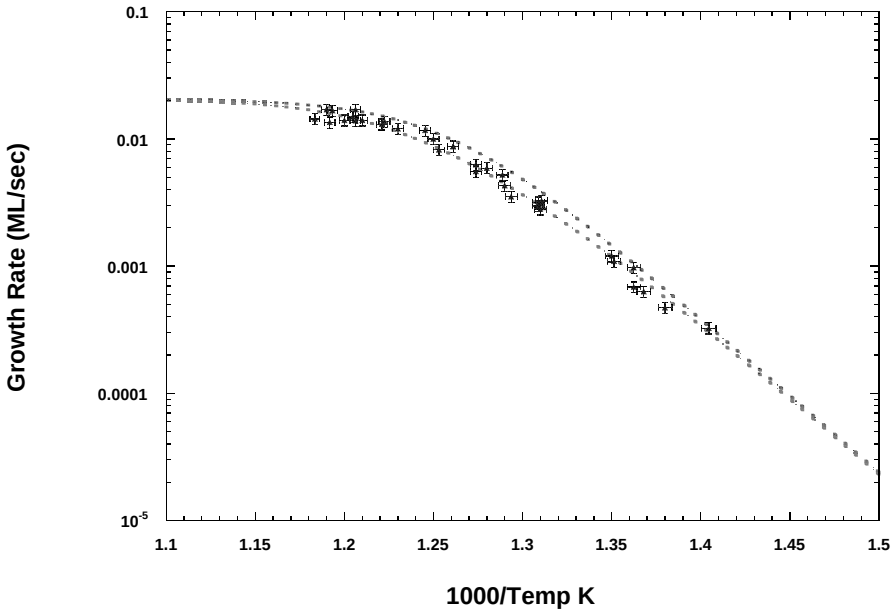


Figure 5.9: Growth rate measured using RHEED intensity oscillations along with fits for first and second order adsorption growth models. Hydrogen desorption is first order for both. It can be seen that there is little difference in the fit from the two models although the second order model fits slightly better. The two models agree at coverages of 1 at low temperatures and 0 at high temperatures

fluxes where the steady state hydrogen coverage is low, the growth rate is limited by the rate of adsorption and hence incoming flux. However, the measurements have shown two phenomena thus far unaccounted for in the established models of the growth process, these will be discussed later but initially the limitations of this model will be analysed.

The steady state hydrogen coverage depends on the balance between the rate of hydrogen generation from adsorption and the pyrolysis of disilane, of which six H atoms are generated for every disilane molecule adsorbed, and the rate of desorption where two H atoms desorb as molecular hydrogen. If the process of disilane adsorption and H_2 desorption requires one vacant site and one H occupied site respectively, then the steady state hydrogen coverage can be given as follows:

$$\frac{d\theta_{1st}}{dt} = 6SJ(1-\theta) - 2k_d\theta = 0 \tag{5.8}$$

J is measured in monolayers per second and S is a sticking coefficient and simply represents

the fraction of Si from the incident flux that chemisorbs. k_d is the rate constant for hydrogen desorption and is given by $k_d = k_{d_0} exp(-E_d/k_B T)$ where k_{d_0} is the pre-exponential and E_d the activation energy of desorption. At steady state the rate of change of the hydrogen coverage is zero, therefore we can solve the above equation for θ:

$$\theta_{1st} = \frac{3SJ}{3SJ + k_d} \tag{5.9}$$

The growth rate depends on the number of free sites and substituting the result for θ into the following equation gives the expression used for fitting experimental results.

$$GR_{1st} = 2SJ(1 - \theta) \tag{5.10}$$

This is termed the first order model and the factor of two represents the fact that two silicon atoms are deposited for every disilane molecule. If the disilane adsorption process requires two sites, as the reaction pathway requires, the model is as follows and is termed the second order growth model:

$$\frac{d\theta_{2nd}}{dt} = 6SJ(1 - \theta)^2 - 2k_d\theta = 0 \tag{5.11}$$

$$\theta_{2nd} = \frac{6SJ + k_d - \sqrt{12k_dSJ + (k_d)^2}}{6SJ} \tag{5.12}$$

$$GR_{2nd} = 2SJ(1 - \theta)^2 \tag{5.13}$$

The two models are shown in Figure 5.9 with the data for the growth rate measured using the period of RHEED intensity oscillations. The growth was performed using a gas line pressure of 0.1 Torr which is equivalent to a beam pressure (BEP) of 2.4x10^{-6} mbar. The incident flux I is related to the BEP in mbar as follows

$$I = \frac{101P}{\sqrt{2\pi mkT}} \tag{5.14}$$

T is assumed to be 300 K, room temperature and the temperature of the source. The flux in units of ML/sec, J, is given by

$$J = \frac{I}{N_0} \tag{5.15}$$

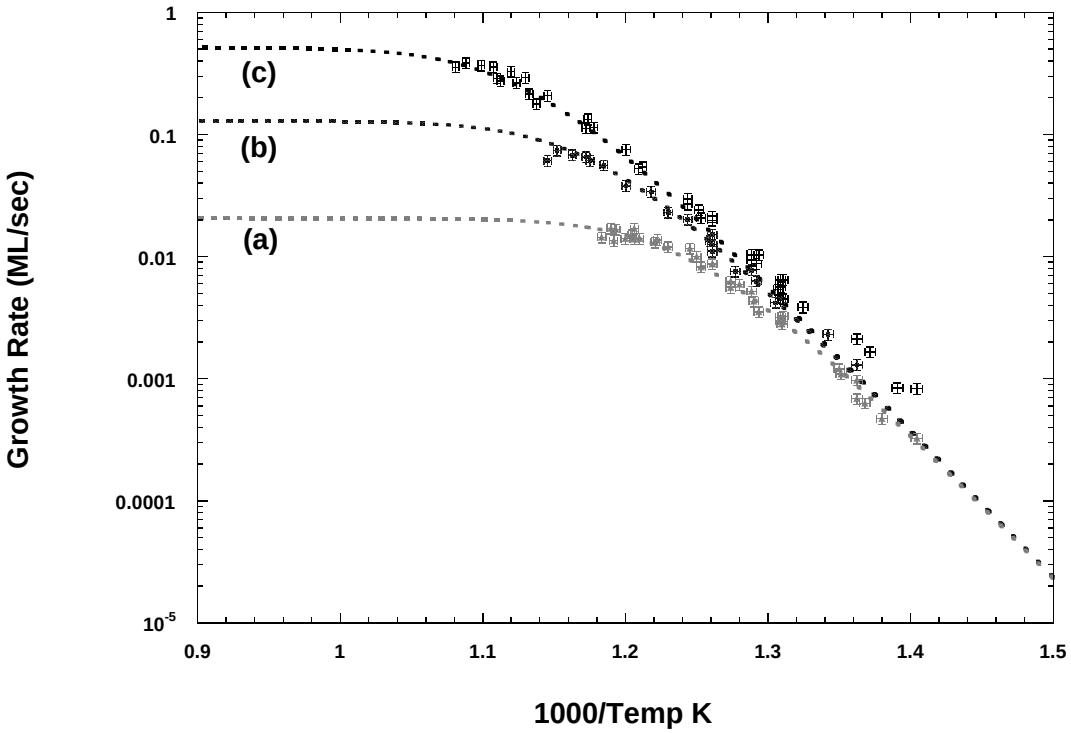


Figure 5.10: Growth rate measured using RHEED intensity oscillations for various fluxes along with fits for second order adsorption growth models. The model fits the data well with no modifications required to simulate the flux dependence at high temperatures.

where N_0 is the surface dangling bond density on the Si(001) surface and is assumed to be 6.8 x $10^{18} m^{-2}$

The model in figure 5.9 uses a sticking coefficient S of 0.015, a desorption rate pre-exponential k_{d_0} of 5 x $10^{13} s^{-1}$ and an activation energy E_d for desorption of 2.4 eV. This is in excellent agreement with the TPD studies of chapter 4 (pre-exponential $3.16 \times 10^{14} s^{-1}$ energy 2.48 eV) and the MBMS study (energy 1.8 eV). It can be seen that there is little difference in the fit from the two models although the second order model fits slightly better. Hirose *et al* [30] showed that the model for growth rate is less sensitive to the order of the adsorption process than the model for hydrogen coverage. Since the general consensus is that the adsorption process is second order this has been used to fit the complete set of RHEED data, see Figure 5.10

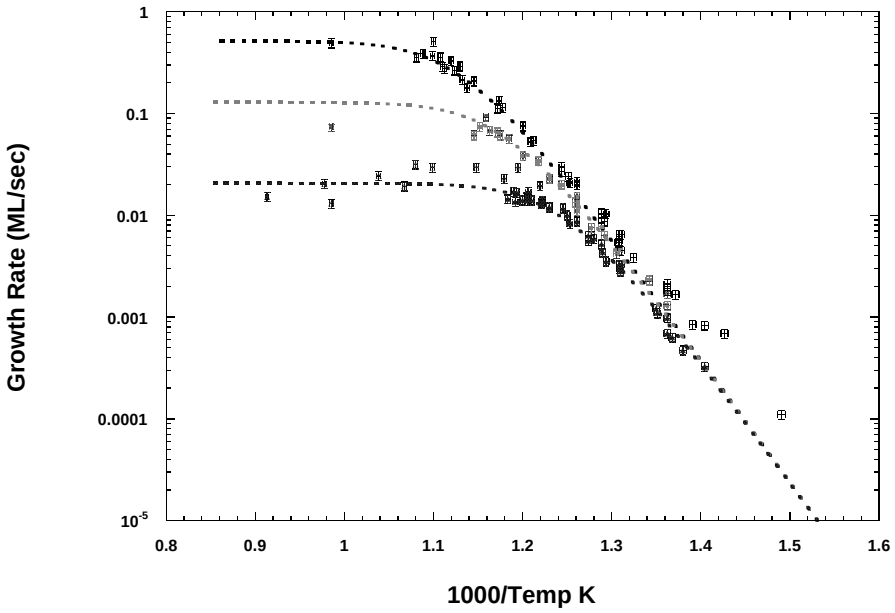


Figure 5.11: The second order adsorption growth model fits the RHEED data well but the growth rate temperature dependence measured at very high temperatures using XRD is not predicted by the standard model

5.4.4 Modelling the Growth Phenomenon

In Figure 5.11 the ex-situ XRD measurements of the growth rate are plotted with the simulated result using the current second order model. It is clear that the model could not produce a drop in growth rate at high temperatures and it is also evident that the flux dependence at low temperatures could not accounted for using the current model.

The flux dependence at low temperatures is illustrated more clearly in figure 5.12 where the growth rate is plotted against flux along with fits predicted by the standard second order adsorption model. The dotted line shows the growth rate for a hydrogen coverage of 0.9ML and a sticking coefficient S of 0.015, for all points along this dotted line the growth rate is given by the following equation:

$$GR = 2SJ(1-0.9)^2 = 0.0003J \tag{5.16}$$

It is clear that the models for the various temperatures show a similar form for the same hydrogen coverage as expected. At very large fluxes the model predicts that the growth rate becomes independent of flux since the steady state hydrogen coverage is approximately

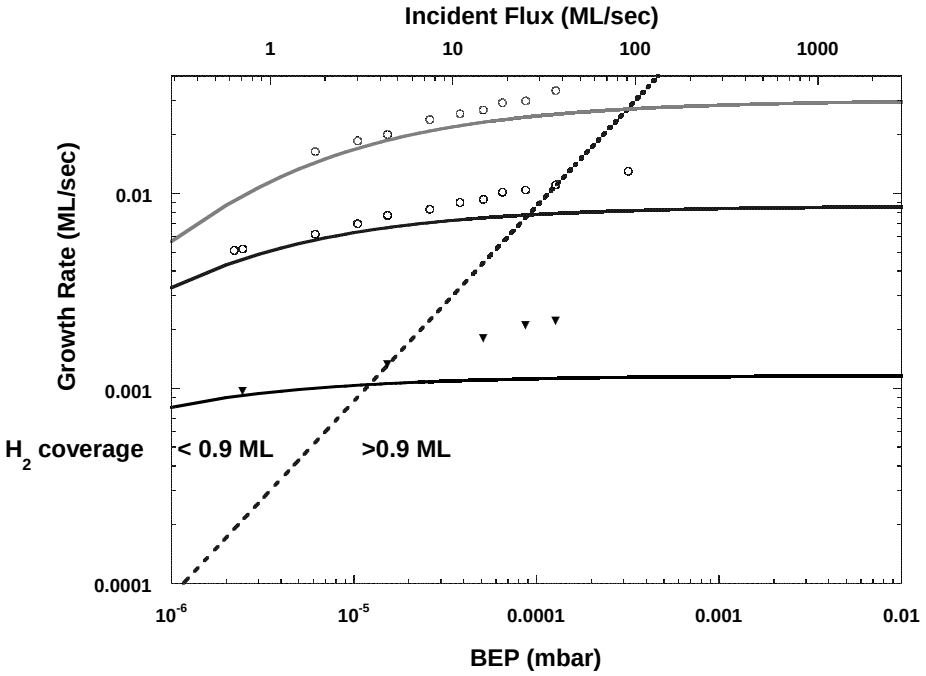


Figure 5.12: Growth rate dependence on incident flux measured using XRD and RHEED intensity oscillations. The dotted line is given by $GR = 2SJ(1-0.9)^2 = 0.02SJ$. The growth rates were recorded at 462 °C (bottom), 503°C (middle) and 531 °C (top). The solid lines show the growth rate dependence on BEP predicted by the standard second order model.

1ML. It can be seen that at low hydrogen coverages the model fits the data but with increasing incident flux the data seems to bear a power relationship to the flux with the power being approximately 0.2 (GR $\propto J^{0.2}$). This is not accounted for in any of the established growth models. It is clear that a new model must be constructed to explain these observed phenomena.

In figure 5.12 the incident flux is related to the beam equivalent pressure by the relation 2.9 this pressure was measured directly above the substrate during identical growth conditions. The effect of the high background of disilane is thus accounted for since an isotropic velocity distribution and not a molecular beam is assumed. If there were no background and growth occurred purely from the beam only the value of the calculated sticking coefficient would be altered. The beam and background are assumed to be of the same temperature throughout all experiments.

We shall now apply several extensions to the standard second order model and discuss their justification and merit. The first model depicted in Figure 5.13 is Model 1 and

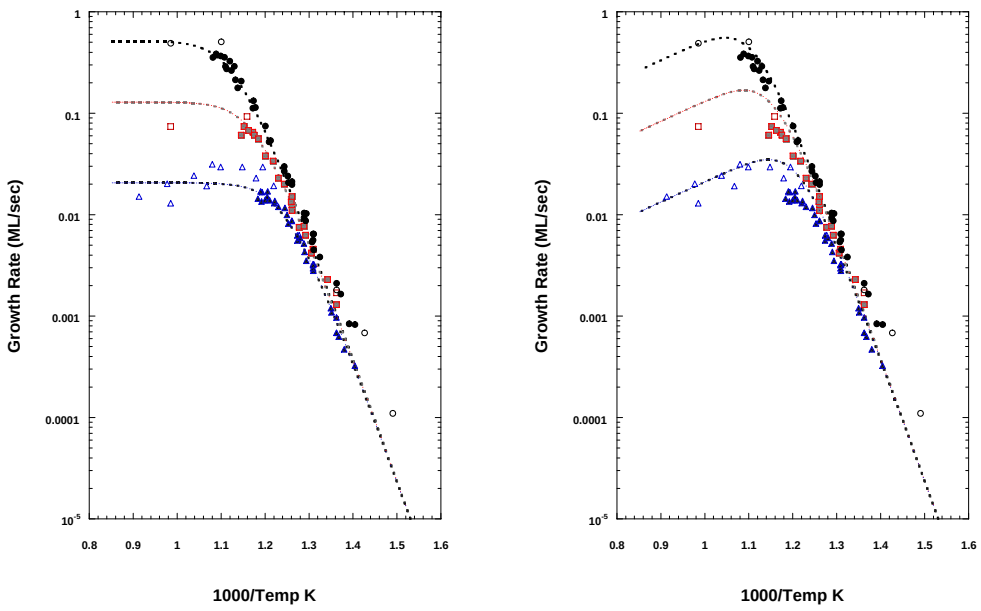


Figure 5.13: Growth models 1 and 2: Model 1 (left) is the standard model with second order disilane adsorption and first order hydrogen desorption. Model 2 (right) is the same as model 1 but with a temperature dependent sticking probability

is the standard model where adsorption requires two sites and desorption is a first order process, this is the model described by equations 5.11, 5.12 and 5.13. It is clear this model fails to fit the data at low temperatures where the growth rate is dependent on flux and at high temperatures where there is a decrease in growth rate with temperature.

A decrease in growth rate at high temperatures implies that the amount of silicon adsorbing is a smaller fraction of the incident flux than at lower temperatures for the same incident flux. This process can be modelled by desorption from a precursor state but no direct evidence exists for the presence of such a state. A simple model, model 2, introduces a trapping probability that is temperature dependent, α, to modify J. J will now be given by:

$$J = \frac{\alpha I}{N_0} \tag{5.17}$$

The sticking probability S used in earlier models is now replaced by the term α where α should vary from 1 at very low temperatures to 0 at very high temperatures. The variation

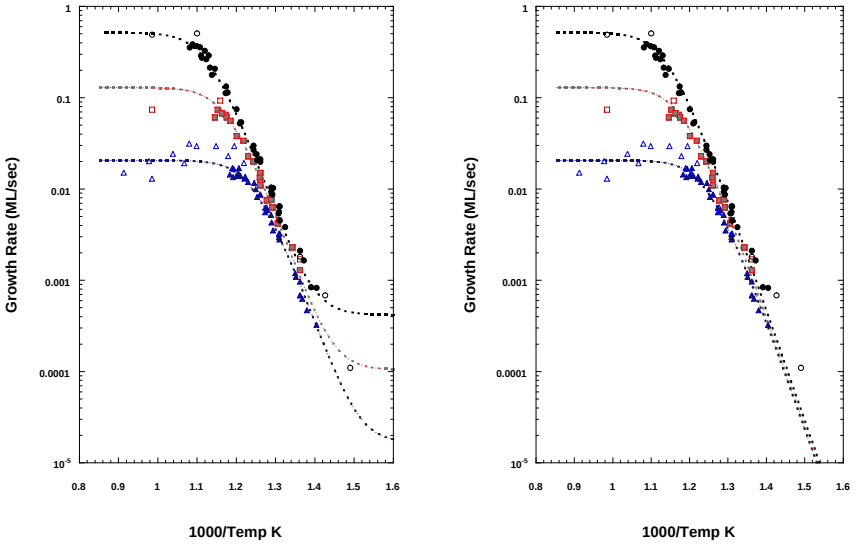


Figure 5.14: Growth models 3 and 4: Model 3 (left) is the standard model 1 but with a flux dependent abstraction. Model 4 (right) is the same as model 3 but with the flux dependent abstraction thermally activated.

of α with temperature is explained as due to an increased desorption from a precursor state back into the gas phase at higher temperatures. α is assumed to have the form:

$$\alpha = \frac{\alpha_a}{1 + \alpha_a} \tag{5.18}$$

where α_a is exponentially dependent on temperature:

$$\alpha_a = 1.5 \times 10^{-4} exp\left(\frac{0.4e}{k_B T}\right) \tag{5.19}$$

The success of model 2 in modelling the high temperature growth characteristics is clearly demonstrated in Figure 5.13. However the flux dependence at low temperatures is not modelled accurately.

As discussed earlier at low temperatures where hydrogen desorption is negligible and where hydrogen is known to passivate the surface, a flux dependence must be due to some form of flux initiated desorption or removal of hydrogen. A mechanism through which growth could proceed is by the removal of hydrogen by a disilane fragment produced by

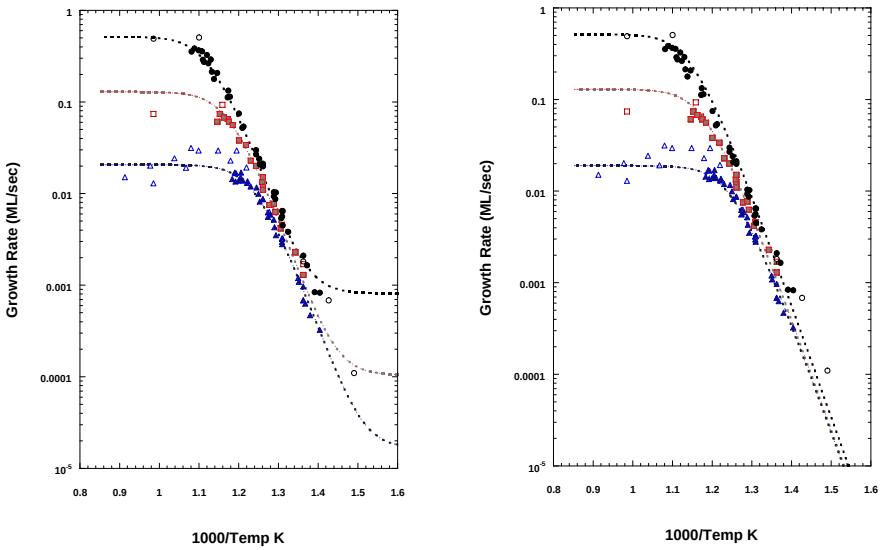


Figure 5.15: Growth models 5 and 6: Model 5 (left) is the standard model but with the abstraction depending on the flux to the power of $\frac{1}{2}$. Model 6 (right) is the same as model 5 but with the flux dependent abstraction thermally activated

adsorption. It is possible disilane could deposit a silicon adatom and two hydrogen atoms but remove one hydrogen atom in the form of silane into the gas phase. The removal of hydrogen would produce dangling bonds to which additional disilane can adsorb. In other words, hydrogen is abstracted by the desorption of silane. However the modulated beam experiments showed no thermally activated silane desorption but this does not dismiss silane desorption completely given the absolute change in the growth rate is exceedingly low. We will reserve discussion until later and for the present an extra term can be simply introduced into the standard model. The effectiveness of this will then be discussed. This term represents another desorption process with rate constant k_{abs} which is first order with respect to hydrogen coverage θ and flux J. The rate of change of hydrogen coverage for model 3 is now given by:

$$\frac{d\theta}{dt} = 6J(1-\theta)^2 - 2k_d\theta - k_{abs}\theta J = 0 \tag{5.20}$$

The solution to this equation is given in appendix E. For the fit in figure 5.14 $k_{abs} = 5\times10^{-3}$ and the trapping probability is fixed at $\alpha = 0.015$. Model 3 produces a tail off of the growth rate with decreasing temperatures where the thermally activated hydrogen desorption is

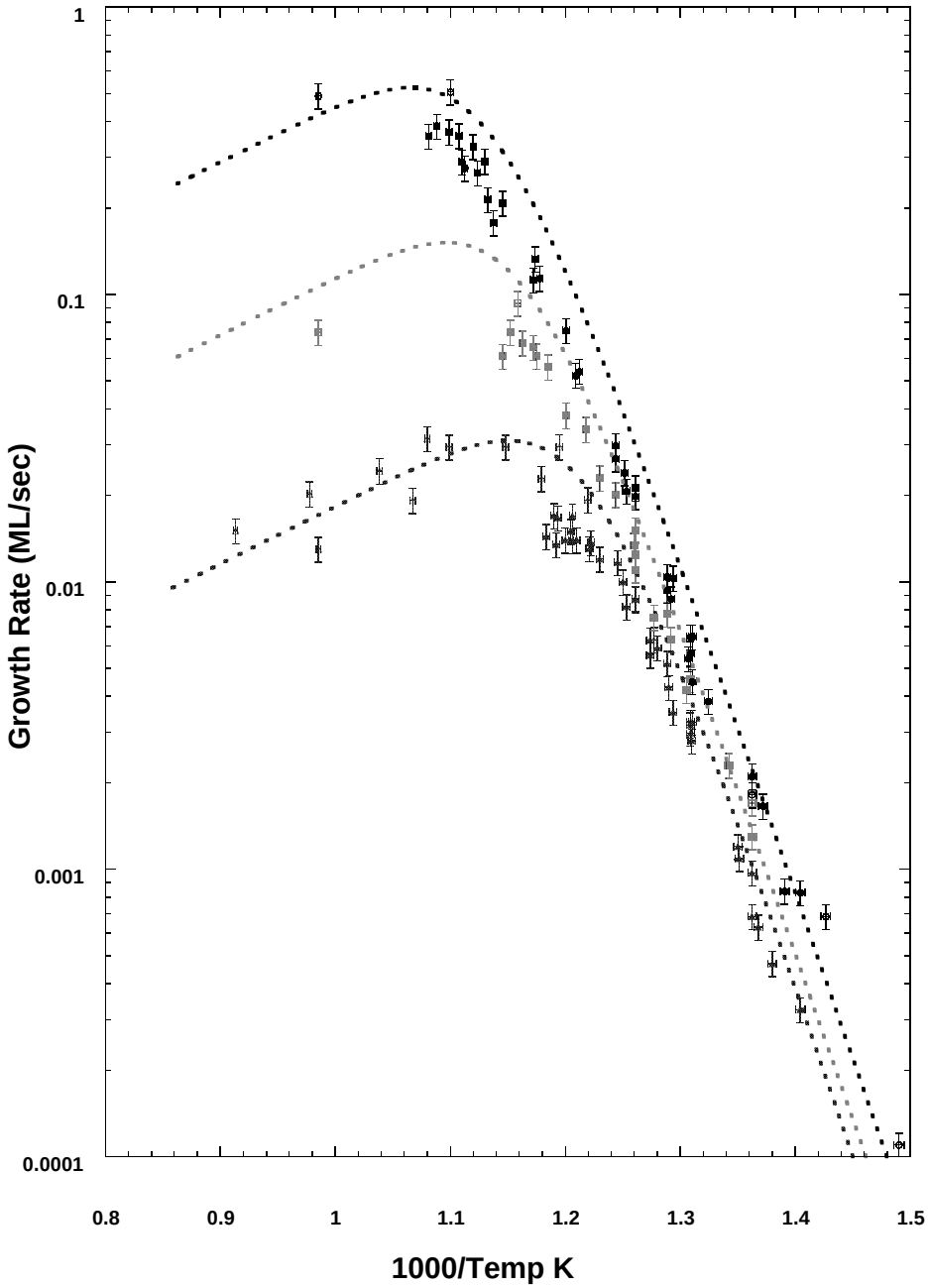


Figure 5.16: Growth model 7 is a combination of the standard growth model 1 with model 6. The model incorporates a hydrogen abstraction reaction dependent on $J^{\frac{1}{2}}$ and both the abstraction reaction and the trapping probability are temperature dependent. Growth from a BEP = $6{\times}10^{-5}$ circles, BEP = $1.5{\times}10^{-5}$ squares and BEP = $2.4{\times}10^{-6}$ triangles. RHEED data points solid XRD data points open.

no longer rate limiting in the overall growth process. The growth rate depends solely on the incident flux. This model was dismissed by probing the growth rate at very low temperatures using XRD. RHEED intensity oscillations will be too susceptible to noise at these extremely slow growth rates. Growth rate measurements at 1000/K = 1.5 show the growth rate does not level off at low temperatures as modelled by model 3. Another model was constructed in which the abstraction of model 3 is thermally activated and k_{abs} is given by $k_{abs} = 1 \times 10^{14} exp\left(\frac{-2.4e}{k_b T}\right)$. The levelling off is no longer present in this model and the fit is better however the growth rate dependence on flux is still not modelled correctly.

Two further models were constructed which were both identical to 3 and 4 but the process of abstraction was no longer first order but of fractional order $\frac{1}{2}$ which is similar to the flux dependence of $J^{\frac{1}{5}}$ hinted at in the gradient of the flux dependence shown in figure 5.12

$$\frac{d\theta}{dt} = 6J(1-\theta)^2 - 2k_d\theta - k_{abs}\theta J^{\frac{1}{2}} = 0 \tag{5.21}$$

The solution to this equation along with a summary of all the growth models is given in appendix E. Figure 5.15 clearly shows the abstraction must be thermally activated as model 5 still produces the levelling off at low temperatures. Model 6 appears to have modelled the growth rate at low temperatures correctly but the growth rate decrease at high temperatures is not accounted for, however this was modelled correctly by Model 2. It seems reasonable that an accurate model, model 7, should combine models 2 and 6, the result of this is shown in 5.16.

The temperature dependent trapping probability results in model 7 fitting better at the low temperatures as the trapping increases at low temperatures and since more flux is present the abstraction process will be accelerated. The complete model 7 is given as follows:

$$\frac{d\theta}{dt} = 6J(1-\theta)^2 - 2k_d\theta - k_{abs}\theta J^{\frac{1}{2}} = 0 \tag{5.22}$$

$$\theta = \frac{8\frac{1}{3} \times 10^{-2}}{J}\left[12J + 2k_d + k_{abs}\sqrt{J} - \sqrt{48Jk_d + 24J^{\frac{3}{2}}k_{abs} + 4k_d^2 + 4k_d k_{abs}\sqrt{J} + k_{abs}^2 J}\right] \tag{5.23}$$

$$GR = 2J(1-\theta)^2 \tag{5.24}$$

Where the variables are given as follows:

$J = \frac{\alpha I}{N_0}$

$I = \frac{101P}{\sqrt{2\pi mkT}}$

$\alpha = \frac{\alpha_a}{1+\alpha_a}$

$N_0 = 6.8 \times 10^{18}$

$m = 62 \times 1.66 \times 10^{-27}$

$k_d = 5 \times 10^{13} exp\left(\frac{-2.4e}{k_b T}\right)$

$\alpha_a = 1.5 \times 10^{-4} exp\left(\frac{0.4e}{k_B T}\right)$

$k_{abs} = 1 \times 10^{14} exp\left(\frac{-2.4e}{k_b T}\right)$

It should be noted that Model 7 is based on some speculation and no direct evidence exists for a temperature dependent trapping probability. However, silane desorption has been reported [48] during silicon growth from disilane but studies reported earlier show no thermal activation for such a process, this is in disagreement with the postulates for model 7.

5.5 Summary

Disilane adsorption has been studied extensively in this section and the conclusions can be summarised as follows:

- The reaction pathway for disilane adsorption has been identified. The initial adsorption step produces no silane but results in two trihydride fragments on the surface.
- The resulting dissociation is sequential with no hydrogen released into the gas phase and results in a passivated surface where thermal desorption is negligible.
- Two growth phenomena not predicted by the established growth model are observed and modelled.
- Growth rate modelling uses a temperature dependent trapping probability and a flux dependent hydrogen desorption to fit the data.

Chapter 6

Kinetics of Growth from Silane

6.1 Introduction

Chapter 5 reported a systematic study of the growth of silicon from disilane on the Si(001) surface. When disilane adsorbed on a clean surface the type of silicon hydride species were found to depend on the rate of disilane decomposition compared to the rate of the initial adsorption. The rate of decomposition of adsorbed disilane was found to be thermally activated so at high substrate temperatures and low flux the surface hydride species are predominately monohydride. Chapters 4 and 5 also demonstrated that as the substrate temperature is decreased or the incident disilane flux increased larger and larger silicon hydride units exist in stability on the surface. The availability of dangling bonds directly effects the stability of these adsorbed silicon hydride units and hydrogen completely passivates these dangling bonds. In this chapter a similar study to that for disilane adsorption on the Si(001) surface is performed using silane as the growth precursor. The results are compared and contrasted with those reported in Chapters 4 and 5.

6.2 Hydrogen Desorption from a Silane Exposed Surface

Temperature programmed desorption was used to study any differences in hydrogen desorption between a surface previously exposed to disilane or silane. Figure 6.1 shows the desorption spectra from a Si(001)surface after exposure to disilane or silane. The disilane dose was from a 1 Torr gas line (BEP = 5.2×10^{-5} mbar) for 1 minute at 430 °C and the silane dose was from a gas line pressure of 2 Torr (BEP = 0.15×10^{-3} mbar) for 10 minutes at 200°C .

It is clear in both TPD spectra the desorption is occurring predominately from

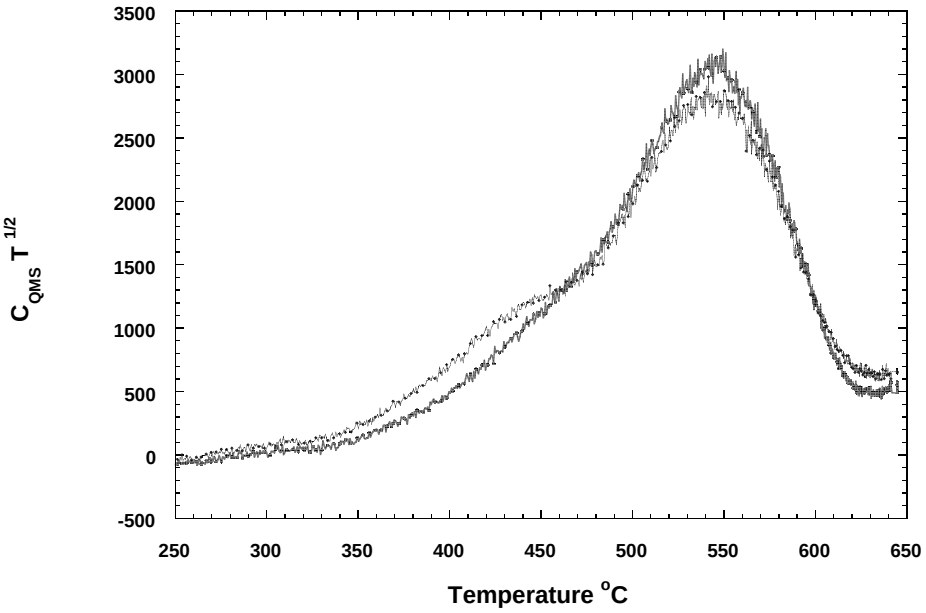


Figure 6.1: Temperature programmed desorption from a Si(001) surface exposed to silane and disilane. The disilane dose was from a 1 Torr gas line (BEP = 5.2×10^{-5} mbar) for 1 minute at 430 °C and the silane dose was from a gas line pressure of 2 Torr (BEP = 0.15×10^{-3} mbar) for 10 minutes at 200°C .

the monohydride β_1 phase but for the silane dosing case a small β_2 shoulder is seen. This is in contrast to disilane adsorption under similar dosing conditions where a considerable β_2 peak is in the desorption spectra, see Figure 4.1.

The interpretation of this is that the adsorption rate of silane and hence the rate of production of silicon hydride radicals on the surface is much smaller compared with the rate of decomposition of these hydride radicals (at a substrate temperature of 200°C and a BEP of 0.15×10^{-3} mbar) since dangling bonds must have been available for the adsorbed silane to decompose. For a much smaller disilane BEP of 5.2×10^{-5} mbar at the same temperatures, disilane is adsorbing at a greater rate in relation to decomposition compared to the case for silane and leads to a much higher concentration of dihydride when the surface is fully passivated. These TPD spectra clearly demonstrate a smaller sticking probability for silane in comparison to disilane.

6.3 Adsorption of Disilane on a Clean Si(001) Surface Studied by TMG

TPD experiments show that a 10 minute dose at a BEP of 0.15×10^{-3} mbar at 200°C gives a hydrogen coverage similar to a known fully passivated surface produced from disilane at 1 minute, 430°C BEP = 5.2×10^{-5} mbar. The surfaces are predominately monohydride. Such a dosage can then be used in a Temperature Modulated Growth (TMG) experiment to probe how much silicon is deposited per cycle of adsorption on a clean Si(001) surface. The sample structure and measurement method is identical to those reported in section 5.3.1.

The thickness of the TMG layers was indicative of silane adsorption for a 10 minute 2 Torr dose at 200 °C depositing 0.2 $\pm$ 0.04 ML per cycle. For silane a dose at 1 Torr at 320 °C for 5 mins, 0.18 $\pm$ 0.04 ML per cycle was produced.

Silane consists of one silicon and four hydrogen atoms and if silane was to adsorb in a similarly complete way as disilane does at high temperatures/low fluxes it may be expected that 1/4 ML of silicon would be deposited per cycle. It is not clear if this is the case in the experiments reported here but this is within the experimental uncertainty. It is possible that the surface has not been exposed to silane long enough so as to produce a fully passivated/covered surface.

The experimentally findings are consistent with the reaction pathways reported in the literature:

$$SiH_4(g) + 2\underline{Si}- \rightarrow \underline{Si} - H + \underline{Si} - SiH_3 \tag{6.1}$$

$$\underline{Si} - SiH_3 + \underline{Si}- \rightarrow \underline{Si} - H + \underline{Si} - SiH_2 \tag{6.2}$$

$$\underline{Si} - SiH_2 + \underline{Si}- \rightarrow \underline{Si} - H + \underline{Si} - SiH \tag{6.3}$$

and the overall reaction:

$$SiH_4(g) \rightarrow Si + 2H_2(g) \tag{6.4}$$

6.4 Steady State Growth Rate Measurements

RHEED oscillations and XRD layer thickness evaluations were employed to measure the growth rate of silicon on the Si(001) surface using silane as the growth precursor. Figure 6.3 shows the growth rate measurements for a 2 Torr silane gas line pressure (BEP = 0.15×10^{-3} mbar) along with those from disilane at a gas line pressure of 0.1 Torr (BEP = 2.40×10^{-6} mbar).

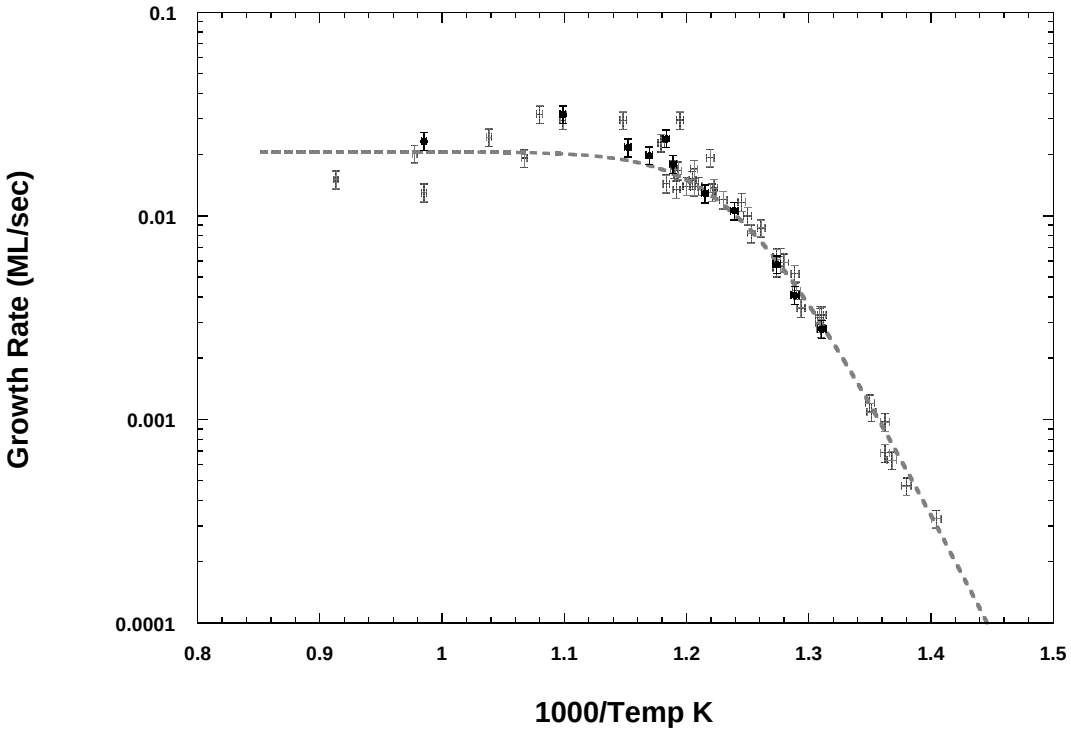


Figure 6.2: Arrhenius plot of the growth rate of silicon from silane (solid circles) and disilane (error bars only) on the Si(001) surface. The dotted line shows the fit for disilane from the standard model 1, see chapter 5

The growth rate shows an identical temperature dependence for both silane and disilane precursors, however, the BEP of the silane is over 60 times greater than that for the growth from disilane. Clearly the barrier to hydrogen desorption is the same to that for growth from disilane but the sticking probability, which defines how much of the incident flux actually chemisorbs, is much smaller for growth from silane. Since the growth rate is similar for both silane and disilane under the incident fluxes as in Figure 6.3, a quick analysis can calculate the ratio of the sticking coefficients by comparing the fluxes incident on the surface using equation 2.8.

$$\frac{S_{(Si_2H_6)}}{S_{(SiH_4)}} = \frac{4.179 \times 10^{20}}{2 \times 4.878 \times 10^{18}} = 43 \tag{6.5}$$

The sticking coefficient for the simple growth model used in chapter 5 for disilane was 0.015

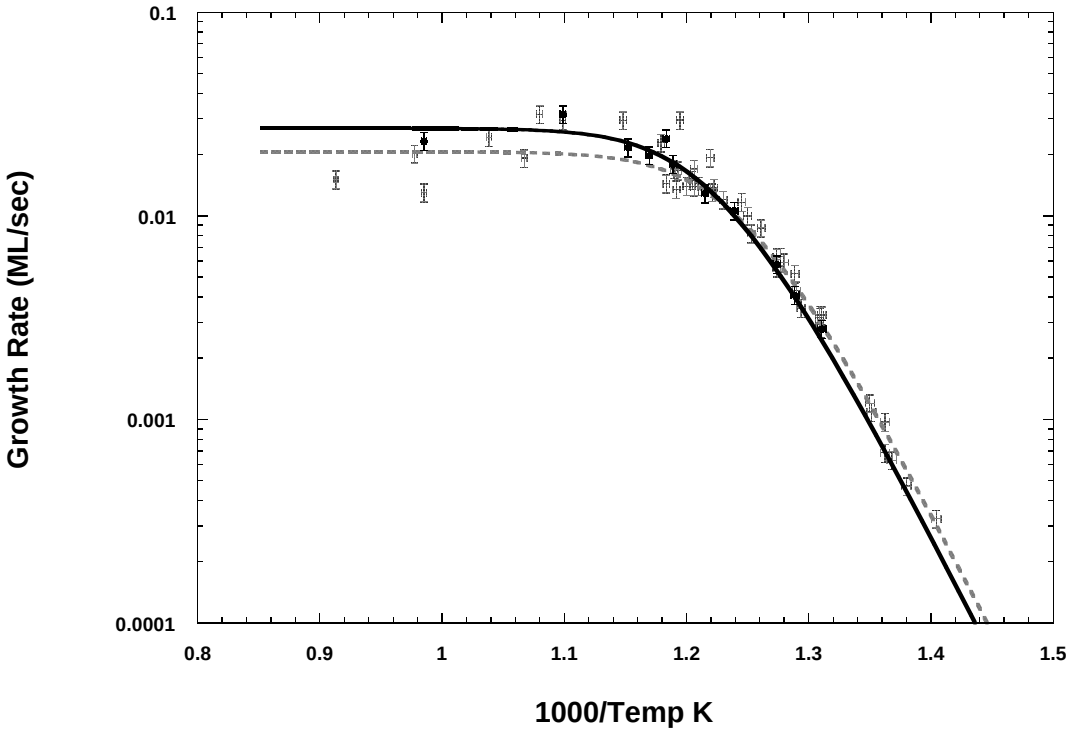


Figure 6.3: Arrhenius plot of the growth rate of silicon from silane (solid circles) and disilane (error bars only) on the Si(001) surface. The dotted line shows the fit for disilane and the solid line the fit from the silane growth model

this means the sticking coefficient for silane is around 3.5×10^{-4} in excellent agreement with [20]. This lower sticking probability is incorporated into the growth model in section 6.5.

A reduction in growth rate at high temperatures is also observed similar to the disilane case. This is again attributed to the limited lifetime in the precursor state.

6.5 Steady State Growth Rate Modelling

For the growth of silicon from silane the model of chapter 5 needs to be slightly modified since silane consists of only one silicon atom and four hydrogen. The rate of change of hydrogen coverage using a second order adsorption model is therefore given by:

$$\frac{d\theta_{2nd}}{dt} = 4SJ(1-\theta)^2 - 2k_d\theta = 0 \tag{6.6}$$

at steady state this can be solved to give:

$$\theta_{2nd} = \frac{4SJ + k_d - \sqrt{8k_dSJ + (k_d)^2}}{4SJ} \tag{6.7}$$

and the growth rate is given by:

$$GR_{2nd} = SJ(1-\theta_{2nd})^2 \tag{6.8}$$

This second order adsorption model assumes silane requires two sites to adsorb similar to the case for disilane and the fit is shown in Figure 6.3. The hydrogen desorption parameters are the same as for the disilane model $E_d = 2.4$ eV and $k_{d_0} = 5{\times}10^{13}$ but a sticking probability of $0.45{\times}10^{-3}$ is necessary for a good fit. For a fit from a first order adsorption model the desorption activation energy must be lowered and this is not thought to be realistic since the TPD from a silane exposed surface does not show any shift in peak position indicative of a lower energy pathway to desorption.

6.6 Summary

In this chapter a study of the growth of silicon on the Si(001) surface from silane has been undertaken. The conclusions can be summarised as follows:

- After silane adsorbs the resulting dissociation is sequential with no hydrogen released into the gas phase and results in a passivated surface at temperatures where thermal desorption is negligible. All four hydrogen atoms remain on the surface depositing one silicon atom. This is consistent with the studies of Gates *et al* [23] [21] [22] where:

$$SiH_4(g) + 2\underline{Si}- \rightarrow \underline{Si} - H + \underline{Si} - SiH_3 \tag{6.9}$$

$$\underline{Si} - SiH_3 + \underline{Si}- \rightarrow \underline{Si} - H + \underline{Si} - SiH_2 \tag{6.10}$$

$$\underline{Si} - SiH_2 + \underline{Si}- \rightarrow \underline{Si} - H + \underline{Si} - SiH \tag{6.11}$$

- In the growth rate modelling the hydrogen desorption parameters are the same as for the disilane model $E_d = 2.4$ eV and $k_{d_0} = 5{\times}10^{13}$ but a sticking probability of $0.45{\times}10^{-3}$ is necessary for a good fit.

Chapter 7

Kinetics of Growth from Germane

7.1 Introduction

In previous chapters the emphasis has been on homoepitaxial growth where the gas precursors deposited silicon on the Si(001) surface. The resulting growth is strain free and reaches a steady state hydrogen coverage almost immediately. This chapter reports on studies of the deposition of germanium from germane (GeH_4) on the clean Si(001) surface and steady state heteroepitaxial SiGe growth from disilane and germane at a constant flux ratio and temperature. For the growth of germanium or SiGe on Si(001) it can take an appreciable time for a steady state to be reached.

7.2 Hydrogen Passivation Effect on Alloy and Germane Dosed Surfaces

It has been shown that the presence of germanium on a silicon surface enhances the growth rate at low temperatures/high fluxes by producing a more facile pathway to desorption of hydrogen which is known to passivate the adsorption sites. It is in this regime that RHEED intensity oscillations are easily observed and since a growth rate increase can indicate the presence of germanium, RHEED can be used to indirectly probe the presence of germanium.

A clean silicon surface was given two exposures to germane, the first was for 1 minute at 270 °C from a gas line pressure of 1 Torr and the second was a longer dose for 3 minutes. A longer dose should deposit more germanium on the surface which would be indicated by an increase in the growth rate on this surface from disilane gas. The RHEED oscillations recorded during growth from disilane on such surfaces at 550°C are shown in

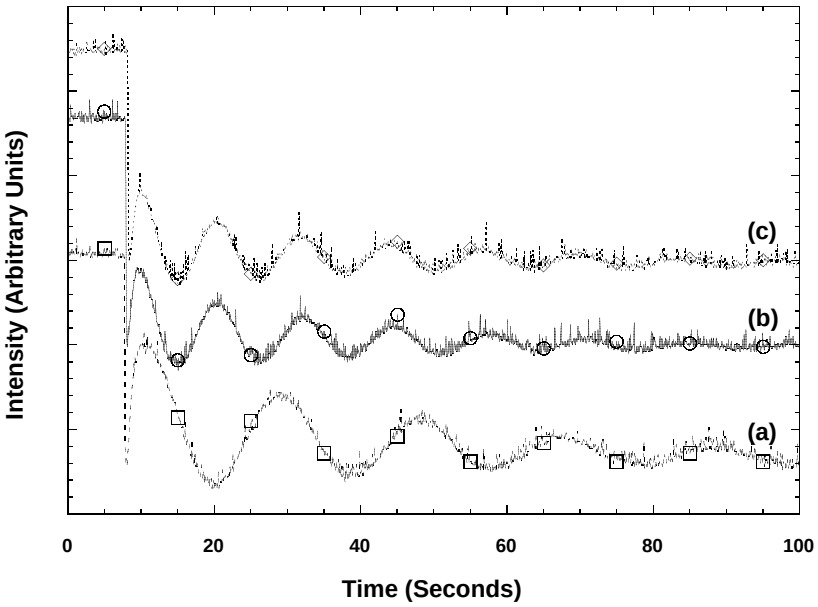


Figure 7.1: RHEED intensity oscillations recorded from growth from disilane. (a) is recorded from growth on a clean silicon surface. (b) is from growth on a surface previously exposed to germane for 1 minute, (c) is from growth on a surface exposed to germane for 3 minutes. No difference in oscillation period is seen between (b) and (c) meaning the same amount of germane was deposited in each case

Figure 7.1. It is clear that the germanium deposited enhances the growth rate but the growth rate enhancement is the same for the 1 minute dose as it is for the 3 minute dose. It can be inferred that the amount of germanium deposited is the same for both doses, this can be explained by the self-passivating effect of the hydrides of silicon and germanium. The hydrogen associated with the germanium in germane remains on the surface after the initial adsorption and passivates the surface preventing further adsorption. This concept of self-passivation will be used further in section 7.3

Figure 7.1 demonstrated the effect of self-passivation but RHEED intensity oscillations can also be used to test the passivation from silicon hydrides on the adsorption germane. Figure 7.2 (a) shows RHEED intensity oscillations recorded from homoepitaxial growth on the Si(001) surface, the remaining curves (b) and (c) are from growth from disilane on a surface previously exposed to disilane at 400°C followed by exposure to germane at a temperature of 270°C for 3 minutes. The purpose of this was to test the ability of a disilane produced monohydride surface on preventing germanium adsorption from germane.

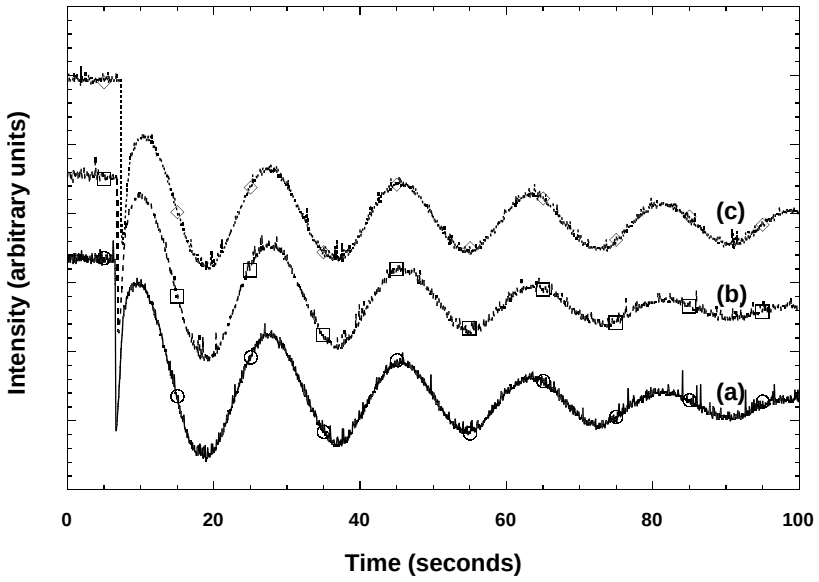


Figure 7.2: (a) shows RHEED intensity oscillations recorded from homoepitaxial growth on the Si(001) surface, the remaining curves (b) and (c) are from growth from disilane on a surface previously exposed to disilane followed by exposure to germane. Disilane exposure times are 10 seconds for (b) and 1 minute for (c). The surface produced from disilane exposure prevents germane adsorption.

It is clear from figure 7.2 that only a 10 second dose of disilane is required to fully passivate the surface, no difference is seen in all three traces.

Figure 7.1 showed that no difference in disilane growth rate enhancement existed for surfaces previously exposed to germane for 1 and 3 minutes, the 1 minute dose deposited the same amount of germanium as the 3 minute dose. This is the same phenomenon that allowed the Temperature Modulated Growth experiments reported for disilane and silane in chapters 5 and 6 respectively. RHEED oscillations were recorded from growth from disilane after various numbers of germane doses performed in a similar fashion to those in TMG. After each exposure to germane the sample is annealed to desorb the hydrogen. Figure 7.3 shows RHEED oscillations from (a) homoepitaxial growth (b) growth from disilane after exposure to germane and (c) growth from disilane after two TMG exposures to germane. It is clear that with every dose the growth rate from disilane is enhanced, however, with every dose the quality of the oscillations is degraded. Oscillations were not observed from surfaces after 3 TMG cycles.

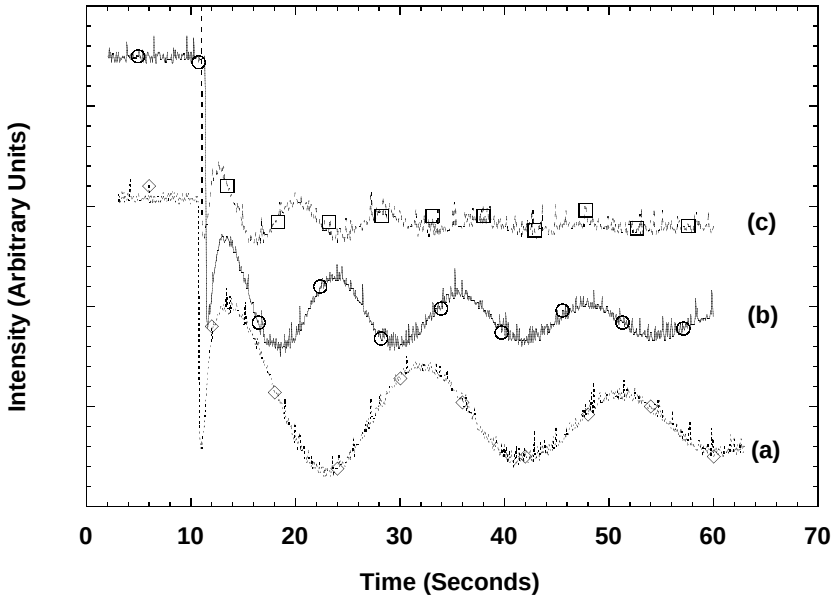


Figure 7.3: RHEED intensity oscillations recorded after a form of temperature modulated growth for germane dosing. (a) is from growth from disilane on the clean surface. (b) is from growth from disilane on a surface exposed to germane. (c) is from growth from disilane on a surface exposed to two cycles of germane dosing and annealing

TMG like experiments using germane are described in the next section where Temperature Programmed desorption is used to study the effect of germanium on hydrogen desorption.

7.3 Hydrogen Desorption During Temperature Modulated Growth

The effect of the germanium on hydrogen desorption can be measured more directly using temperature programmed desorption (TPD). Figure 7.4 shows the TPD spectra from a surface exposed to disilane at 430°C for 1 minute from a gas line pressure 1 Torr and germane at 200 °C for 10 minutes from a gas line pressure of 2 Torr. The effect of the surface germanium is clearly demonstrated as a shift in the peak desorption rate from 550°C to lower temperatures, the germanium results in more facile hydrogen desorption. The presence of another peak at lower temperatures 400°C is also seen, this is at a temperature

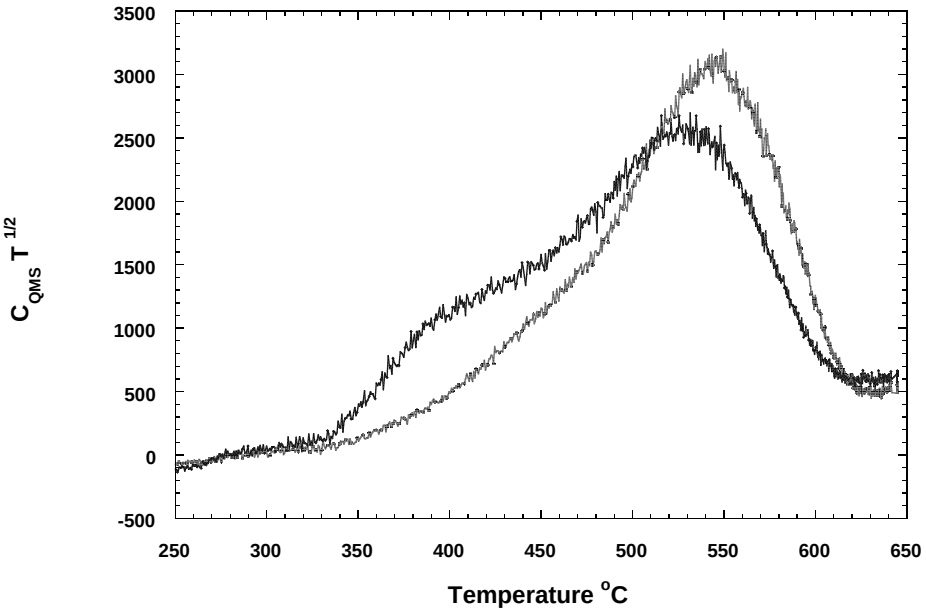


Figure 7.4: Temperature programmed desorption from a Si(001) surface exposed to disilane from a gas line pressure of 1 torr at 430°C falling for 1 min and germane at 200°C from a gas line pressure of 2 torr for 10 mins. The ramp rate used was 4°C per second.

much lower than that expected from the dihydride phase (460°C) and it is postulated this relates to desorption from a germanium related site and is termed the α peak. The area of the peaks from disilane exposure are of similar area and it is known that this disilane dose creates a passivated surface against further disilane adsorption depositing 1/3 ML of silicon. Therefore it can be inferred that the germane dosing has produced a passivated surface, this is confirmed when a longer dose time produces no change to the TPD spectra consistent with the RHEED investigation in the previous section.

A study was performed to observe the effect of repeated dosing of germane on the hydrogen desorption. This experiment uses conditions exactly the same as the temperature modulated growth experiments reported in chapter 4, however the layer thickness experiment was not performed since the growth mode would not be two dimensional and the amount of germane deposited per cycle would be meaningless. The aim is to produce a controlled surface germanium coverage using the self-passivation effect.

Figure 7.5 shows the result of TPD from a Si(001) surface after repeated dosing using germane. The germane exposure for each cycle was for 10 mins from a gas line pressure

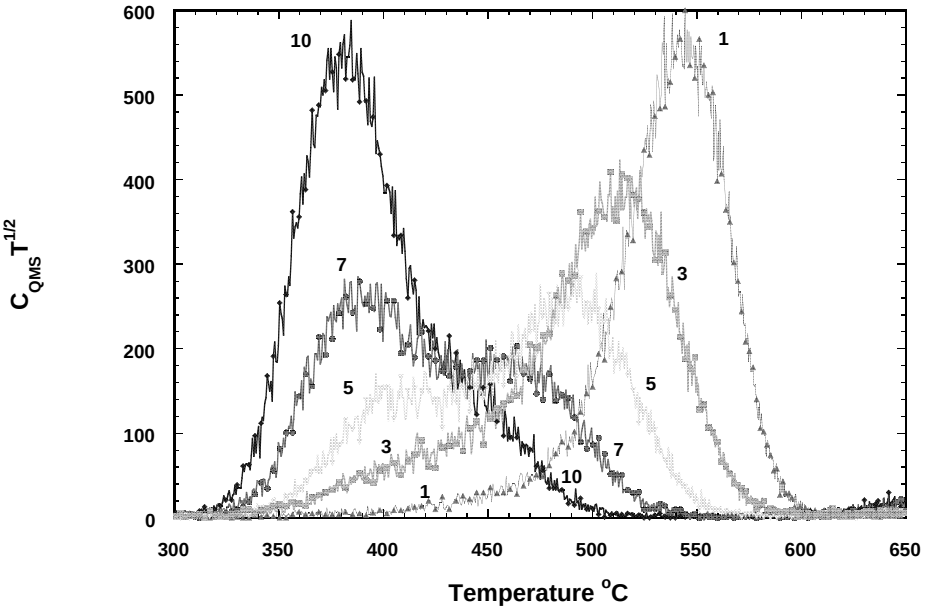


Figure 7.5: Temperature programmed desorption from a Si(001) surface repeatedly exposed to germane. The germane dose was at 340°C for 10 minutes from a gas line pressure of 1 torr. The ramp rate used was 4 °C per sec. The numbers in bold refer to the number of exposures to germane.

of 1 Torr, this dosage dose not create a fully passivated surface for each cycle but the TPD spectra serve to show the effect of an increasing surface germanium concentration. The TPD spectra show the gradual shift of the β_1 peak from 550°C to lower temperatures with the appearance of another peak at around 400°C for 3 cycles, this peak has been labelled as the α peak

This shift has been postulated as due to surface germanium weakening the Si-H bond [81]. Other groups [40] have used the presence of a new β_1^* peak which is thought to be due to desorption from mixed dimers. This model used by Kim *et al* [40] seems to satisfactorily explain the shift of the β_1 peak to lower temperatures in the presence of surface germanium. An effect that should be considered is diffusion of hydrogen between silicon and germanium sites during the temperature ramp. The increased strength of the Si-H bond will mean any H diffusion will result in the preferential formation of Si-H bonds. However the greater concentration of hydrogen on the silicon sites means diffusion will also occur from the occupied silicon sites to areas of germanium free of hydrogen.

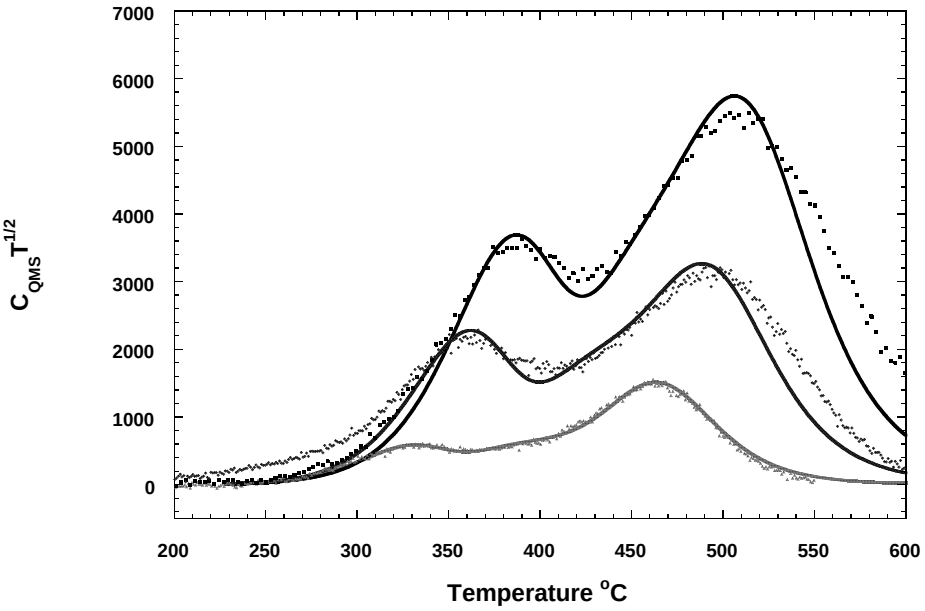


Figure 7.6: TPD recorded from temperature modulated growth from germane on a silicon surface after 4 exposure and annealing cycles but with various TPD ramp rates. The ramp rates used are 0.5, 2 and 5 °C per sec. The germane dose was for 10min from a gas line at 2 torr with a substrate temperature of 200°C

A TPD study of four germane doses which are known to produce a passivated surface is shown in Figure 7.6. The three spectra are from differing temperature ramp rates of 0.5°C /sec, 2°C /sec and 5°C /sec and have not been modified for ramp rate to aid clarity. It can be seen the form of the spectra alter significantly with ramp rate the shape of the spectra hint at three peaks which all have a different dependence on the temperature ramp rate.

The model used in chapter 4 was used to fit three independent peaks to the observed spectra, the use of three independent peaks is somewhat unrealistic since if the middle peak is indeed from a dihydride phase then there is a possibility that during the temperature ramp some of this dihydride can decay into the monohydride phase before desorption. The following parameters were used to fit the data: β_1 energy = 2.2 $\pm$0.4 eV pre-exponential = $3.18\times10^{13}s^{-1}$ β_2 energy = 1.24 $\pm$0.4 eV pre-exponential = $4.27\times10^{7}s^{-1}$ α energy = 1.3 $\pm$0.4 eV pre-exponential = $1.33\times10^{9}s^{-1}$

7.4 Steady State SiGe Growth Rate Measurements

As in the case of growth from disilane, hydrogen plays an important role through its passivation effect against further adsorption of the hydrides of silicon or germanium. While it is clear from previous sections that a number of hydrogen desorption routes are available, it is still beneficial to examine the growth rate in detail and attempt to produce a hydrogen coverage rate equation based model for the overall growth reaction.

It is already clear in the literature that the introduction of a different gas precursor, germane, will effect growth through changes in sticking probability and hydrogen desorption rate. There will also be differences to homoepitaxial growth since incorporation into the growing layer will depend on the segregation of germanium from the sub-layers to the growing layer. However this thesis is not concerned with segregation and will concentrate on the initial adsorption of germanium on the clean Si(001) surface and growth on a SiGe surface that has reached a steady state. Studies of the phenomenon of segregation have been widely reported elsewhere [111].

Recording RHEED intensity oscillations from SiGe growth on a Si(001) surface is problematic since the strain produced from the incorporated germanium eventually results in 3D growth and growth can no longer be monitored with RHEED. In all the experiments before SiGe growth was initiated at the specified temperature, a large buffer was grown and annealed at 800°C for 10 minutes. This ensured a good starting surface. Disilane and germane were then introduced into the deposition chamber from gas line pressures of 0.2Torr and 0.05 Torr respectively and the period of the intensity of the specularly reflected electron beam measured. After the SiGe is grown the substrate is heated to 850°C for 10 minutes to desorb the germanium before the Si buffer is grown. The germanium fraction in the film grown is approximately 4% though the surface concentration is expected to be different due to the germanium surface segregation.

A set of RHEED intensity oscillations are shown in figure 7.7. The period of the oscillations is initially seen to decrease and eventually reaches a steady rate, however at this point the intensity of the oscillation has diminished considerably. The presence of germanium on the surface clearly increases the growth rate under these conditions of flux and temperature and the oscillations also show a move towards bi-layer growth. A possible reason for these observations can be postulated as follows; At these temperatures the steady state hydrogen coverage is expected to be considerable and the increase in growth rate is due to an increased rate of hydrogen desorption. The gradual decrease in oscillation period can be explained as due to a gradual increase in the surface concentration of germanium.

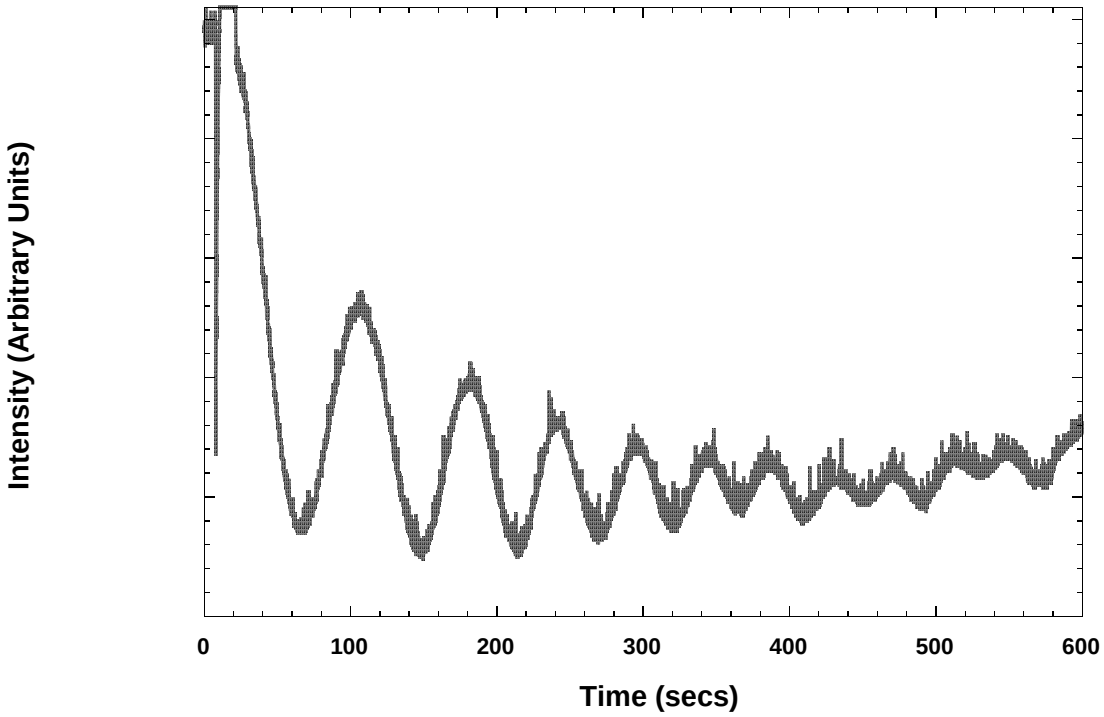


Figure 7.7: RHEED intensity oscillations from SiGe growth on a clean Si(001) surface. After introduction of the gas into the chamber the period of oscillations decreases until a steady state is reached, before the oscillations disappear a transition to bilayer growth is indicated

Under steady state the rate of incorporation of germanium into the subsurface layer must be equal to the rate of adsorption of germanium on the growing layer, however the surface concentration of germanium is greater than that in the subsurface layer and it is the gradual build up of this population that accounts for the gradual decrease in oscillation period. During this gradual build up in the surface germanium the incorporated concentration of germane into the subsurface layers will be lower than when this population has reached steady state.

RHEED oscillations were recorded over the temperature range 480°C to 580°C and the resulting growth rates plotted against 1000/T in Figure 7.8. At low temperatures the growth rate is much greater than that for growth from disilane from a gas line at 0.25 Torr which is know to give a similar BEP. At high temperatures, however, the growth rate

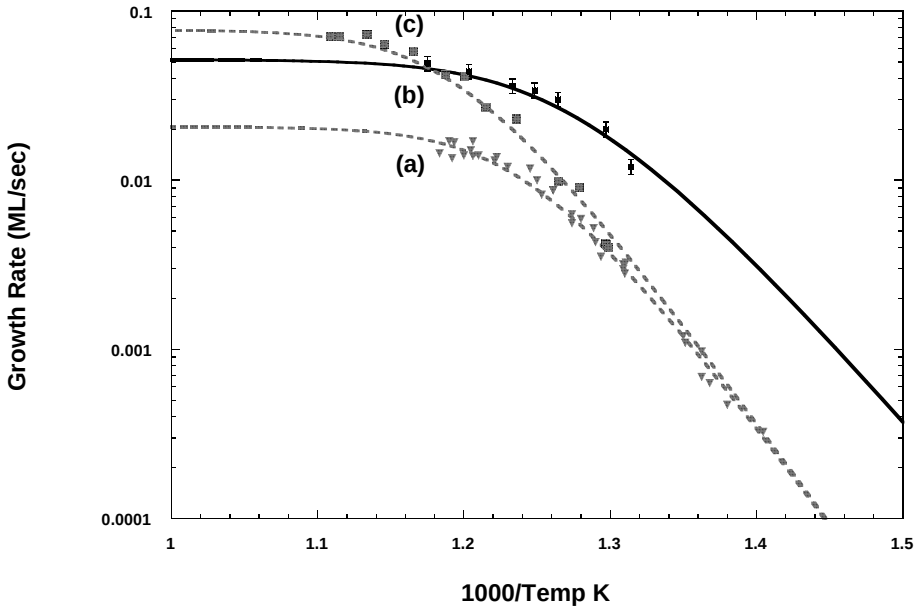


Figure 7.8: Arrhenius plot of the growth rate of silicon and SiGe. The silicon was grown from disilane at gas line pressures of 0.1 Torr (solid triangles) and 0.25 Torr (solid squares). The SiGe growth (solid circles)is from gas line pressures of disilane (0.2 Torr) and germane (0.05 Torr). The solid line is produced from a simple SiGe growth model and serves mainly to guide the eye.

is less than that from disilane. A simplistic growth model can be constructed to explain this behaviour. It is assumed the disilane deposits all the growing material, silicon, and the germane deposits "magic" atoms which do not contribute to growth but do effect the sticking probability and hydrogen desorption parameters. Therefore the model used is that used in Chapter 4 for disilane. The parameters used are as follows; sticking probability 0.01, activation energy for hydrogen desorption 2 eV with a pre-exponential 8×10^{11}. For disilane growth they are 0.015, 2.4eV and 5×10^{13}.

The result of this model appears to confirm the postulate that surface germanium increases growth rate at low temperatures by aiding hydrogen desorption, the activation energy is reduced from 2.4eV for homoepitaxial growth to 2eV. Surface germanium also inhibits the adsorption of disilane and hence the amount of silicon deposited as the sticking probability appears to be reduced from 0.015 to 0.01.

7.5 Summary

The study reported in this chapter has highlighted many important effects that germanium has on the adsorption of silicon/germanium and the desorption of hydrogen. These can be summarised as follows:

- Surface Germanium presents a lower energy pathway for hydrogen desorption into the gas phase. This is seen in an increased growth rate compared to that from disilane in the low temperature/high coverage regime of growth.

- Surface germanium results in a lower sticking coefficient. This is seen as a decreased growth rate compared to that from disilane in the high temperature/low coverage regime of growth.

- The monohydride phase produced from disilane and germane is unreactive to further germane.

- Repeated germane dosing followed by TPD showed a shift in peak position of the monohydride peak. This was thought to be due to the monohydride peak consisting of desorption from Si-Si dimers and a Si-Ge mixed dimer state, the β_1^* peak. The emergence of another peak at lower temperatures was thought to be from the germanium monohydride phase, the α peak.

- TPD spectra show three peaks. TPD modelling gives β_1 energy = 2.2 $\pm$0.4 eV pre-exponential = $3.18\times10^{13}s^{-1}$ β_2 energy = 1.24 $\pm$0.4 eV pre-exponential = $4.27\times10^{7}s^{-1}$ α energy = 1.3 $\pm$0.4 eV pre-exponential = $1.33\times10^{9}s^{-1}$ all were modelled with first order desorption.

Chapter 8

Conclusion

This thesis reported an extensive study of the growth of Si and SiGe from disilane, silane and germane precursors on the Si(001) surface. The experimental findings confirm some of the existing knowledge reported in the literature and have identified the reaction pathway in the disilane pyrolysis reaction. Some new features in the growth/reaction rate as functions of temperature and flux have also been identified. This chapter summarises the findings and conclusions from these studies.

8.1 Hydrogen Desorption Studies

The focus of of this part of the investigation is the the desorption of molecular hydrogen, a reaction product of the disilane pyrolysis reaction. Temperature programmed desorption was used to probe the phase of hydrogen on the surface under different disilane dosing conditions. The main findings are that exposure of the Si(001) surface to disilane at 430°C for 1 minute produced a single peak in the TPD spectra and this is attributed to the desorption from the monohydride phase termed the β_1 peak. For exposure at lower temperatures another peak was observed and this was thought to be due to desorption from the dihydride phase termed the β_2 peak . The dihydride β_2 peak was never observed without the presence of the monohydride β_1 peak. The monohydride phase was found to prevent the formation of the dihydride phase at lower temperatures and this is thought to be through a site blocking effect.

The modelling of the TPD spectra assumed first order desorption and produced an activation energy for desorption from the monohydride phase of 2.48 $\pm$0.4 eV and pre-exponential of 3.16×10^{14}. An activation energy for the β_2 peak was calculated as 1.22 $\pm$0.4 eV with a pre-exponential of 4.27×10^{7}. Hydrogen desorption was observed to be first order

from high surface coverages but shifts to higher order at very low coverages.

8.2 Pyrolysis Reaction Pathways

To identify the reaction pathway, modulated beam mass spectrometry was used to establish the reaction products leaving the surface and their temperature dependence. Silane or silicon hydride radicals were not detected in the species leaving the surface whereas molecular hydrogen desorption has been observed with a flux correlated to the growth rate temperature behaviour. The overall pyrolysis reaction occurs as:

$$Si_2H_6 \rightarrow 2Si + 3H_2(g) \tag{8.1}$$

and silane or silicon hydride radicals are not seen as reaction products at temperatures above 400°C . However the process of silicon hydride desorption cannot be ruled out since it is probable that any signal due to silicon hydride could be swamped by that from unreacted disilane reflected from the surface.

MBMS was also used to study hydrogen desorption and this was found to be thermally activated with an activation energy of 1.8 eV, in good agreement with the literature as reviewed in chapter 2. At high temperatures, the desorption rate saturates and this is correlated with the saturation of growth rate as the rate limiting step changes in the overall pyrolysis reaction.

8.3 Disilane Adsorption and the Pathway for Dissociation of Silicon Hydride Radicals

Upon adsorption of disilane molecules on the Si(001) surface, silicon hydrides are produced. This confirms the details of the overall reaction, but there are two alternatives in the pathway of dissociation of SiH_2 into the monohydride phase identified in the TPD study:

$$\underline{Si} - SiH_3 + \underline{Si} - \rightarrow \underline{Si} - SiH_2 + \underline{Si} - H \tag{8.2}$$

$$\underline{Si} - SiH_2 + \underline{Si} - \rightarrow \underline{Si} - SiH + \underline{Si} - H \tag{8.3}$$

However, the dihydride phase may decompose to release hydrogen:

$$2(\underline{Si} - SiH_2) \rightarrow 2(\underline{Si} - SiH) + H_2(g) \tag{8.4}$$

The amount of Si deposited to achieve a surface fully passivated by hydrogen differs in the two alternatives. Using temperature modulated growth, it is shown that 1/3ML of silicon is deposited in the process of producing fully passivated surface at 430°C and reaction pathway shown in equation 8.3 is dominant and is the important pathway for growth from hydrides.

At lower temperatures, an investigation based on TMG shows that higher hydrides are produced as the decomposition of SiH_2 radicals becomes slow compared with the adsorption of disilane. This leads to the deposition of 1/2 ML silicon while achieving a fully passivated surface.

8.4 Rate Limiting Steps in the Growth of Si from Hydrides

The MBMS study of H_2 desorption indicated that the desorption of molecular hydrogen is the rate limiting step at low temperatures and disilane supply becomes the bottleneck in the overall growth reaction at high temperatures. In all this, hydrogen coverage plays a vital role due to its passivation effect.

The temperature and flux dependence of growth rate is investigated using careful *in-situ* RHEED and *ex-situ* XRD measurements. The findings broadly agree with the current understanding but with two exceptions. These are the reduction of growth rate at high temperatures and a flux dependence at low temperatures. Two terms are introduced into the rate equation for the surface hydrogen coverage to account for the new findings. (1) a temperature dependent lifetime in the precursor state and (2) a flux dependent desorption term $k_{abs}\theta\sqrt{J}$ attributed to an abstraction mechanism. Based on the basic reaction pathway identified, the overall model is given by:

$$\frac{d\theta}{dt} = 6J(1-\theta)^2 - 2k_d\theta - k_{abs}\theta J^{\frac{1}{2}} = 0 \tag{8.5}$$

$$GR = 2J(1-\theta)^2 \tag{8.6}$$

The temperature dependent lifetime of the precursor state is implemented as a temperature dependent effective flux $J = \frac{\alpha I}{N_0}$ where $\alpha = \frac{\alpha_a}{1+\alpha_a}$ and $\alpha_a = 1.5 \times 10^{-4} exp\left(\frac{0.4e}{k_B T}\right)$.

8.5 Growth from Silane

The growth of silicon from silane was studied in an identical fashion to that from disilane. TPD indicated the β_1 and β_2 peaks as was seen for dosing from disilane. A

temperature modulated growth experiment was performed for silane at low temperatures and it was found that 0.2 ± 0.04 ML of silicon were deposited per cycle. This suggests that the silane adsorbs in similarly sequential way to disilane. The result is one silicon atom adsorbs for every four hydrogens. The results are consistent with the following reactions:

$$SiH_4(g) + 2\underline{Si} - \rightarrow \underline{Si} - H + \underline{Si} - SiH_3 \tag{8.7}$$

$$\underline{Si} - SiH_3 + \underline{Si} - \rightarrow \underline{Si} - H + \underline{Si} - SiH_2 \tag{8.8}$$

$$\underline{Si} - SiH_2 + \underline{Si} - \rightarrow \underline{Si} - H + \underline{Si} - SiH \tag{8.9}$$

RHEED intensity oscillations and XRD growth rate measurements were made and the established model used to derive the kinetic parameters. This model appeared to fit the data but it is possible a flux dependence at low temperatures and growth rate decrease at high temperatures exists as it did for the case of disilane. The hydrogen desorption parameters are the same as for the disilane model $E_d = 2.4$ eV and $k_{d_0} = 5{\times}10^{13}$ but a sticking probability of $0.45{\times}10^{-3}$ is necessary for a good fit. This is many orders of magnitude smaller than the sticking probability of disilane.

8.6 The Influence of Germanium on the Growth of Alloys

The effect of surface germanium on the adsorption and desorption kinetics has been studied. Surface germanium is found to present a lower energy pathway for hydrogen desorption into the gas phase. This is evident as an increase in growth rate at low temperatures compared to that from disilane. A decrease of growth rate at high temperatures is explained as a decrease in sticking coefficient.

Repeated germane dosing followed by TPD showed a shift in the peak position of the monohydride peak. This was thought to be due to the monohydride peak consisting of desorption from Si-Si dimers and a Si-Ge mixed dimer state, the β_1^* peak. The emergence of another peak at lower temperatures was thought to be from the germanium monohydride phase, the α peak. RHEED studies confirm that hydrogen is also effective in passivating the surface against further adsorption of germane.

Modelling of the TPD is achieved using a first order desorption model. The activation energy for desorption from the monohydride phase is 2.48 eV with a pre-exponential of $3.16{\times}10^{14}$. For desorption from the dihydride phase the activation energy is 1.22 eV with a pre-exponential of $4.27{\times}10^{7}$ and for desorption from the germanium monohydride phase 1.3 eV and a pre-exponential of $1.33{\times}10^{9}$. These parameters are all in good agreement with the literature, however, the energy term for dihydride desorption is low.

8.7 Future Work

The extension of all the work reported here would obviously be beneficial. A study to clarify the precise cause of the observed flux dependence of the growth rate from disilane at low temperatures is needed. A study of the high temperature drop in growth rate should also be undertaken. The identification of a precursor state with a temperature dependent lifetime could explain the observed effects.

The work on growth of SiGe is clearly preliminary. An extensive study is required as the growth of SiGe alloy is also affected by the Ge surface segregation. These complicated processes make it difficult to establish a simple rate equation model, unlike the case of growth from disilane.

Another area where the use TPD and other surface sensitive tools is likely to be effective is the investigation of arsenic and its effect on the growth of silicon, SiGe from hydride precursors.

8.8 Publications

[1] E.S. Tok, N.J. Woods, R.W. Price, A.G. Taylor and J. Zhang. Optical second harmonic generation studies of epitaxial growth of Si and SiGe. *J. Crys. Growth* 209:297-301, 2000

[2] R.W. Price, E.S. Tok and J. Zhang. Probing the silane, disilane and germane adsorption kinetics on the silicon (001) surface. *J. Crys. Growth* 209:306-310, 2000 Presented at the 7th international conference on chemical beam epitaxy and related growth techniques (ICCBE-7) Tsukuba, Japan July 28-30 1999.

[3] E.S. Tok, R.W. Price, A.G. Taylor and J. Zhang. Oscillatory optical second-harmonic generation from Si(001) surfaces during thin-film epitaxy. *Appl. Phys. Lett.* 76:933-935, 2000

[4] R.W. Price, E.S. Tok and J. Zhang. Probing the disilane adsorption kinetics: An alternative approach *Phys. Rev. B* 59:R5292-R5295, 2000

Appendix A

List of Abbreviations

AES Auger Electron Spectroscopy

AFM Atomic Force Microscopy

ALE Atomic Layer Epitaxy

APCVD Atmospheric Pressure Chemical Vapour Deposition

CVD Chemical Vapour Deposition

FVM Frank-van der Merwe

GSMBE Gas Source Molecular Beam Epitaxy

HREELS High Resolution Electron Energy Loss Spectroscopy

HRXRD High Resolution X-ray Diffraction

LEED Low Energy Electron Diffraction

LEO Linear Electro-Optic Effect

LITD Laser Induced Thermal Desorption

LPE Liquid Phase Epitaxy

MBE Molecular Beam Epitaxy

ML Monolayer

MBMS Modulated Beam Mass Spectroscopy

MEIS Medium Energy Ion Scattering

MOCVD Metal Organic Chemical Vapour Deposition

MOS Metal Oxide Semiconductor

MIRIRS Multiple Internal Reflection Infrared Spectroscopy

RAS Reflectance Anisotropy Spectroscopy

RBS Rutherford Back Scattering

REMPI Resonance Enhanced Multiphonon Ionisation

RHEED Reflection High Energy Electron Diffraction

RT Room Temperature

SHG Second Harmonic Generation

SIMS Secondary Ion Mass Spectroscopy

SK Stranski-Krastanov

STM Scanning Tunnelling Microscopy

STS Scanning Tunnelling Spectroscopy

TEM Transmission Electron Microscopy

TMG Temperature Modulated Growth

TOFMS Time of Flight Mass Spectroscopy

TPD Temperature Programmed Desorption

UHV Ultra High Vacuum

UPS Ultra-violet Photo-electron Spectroscopy

VW Volmer-Weber

Appendix B

The Boltzmann Distribution

The total energy of a system can be considered to depend on the combined state of its constituent parts. These constituent parts, microstates, can occupy different energy states.

The number of microstates with energy E(n) is given by the number of ways in which n indistinguishable states can be selected out of a total of N sites, this number, $\Omega(n)$, is called the statistical weight of the macrostate with energy E(n). We postulate that all microstates compatible with the given constraints of the system are equally likely to occur and that equilibrium corresponds to that value of α for which $\Omega(E, V, N, \alpha)$ attains its maximum value, with E, V, N fixed. Boltzmann defined the entropy of a system by

$$S(E, V, N, \alpha) = k_B ln\Omega(E, V, N, \alpha) \tag{B.1}$$

The probability p of the system in a state r is proportional to the number of states compatible with this energy. If we consider a small energy interval containing only one energy level this will usually correspond to several different states of the system.

$$p_r = const.\Omega_2(E_0 - E_r) \tag{B.2}$$

using

$$p_r = const.e^{\frac{S_2(E_0 - E_r)}{k_B}} \tag{B.3}$$

and Taylors theorem, $\frac{dS_2(E_0)}{dE_0} = \frac{1}{T}$ and $E_0 >> E_r$ gives

$$p_r = \frac{1}{Z} e^{\frac{-E_r}{k_B T}} \tag{B.4}$$

where the normalisation constant Z is given by

$$Z = \sum_r e^{\frac{-E_r}{k_B T}} \tag{B.5}$$

Equation B.4 is the Boltzmann distribution and gives the probability that a system when placed in a heat bath at a temperature T should be in a particular state.

B.0.1 The Maxwell Velocity Distribution

Using the Boltzmann distribution we can now go on to find the velocity distribution of the gas particles.

It is straightforward to show that the density of states for standing waves with wave vector k and hence for particle with momentum $p = \frac{hk}{2\pi}$

$$f(k)dk = \frac{Vk^2 dk}{2\pi^2} \tag{B.6}$$

$$f(p)dp = \frac{V 4\pi p^2 dp}{h^3} \tag{B.7}$$

The Boltzmann distribution gives the probability a particle will be a translational energy state:

$$p_s = \frac{1}{Z_1^{tr}} e^{\frac{-p^2}{2mk_B T}} \tag{B.8}$$

where the normalisation constant Z_1^{tr} is given by

$$Z_1^{tr} = \int_0^\infty f(p)dp e^{\frac{-E_r}{k_B T}} \tag{B.9}$$

substituting in equation B.7 and solving gives

$$Z_1^{tr} = V \left(\frac{2\pi m k_B T}{h^2} \right)^{\frac{3}{2}} \tag{B.10}$$

combining B.4, B.10, $E^{tr} = \frac{p^2}{2m} = \frac{m^2\nu^2}{2m}$ and $\bar{n}(p) = Np_s$ gives the mean number of particles in a state with momentum magnitude p

$$\bar{n}(p) = \frac{N}{V}\left(\frac{h^2}{2\pi m k_B T}\right)^{\frac{3}{2}} e^{\frac{-p^2}{2mT}} \tag{B.11}$$

combining this with B.7 gives the probability that a particle in the gas posses momentum of magnitude in the range p to $p + dp$

$$P(p)dp = \frac{1}{N} f(p)dp\bar{n}(p) \tag{B.12}$$

giving

$$P(p)dp = \frac{4\pi p^2 dp}{(2\pi m k_B T)^{\frac{3}{2}}} e^{\frac{-p^2}{2mk_B T}} \tag{B.13}$$

Normalising and substituting $p = m\nu$ we get the probability that a particle will have a speed in the interval ν to $\nu + d\nu$, the Maxwell speed distribution:

$$P(\nu)d\nu = 4\pi\nu^2 d\nu \left(\frac{m}{2\pi k_B T}\right)^{\frac{3}{2}} e^{\frac{-m\nu^2}{2k_B T}} \tag{B.14}$$

Using $\frac{dE}{d\nu} = m\nu$ it is possible to show:

$$P(E)dE = \frac{2}{\sqrt{\pi}(k_B T)^{\frac{3}{2}}} \sqrt{E} dE e^{\frac{-E}{k_B T}} \tag{B.15}$$

and

$$\bar{E} = \frac{3}{2} k_B T \tag{B.16}$$

From the Maxwell speed distribution we can calculate ν_{max}, $\bar{\nu}$ and using $\bar{E} = \frac{1}{2}m\nu^2$, $\bar{\nu}^2$:

$$\nu_{max} = \sqrt{\frac{2k_B T}{m}} \tag{B.17}$$

$$\bar{\nu} = \frac{2}{\sqrt{\pi}}\sqrt{\frac{2k_BT}{m}} = \frac{2}{\sqrt{\pi}}\nu_{max} \tag{B.18}$$

$$\bar{\nu^2} = \frac{3k_BT}{m} = \sqrt{\frac{3}{2}}\nu_{max} = \frac{8}{3\pi}\bar{\nu^2} \tag{B.19}$$

Combining the above result with equations 2.5, 2.7, B.18, the ideal gas relation and $n = \frac{N}{V}$ gives the molecular impingement rate

$$I = \frac{P}{\sqrt{2\pi m k_B T}} \tag{B.20}$$

Appendix C

Reflection High Energy Electron Diffraction

To study the surface of a material a method must be employed that uses imaging radiation of a comparable wavelength to the surface features. Since the smallest surface features are of the order 0.10nm, visible radiation, wavelength 300-700nm, cannot be used. Shorter wavelength X-Rays may be used but they are generally not surface specific, it is therefore necessary to use radiation which interacts strongly with the material or is introduced to the surface at a glancing angle. This can be achieved by utilising the wave nature of high energy electrons. When the electrons are introduced at a glancing angle the technique is titled Reflection High Energy Electron Diffraction (RHEED) and this geometry together with the energy range used ensures surface sensitivity. RHEED lends itself well to the technique of Molecular Beam Epitaxy (MBE) since the electron beam source and detector can be placed well away from the substrate allowing room for effusion cells and other molecular beam sources.

C.0.2 RHEED Patterns

As opposed to conventional X-ray diffraction, RHEED is essentially a surface technique meaning that the three dimensional symmetry is broken and hence the familiar reciprocal lattice normally associated with diffraction must be re-considered. The result of reducing one of the dimensions of the real lattice is to produce 'rods' in the reciprocal space due to the relaxation of the so called Laue conditions. The Laue condition states that the difference of the incident wave vector k and the diffracted wave vector k' must be factor of any reciprocal lattice vector.

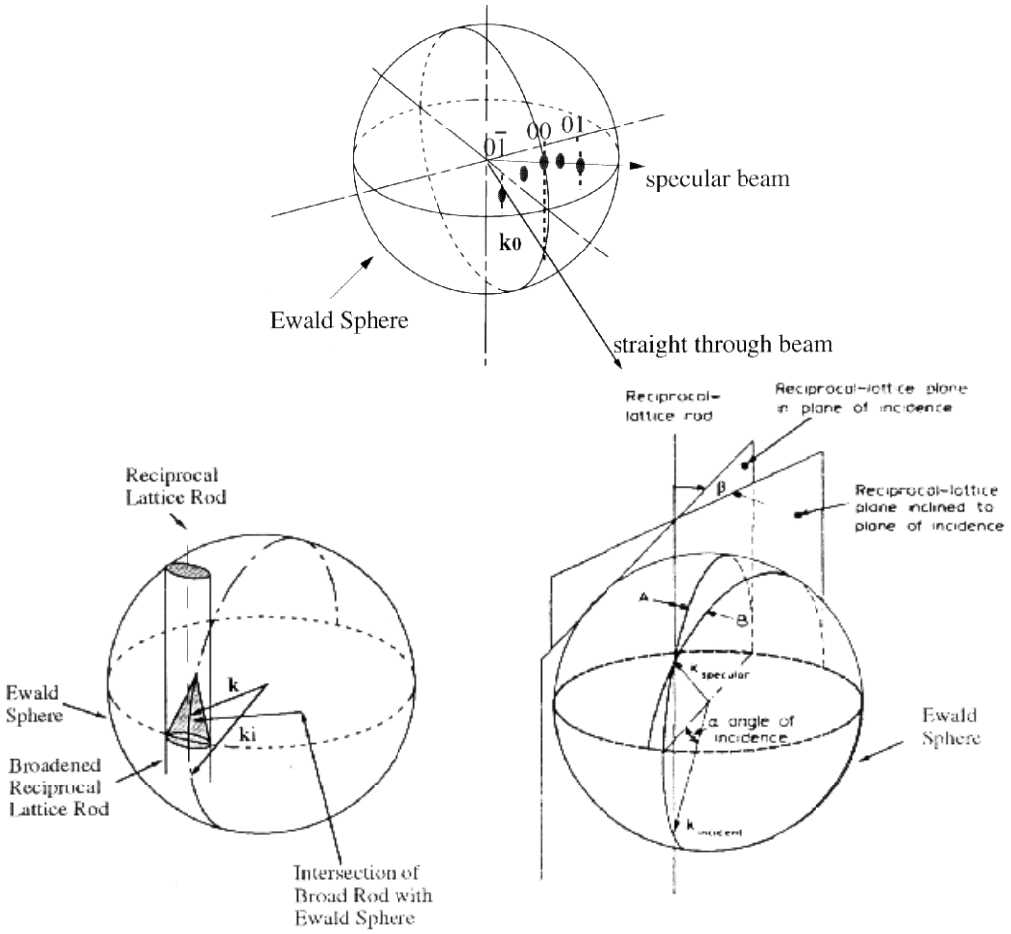


Figure C.1: The Ewald Sphere construction and reciprocal lattice rods. The bottom eft hand figure illustrates the effect of broad lattice rods and the bottom right hand figure the origin of arrowhead shaped features [64]

$$k - k' = \Delta k = G \tag{C.1}$$

For the two dimensional surface the Laue conditions are relaxed to give the following condition:

$$\Delta k_{||} = \Delta G_{||} \tag{C.2}$$

where the $_{||}$ symbol denotes the component of the vector parallel to the surface.

For elastic scattering energy conservation also requires that the magnitude of these two vectors be equal.

$$|k| = |k'| \tag{C.3}$$

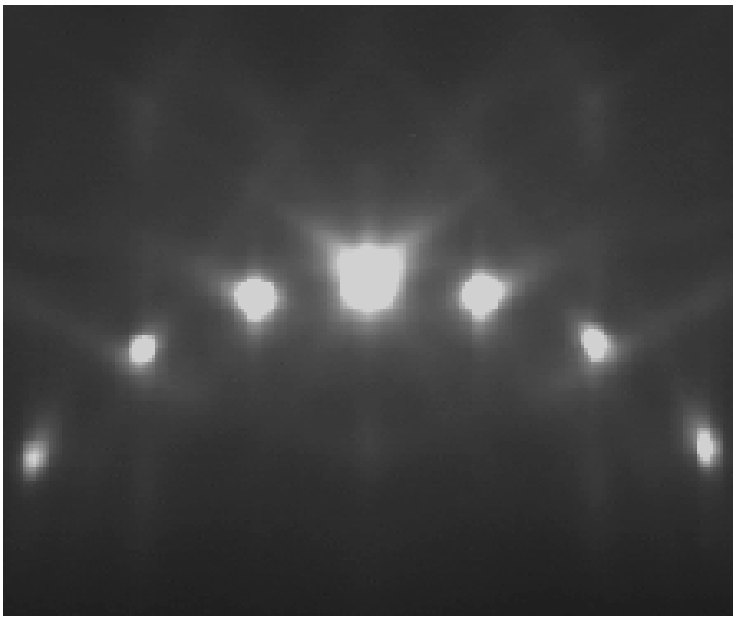


Figure C.2: RHEED pattern of a clean (2x1)(1x2) reconstructed Silicon(100) surface taken in the [110] direction

Since the incident and scattered wave vectors are of equal magnitude and exist in three dimensions they must lie on a sphere in reciprocal space with radius $k = k'$ centred on the termination of the k vector. This is called the Ewald Sphere and where it intersects the reciprocal lattice rods a diffraction 'beam' will be produced in that direction, see figure C.1. Where the 'beam' hits the phosphor screen a spot will be seen. However, not all the spots one expects to observe are present in the diffraction pattern, this is due to interference effects dependent on the position of the atoms in the unit cell. Within the framework of the kinematic theory of electron diffraction, this is accounted for in the Structure Factor which is zero for certain polar directions.

C.0.3 Features of RHEED Patterns

For a theoretically perfect two dimensional lattice, the reciprocal space rods are one dimensional, however, if the surface layer has any thickness, the reciprocal lattice rods are broken up into 'beads' along the length of the rods. The length of these 'beads' is determined by the thickness of the layer. The thicker the layer, the shorter the beads, obviously, as the layer thickness increases the reciprocal rods will approach the spots of the familiar three dimensional reciprocal lattice. However, there are other reasons for the relaxation of the Laue conditions even in the absence of a surface layer. The sudden termination of the bulk structure and the limited penetration depth of the electron beam will also create

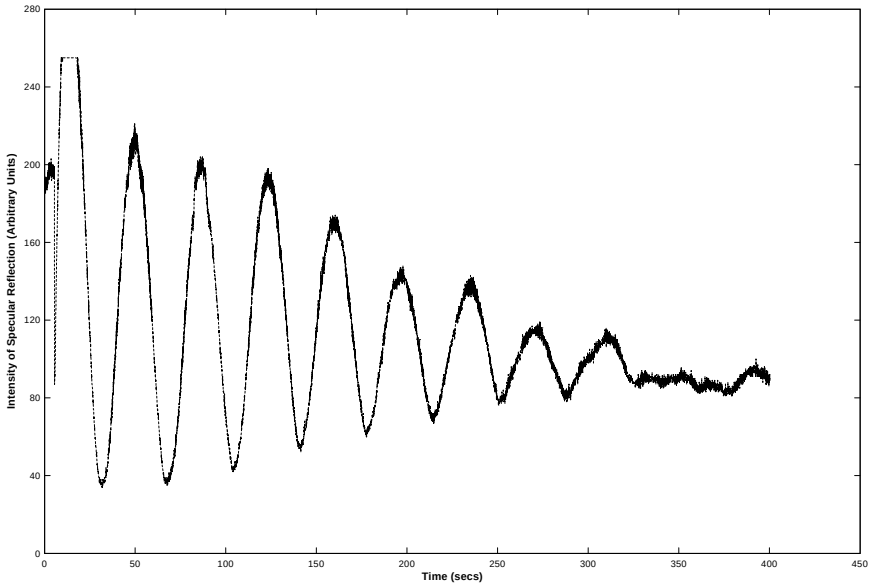


Figure C.3: RHEED oscillations during growth from a gas line pressure of 10 Torr with a substrate temperature of 550 °C . The growth rate is calculated at 0.027 ML/sec

reciprocal lattice rods. If the spatial frequency of the surface layer is perturbed for any reason, this will result in a broadening of the reciprocal rods. Since the points in reciprocal space of a perfectly periodic, infinite lattice have no size, any decrease in the periodicity will increase the size of the spot (the spot size is in fact a measure of the size of the crystal) so the rod cross-sectional area will increase. The increase in this area will result in elliptical shaped diffraction beams, and hence spots, where the broad rods intersect the Ewald sphere. The same reasoning applies to features with no periodicity they will produce 'sheets' in the reciprocal lattice and hence arcs in the diffraction pattern where they intersect the Ewald sphere. If facets are present on the surface new diffraction features are produced corresponding to the new surface planes. These diffracted beams produce 'arrow head' shaped diffraction spots. An example of a RHEED pattern is given in Figure C.2.

C.0.4 RHEED Intensity Oscillations

The intensity of the RHEED features has been observed to oscillate during layer by layer growth, [64]. This can be explained, albeit over simplified, by considering the reflectivity of the surface. As adatoms arrive at the surface of the substrate and grow via 2D nucleation, they effectively 'roughen' the surface, meaning a coverage of half a monolayer would create the roughest surface, and hence have the lowest reflectivity. When a full layer is deposited the surface will reach a peak in reflectivity. Hence the reflectivity, and thus

the intensity of the *reflected*[1] beam, will oscillate as growth proceeds. The period of these oscillations can thus be used to characterise the growth rate of the system since one period corresponds to one monolayer of growth. However, at high temperatures, the adatoms are more free to migrate[2] around the surface and there will be fewer but larger island nucleation on the surface. If the temperature is high enough, the adatoms are sufficiently mobile to reach step edges on either side of the terraces, where they are more inclined to stay since it can form higher coordinated bonds in comparison to those on the terraces. Growth effectively proceeds by step edges propagating across the top of the lower layer and no island nucleation can occur on the terraces, this means there will be no reduction or increase in reflectivity of the surface and hence RHEED intensity oscillations are not observed. For areas near the step edge, the terrace is 'denuded' of islands since the mean free path of the adatoms is such as to allow them to reach the step edge. The concentration of the adatoms will increase with distance from the step edge. An example of RHEED oscillations are given in Figure C.3

[1] This is the simplification since diffraction effects will also be present

[2] At higher temperatures the adatoms have enough energy to 'hop' over local potential barriers and are thus free to move across the surface

Appendix D

The Quadrupole Mass Spectrometer

The mass spectrometer operates by ionising the molecules to allow the mass to charge filtering, this ionising can have the effect of cracking larger molecules and it is thus important to study this cracking before any conclusion are reached over an individual mass/charge channels behaviour. In this study the majority of the gas in the chamber is disilane therefore a dependence of the cracking pattern of Disilane on ionising electron energy was performed see Figure D.1. It can be seen that for an energy of 16 eV little cracking takes place and it this therefore advantageous to use low energies as this can reduce confusion of the signal with one due to cracking.

The mass spectrometer itself consists of an ioniser region, a quadrupole filter and a detector, the quadrupole filter is separated from the ioniser region by a filter end plate held at earth. For positive ion detection the ioniser floats at a positive potential relative to earth at a bias set by the ion energy control. This ensures the ions are accelerated towards the filter end plate and into the quadrupole region. An additional plate called the focus plate is located between the ioniser and filter end plate may have a potential applied to it to improve the transmission of ions.

The ioniser or source consists of a filament and trap, the filament is held at a negative potential with respect to the source plate and trap, this ensures the electrons emitted from the filament are accelerated to both these regions and it is between these regions the electrons collide with molecules to create the ions.

Once the ions have entered the quadrupole filter they follow complex trajectories governed by the radio-frequency (RF) and direct-current (DC) voltages set on opposing

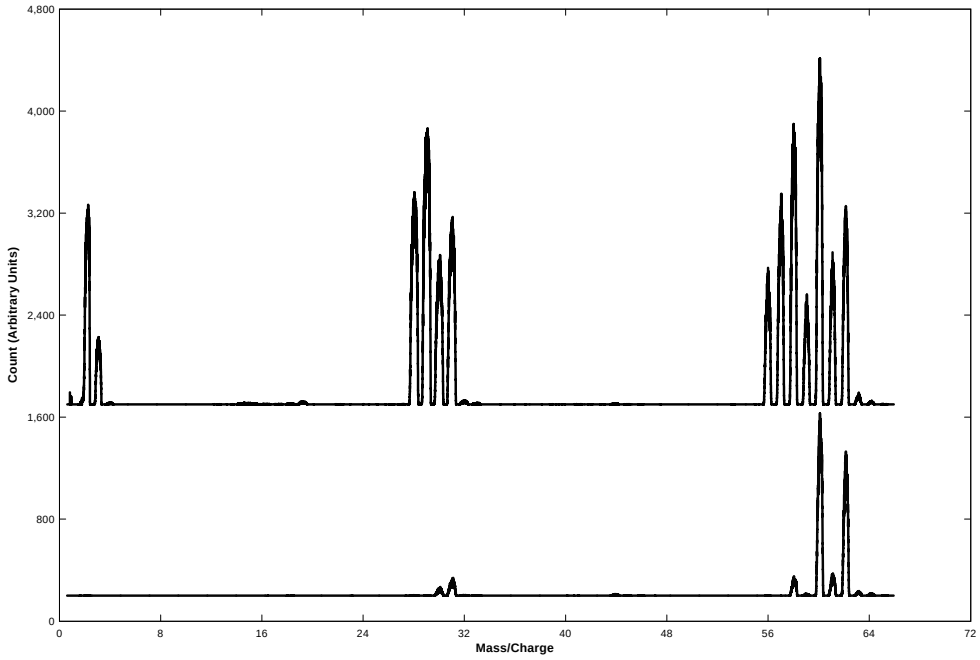


Figure D.1: Cracking pattern of Disilane in a water cooled system at a background pressure of 2.5×10^{-7} mbar. The top trace is from an ion energy of 70 eV and the bottom is 16 eV. ΔM is set at 60%

sets of rods. Ions that pass through the mass/charge filter are then accelerated towards the entrance of the secondary electron multiplier by a negative potential with respect to earth. As the ions interact with the surface of the electron multiplier secondary electrons are generated which are accelerated towards the earthed end of the multiplier where they are detected by the collector. On the way to the collector the generated electrons further collide with the surface of the multiplier where they generate even more electrons, this may occur many times. The initial impact of one ion can end up generating approximately 10^4 electrons.

The detection at the collector may be made in either analogue or pulse counting mode. For analogue operation, as in Figure D.1, the voltage applied to the multiplier entrance is approximately 1000 Volts. In this case the signal is determined simply by measuring the current. In pulse counting mode the multiplier is operated at higher voltages around 3000 Volts and discrete pulses of electrons are detected corresponding to the impact of one ion on the multiplier surface. However at these high voltages the lifetime of the electron multiplier can be seriously reduced.

Appendix E

Growth Rate Modelling Solutions

E.1 Model 1

$$\frac{d\theta}{dt} = 6SJ(1-\theta)^2 - 2k_d\theta = 0 \tag{E.1}$$

$$\theta = \frac{6SJ + k_d - \sqrt{12k_dSJ + (k_d)^2}}{6SJ} \tag{E.2}$$

$$GR = 2SJ(1-\theta)^2 \tag{E.3}$$

$$J = \frac{I}{N_0} \tag{E.4}$$

$$I = \frac{101P}{\sqrt{2\pi mkT}} \tag{E.5}$$

$S = 0.015$

$N_0 = 6.8 \times 10^{18}$

$m = 62 \times 1.66 \times 10^{-27}$

$k_d = 5 \times 10^{13} exp\left(\frac{-2.4e}{k_bT}\right)$

E.2 Model 2

$$\frac{d\theta}{dt} = 6J(1-\theta)^2 - 2k_d\theta = 0 \tag{E.6}$$

$$\theta = \frac{6J + k_d - \sqrt{12k_dJ + (k_d)^2}}{6J} \tag{E.7}$$

$$GR = 2J(1-\theta)^2 \tag{E.8}$$

$$J = \frac{\alpha I}{N_0} \tag{E.9}$$

$$I = \frac{101P}{\sqrt{2\pi mkT}} \tag{E.10}$$

$$\alpha = \frac{\alpha_a}{1+\alpha_a} \tag{E.11}$$

$\alpha_a = 1.5 \times 10^{-4} exp\left(\frac{0.4e}{k_b T}\right)$
$N_0 = 6.8 \times 10^{18}$
$m = 62 \times 1.66 \times 10^{-27}$
$k_d = 5 \times 10^{13} exp\left(\frac{-2.4e}{k_b T}\right)$

E.3 Model 3

$$\frac{d\theta}{dt} = 6J(1-\theta)^2 - 2k_d\theta - k_{abs}\theta J = 0 \tag{E.12}$$

$$\theta = \frac{1}{12J}\left[12J + 2k_d + k_{abs}J - \sqrt{48Jk_d + 24J^2k_{abs} + 4k_d^2 + 4k_dk_{abs}J + k_{abs}^2J^2}\right] \tag{E.13}$$

$$GR = 2J(1-\theta)^2 \tag{E.14}$$

$J = \frac{\alpha I}{N_0}$
$\alpha = 0.015$
$I = \frac{101P}{\sqrt{2\pi mkT}}$
$N_0 = 6.8 \times 10^{18}$
$m = 62 \times 1.66 \times 10^{-27}$
$k_{abs} = 5 \times 10^{-3}$
$k_d = 5 \times 10^{13} exp\left(\frac{-2.4e}{k_b T}\right)$

E.4 Model 4

$$\frac{d\theta}{dt} = 6J(1-\theta)^2 - 2k_d\theta - k_{abs}\theta J = 0 \tag{E.15}$$

$$\theta = \frac{1}{12J}\left[12J + 2k_d + k_{abs}J - \sqrt{48Jk_d + 24J^2k_{abs} + 4k_d^2 + 4k_dk_{abs}J + k_{abs}^2J^2}\right] \tag{E.16}$$

$$GR = 2J(1-\theta)^2 \tag{E.17}$$

$J = \frac{\alpha I}{N_0}$
$I = \frac{101P}{\sqrt{2\pi mkT}}$
$\alpha = 0.015$
$N_0 = 6.8 \times 10^{18}$

$m = 62 \times 1.66 \times 10^{-27}$

$k_{abs} = 1 \times 10^{14} exp\left(\frac{-2.4e}{k_b T}\right)$

$k_d = 5 \times 10^{13} exp\left(\frac{-2.4e}{k_b T}\right)$

E.5 Model 5

$$\frac{d\theta}{dt} = 6J(1-\theta)^2 - 2k_d\theta - k_{abs}\theta J = 0 \tag{E.18}$$

$$\theta = \frac{1}{12J}\left[12J + 2k_d + k_{abs}J - \sqrt{48Jk_d + 24J^2k_{abs} + 4k_d^2 + 4k_dk_{abs}J + k_{abs}^2J^2}\right] \tag{E.19}$$

$$GR = 2J(1-\theta)^2 \tag{E.20}$$

$J = \frac{\alpha I}{N_0}$

$I = \frac{101P}{\sqrt{2\pi mkT}}$

$\alpha = 0.015$

$N_0 = 6.8 \times 10^{18}$

$m = 62 \times 1.66 \times 10^{-27}$

$k_{abs} = 5 \times 10^{-3}$

$k_d = 5 \times 10^{13} exp\left(\frac{-2.4e}{k_b T}\right)$

E.6 Model 6

$$\frac{d\theta}{dt} = 6J(1-\theta)^2 - 2k_d\theta - k_{abs}\theta J^{\frac{1}{2}} = 0 \tag{E.21}$$

$$\theta = \frac{8\frac{1}{3} \times 10^{-2}}{J}\left[12J + 2k_d + k_{abs}\sqrt{J} - \sqrt{48Jk_d + 24J^{\frac{3}{2}}k_{abs} + 4k_d^2 + 4k_dk_{abs}\sqrt{J} + k_{abs}^2J}\right] \tag{E.22}$$

$$GR = 2J(1-\theta)^2 \tag{E.23}$$

$J = \frac{\alpha I}{N_0}$

$I = \frac{101P}{\sqrt{2\pi mkT}}$

$\alpha = 0.015$

$N_0 = 6.8 \times 10^{18}$

$m = 62 \times 1.66 \times 10^{-27}$

$k_{abs} = 1 \times 10^{4} exp\left(\frac{-2.4e}{k_b T}\right)$

$k_d = 5 \times 10^{13} exp\left(\frac{-2.4e}{k_b T}\right)$

E.7 Model 7

$$\frac{d\theta}{dt} = 6J(1-\theta)^2 - 2k_d\theta - k_{abs}\theta J^{\frac{1}{2}} = 0 \tag{E.24}$$

$$\theta = \frac{8\frac{1}{3}\times 10^{-2}}{J}\left[12J + 2k_d + k_{abs}\sqrt{J} - \sqrt{48Jk_d + 24J^{\frac{3}{2}}k_{abs} + 4k_d^2 + 4k_dk_{abs}\sqrt{J} + k_{abs}^2 J}\right] \tag{E.25}$$

$$GR = 2J(1-\theta)^2 \tag{E.26}$$

$J = \frac{\alpha I}{N_0}$
$I = \frac{101P}{\sqrt{2\pi mkT}}$
$\alpha = \frac{\alpha_a}{1+\alpha_a}$
$N_0 = 6.8\times 10^{18}$
$m = 62\times 1.66\times 10^{-27}$
$k_d = 5\times 10^{13} exp\left(\frac{-2.4e}{k_bT}\right)$
$\alpha_a = 1.5\times 10^{-4} exp\left(\frac{0.4e}{k_BT}\right)$
$k_{abs} = 1\times 10^{14} exp\left(\frac{-2.4e}{k_bT}\right)$

Appendix F

Acknowledgements

Thanks to my supervisor Jing Zhang for all his help over the last few years overcoming the numerous rate limiting steps. Thanks also to Eng Soon Tok without whose help I would not be writing this now and thanks to Steve Cussell for all his help building equipment. I must also thank my parents for all their support, a considerable part of which was financial. Can I also say a big thank-you to all those that know me, THANK-YOU.

Bibliography

[1] G. Abstrieter, H. Brugger, T. Wolf, H. Jorke, and H.J. Herzog. Strain-induced two dimensional electron gas in selectively doped si/si$_x$ge$_{1-x}$ superlatices. *Phys. Rev. Lett*, 54:2441, 1985.

[2] I.P. Batra. *Phys. Rev.*, B41:5048, 1990.

[3] E. Bauer and J.H. van der Merwe. Structure and growth of crystalline superlattices: From monolayer to superlattice. *Phys. Rev.*, B33:3657–3671, 1986.

[4] Bean. *J. Appl. Phys.*, 73:2288, 1984.

[5] G. Boishin and L. Surnev. Adsorption of hydroge on a ge covered si(100) surface. *Surf. Sci.*, 345:69–74, 1996.

[6] J. J. Boland. *Phys. Rev. B.*, 44:3, 1991.

[7] T. R. Bramblett, Q. Lu, T. Karasawa, M. A. Hasan, S. K. Jo, and J. E. Greene. Si(100) 2×1 gas source molecular beam epitaxy from si$_2$h$_6$: Growth kinetics and boron doping. *J. Appl. Phys.*, 76:1884–1888, 1994.

[8] D.J Chadi. *Phys. Rev. Lett.*, 41:1064, 1978.

[9] D.J. Chadi. Stablilities of single-layer and bilayer steps on si(001) surfaces. *Phys. Rev. Lett.*, 59:1691–1694, 1987.

[10] J. Comfort and R. Reif. *J. Electrochem. Soc*, 136:2386, 1989.

[11] M. Copel, M.C. Reuter, E. Kaxiras, and R.M. Tromp. Surfactants in epitaxial growth. *Phys. Rev. Lett.*, 63:632–635, 1989.

[12] B. Cunningham, J. O. Chu, and S. Akbar. *Appl. Phys. Lett.*, 59:3574, 1991.

[13] M. P. D'Evelyn, Y. L. Yang, and L. F. Sutcu. *J. Chem. Phys.*, 96:1, 1992.

[14] D. J. Eaglesham, F. C. Unterwald, H. Luftman, D. P. Adams, and S. M. Yalisove. *J. Appl. Phys.*, 74:6615, 1993.

[15] M.K. Farnham and D.R. Olander. The surface chemistry of the thermal cracking of silane on silicon (111). *Surf. Sci*, 145:390, 1984.

[16] R.F.C. Farrow. The kinetics of silicon deposition on silicon by pyrolysis of silane. *Journal Electrochem Soc*, 121:899, 1974.

[17] N. B. H. Flowers, M.C. Jonathan, Y. Liu, and A. Morris. Temperature programmed deosporption of molecular hydrogen from a si(100)2×1 surface: Theory and experiment. *J. Chem. Phys.*, 99:7038–7048, 1993.

[18] F.C Frank and J.H. van der Merwe. *Proc. R. Soc. London Ser.*, A198:205, 1949.

[19] S.M. Gates. Kinetics and mechanisms of surface reactions in epitaxial growth of si from sih4 and si2h6. *J. Crys. Growth.*, 120:269, 1992.

[20] S.M. Gates and C.M. Chiang. Dissociative chemisorption mechanisms of disilane on si(100)-(2x1) and h terminated si(100) surfaces. *Chem. Phys. Lett.*, 1991.

[21] S.M. Gates, C.M. Greenlief, and D.B. Beach. Decomposition of sihx species on si(100)-(2x1) for x = 2,3, and 4. *J. Chem. Phys.*, 93:7493–7503, 1990.

[22] S.M. Gates, C.M. Greenlief, D.B. Beach, and P.A. Holbert. Decomposition of silane on si(111)-(7x7) and si(100)-(2x1) surfaces below 500 0c. *J. Chem. Phys.*, 92:3144, 1990.

[23] S.M. Gates, C.M. Greenlief, S.K. Kulkarni, and H.H. Sawin. Surface reactions in si chemical vapour deposition from silane. *J. Vac. Sci. & Technol.*, A8:2965–2969, 1990.

[24] S.M. Gates and S.K. Kulkarni. Kinetics of surface reactions in very low pressure chemical vapor deposition of si from sih4. *Appl. Phys. Lett.*, 58:2963, 1991.

[25] I. Goldfarb, J.H.G. Owen, D.R. Bowler, G.M Goringe, P. T. Hyden, K. Miki, D. G. Pettifor, and G.A.D. Briggs. In situ obseravtion of gas source molecular beam epitaxy of silicon and germaium on si(001). *J. Vac. Sci. & Technol.*, A16:1938–1943, 1998.

[26] I. Goldfarb, J.H.G. Owen, P.T. Hayden, D.R. Bowler, K. Miki, and G.A.D. Briggs. Gas source growth of group iv semiconductors: (iii) nucleation and growth of ge/si(001). *Surf. Sci.*, 394:105–118, 1997.

[27] C.M. Greenlief and M. Armstrong. Hydrogen desorption from si: How does this relate to film growth? *J. Vac. Sci. & Technol.*, B 13:1810–1815, 1995.

[28] C.M. Greenlief and M. Liehr. Hydrogen desorption kinetics from epitaxially grown si(100). *Appl. Phys. Lett.*, 64:601–603, 1993.

[29] H Hendersen and R.F. Helm. *Surf. Sci.*, 30:310, 1972.

[30] F. Hirose. Modelling growth in si gas source molecular beam epitaxy using si_2h_6. *J. Cryst. Growth.*, 179:108–114, 1997.

[31] F. Hirose and H. Sakamoto. Adsorption mechanisms of si_2h_6 and geh_4 on si(100) 2×1 surfaces. *Appl. Surf. Sci.*, 107:75–80, 1996.

[32] F. Hirose, M. Suemitsu, and N. Miyamoto. Silane adsorption on si(100) 2×1. *J. Appl. Phys.*, 70:5380–5384, 1991.

[33] F. Hirose, M. Suemitsu, and N. Miyamoto. Silane gas source atomic layer epitaxy. *Appl. Surf. Sci.*, 60/61:592–596, 1992.

[34] U. Hofer, L. Li, and T. F. Heinz. Desorption of hydrogen from si(100)2×1 at low coverages: The influence of π bonded dimers on the kinetics. *Phys. Rev. B*, 45:9485–9489, 1991.

[35] X. F. Hu, Z. Xu, D. Lim, M. C. Downer, P. S. Parkinson, B. Gong, G. Hess, and J. G. Ekerdt. In-situ optical second harmonic generation of disilane adsorption and hydrogen desorption during epitaxial growth on si(001). *App. Phys. Lett.*, 71:1376–1378, 1997.

[36] J Hudson. *Surface Science: an Introduction.* 1998.

[37] S.S. Iyer, J.C. Tsnag, M.W. Copel, P.R. Pukrite, and R.M. Tromp. *Appl. Phys. Lett.*, 54:219, 1989.

[38] B. A. Joyce, J. M. Fernandez, M. H. Xie, A. Matsumura, and A. G. Taylor. Growth and doping of si and si/ge films by hydride gas-source molecular beam epitaxy. *J. Cryst. Growth*, 164:214–222, 1996.

[39] B.A. Joyce and P.R. Bradley. *Phil. Mag.*, 14:289, 1966.

[40] H. Kim, T. R. Bramblett, and J. E. Greene. Kinetics of $si_{1-x}ge_x(100)$ growth on si(100) 2×1 by gas source molecular beam epitaxy from si_2h_6 and ge_2h_6. *J. Appl. Phys.*, 84:6372–6381, 1998.

[41] H. Kim, P. Desjardins, J. R. Abelson, and J. E. Greene. Pathways for hydrogen desorption from $si_{1-x}ge_x(001)$ during gas source molecular beam epitaxy snd ultrahigh vacuum chemical vapor deposition. *Phys. Rev. B*, 58:4803–4808, 1997.

[42] H. Kim, N. Taylor, J. R. Abelson, and J. E. Greene. Effects of h coverage on ge segregation during $si_{1-x}ge_x$ gas source molecular beam epitaxy. *J. Appl. Phys.*, 82:6062–6066, 1997.

[43] Y. Koide, A. Furukawa, S. Zaima, and Y. Yasudu. *J. Crys. Gro.*, 115:365, 1991.

[44] K. W. Kolasinski. Dynamics of hydrogen interactions with si(100) and si(111) surfaces. *J. Mod. Phys. B*, 9:2753–2809, 1995.

[45] K. W. Kolasinski, S. F. Shane, and R. N. Zare. Internal state distribution of recombinative hydrogen desorption from si(100). *J. Chem. Phys.*, 96:3995–4006, 1992.

[46] D. D. Koleske and S. M. Gates. Atomic h abstraction of surface h on si: An eley-rideal mechanism. *J. Chem. Phys.*, 101:3301–3309, 1994.

[47] S.K. Kulkarni, S.M. Gates, C.M. Greenlief, and H.H. Swain. Kinetics and mechanics of si2h6 surface decomposition on si. *J. Vac. Sci.& Technol.*, A8:2956, 1990.

[48] S.K. Kulkarni, S.M. Gates, B.A. Scott, and H.H Sawin. Modulated molecular beam scattering of disilane on silicon. *Surf Sci.*, 239:13–25, 1990.

[49] M. Liehr, C.M. Greenlief, M. Offenberg, and S.R. Kasi. Equilibrium surface hydrogen coberage during silicon epitaxy using sih_4. *J. Vac. Sci. & Technol.*, A8:2960–2964, 1990.

[50] D. S. Lin, E. S. Hirschon, T. C. Chiang, R. Tsu, D. Lubben, and J. E. Greene. *Phys. Rev. B.*, 45:7, 1992.

[51] F. M. Lord and J.S. Kittleberger. On the determination of activationenergies in thermal desorption experiments. *Surf. Sci.*, 43:173–182, 1973.

[52] P.M.J. Marée, K. Nakagawa, F.M. Mulders, and J.F. van der Veen. Thin epitaxial ge-si(111) films: Study and control of morphology. *Surf. Sci.*, 191:305–328, 1987.

[53] Y.W. Mo and M.G. Lagally. Anistrotropy in surface migration of si and ge on si(001). *Surf. Sci.*, 248:313–320, 1991.

[54] Y.W. Mo, D.E. Savage, B.S. Swartzentruber, and M.G. Lagally. Kinetic pathways in stranski-krastanov growth of ge on si(001). *Phys. Rev. Lett.*, 65:1020–1023, 1990.

[55] S.M. Mokler, W.K. Liu, N. Ohtani, and B.A. Joyce. Surface reconstructions of si(001) observed using reflection high energy electron diffraction during molecular beam epitaxial growth from disilane. *Appl. Phys. Lett.*, 59:3419–3421, 1991.

[56] S.M. Mokler, W.K. Liu, N. Ohtani, and B.A. Joyce. Relection high energy electron diffraction intensity oscillations and surface reconstructions measured during epitaxial growth of si(001) from si_2h_6 molecular beams. *J. Vac. Sci. & Technol.*, A10:1846–1855, 1992.

[57] S.M. Mokler, W.K. Liu, N. Ohtani, and B.A. Joyce. Si(001) growth dynamics during si gsmbe from disilane. *Sur. Sci.*, 275:16–25, 1992.

[58] S.M. Mokler, N. Ohtani, M. H. Xie, J. Zhang, and B.A. Joyce. In-situ observation of growth rate enhancement during gas source molecular beam epitaxy of $si_{1-x}ge_x$ alloys on si(100) surfaces. *Appl. Phys. Lett.*, 61:2548–2550, 1992.

[59] S.M. Mokler, N. Ohtani, M. H. Xie, J. Zhang, and B.A. Joyce. Growth rate dependence on geh_4 during gas source mbe of $si_{1-x}ge_x$ alloys grown from si_2h_6 and geh_4. *J. Cryst. Growth.*, 127:467–471, 1993.

[60] S.M. Mokler, N. Ohtani, M. H. Xie, J. Zhang, and B.A. Joyce. Surface studies during growth of $si_{1-x}ge_x$/si from gaseous si ans ge hydrides. *J. Vac. Sci. & Technol.*, B 11:1073–1076, 1993.

[61] P. Nachtigall, D. Jordan, and K. C. Janda. Calculation of the si-h bon energies for the monohydirde phase on si(100). *J. Chem. Phys.*, 95:8652–8654, 1991.

[62] K. Nakagawa and M. Masanobu. Reverse temperature dependence of ge segregation during si-molecular beam epitaxy. *J. Appl. Phys.*, 69:3058–3062, 1990.

[63] H. Nakazawa and Suemtisu M. Higher order desorption kinetics of hydrogen from silane/ disilane/, and d/si(100). *Appl. Surf. Sci.*, 130-132:298–303, 1998.

[64] J.H. Neave, P.J. Dobson, B.A Joyce, and N. Norton. *Appl. Phys.*, A31:1, 1983.

[65] B. M. H. Ning and J. E. Crowell. The effect of germanium on the desorption of hydrogen from si(100). *Surf. Sci.*, 295:79–98, 1993.

[66] N. Ohtani, S. Mokler, M.H. Xie, J. Zhang, and B.A. Joyce. Surface hydrogen effects on ge surface segregatiom during silicon gas source molecular beam epitaxy. *Jpn. J. Appl. Phys.*, 33:2311–2316, 1994.

[67] N. Ohtani, S.M. Mokler, J. Zhang, and B.A. Joyce. Bilayer reflection high energy electron diffraction intensity oscliaations observed during growth on double-domain si(001) surfaces. *Appl. Phys. Lett.*, 61:1399–1401, 1992.

[68] N. Ohtani, S.M. Mokler, J. Zhang, and B.A. Joyce. Investigation of surface reconstruction domain behaviour during si-gsmbe. *J. Crys. Gro.*, 127:461–466, 1993.

[69] L.A. Okada, M.L. Wise, and S.M. George. Isothermal h_2 desorption kinetics from si(100)2×1: dependence on disilane and atomic hydrogen precursors. *App. Surf. Sci.*, 82/83:410–416, 1994.

[70] H.J. Osten, J. Klatt, G. Lippert, E. Bugiel, and S. Hinrich. Two-dimensional lattice-mismatched heteroepitaxy of germanium on silicon beyond the critical thickness by introducing a surfactant. *Appl. Phys. Lett.*, 60:2522–2524, 1992.

[71] J.H.G Owen, K. Miki, D.R. Bowler, C.M. Goringe, I. Goldfarb, and G.A.D Briggs. Gas source growth of group iv semiconductors: (i) si(001) nucleation methods. *Surf. Sci.*, 394:79–90, 1997.

[72] J.H.G Owen, K. Miki, D.R. Bowler, C.M. Goringe, I. Goldfarb, and G.A.D Briggs. Gas source growth of group iv semiconductors: (ii) growth regimes and the effect of hydrogen. *Surf. Sci.*, 394:91–104, 1997.

[73] R. People. Physics and applications of ge_xsi_{1-x}/si strained layer heterostructures. *IEEE J. Quan. Elec.*, QE-22:1696–1709, 1986.

[74] A.J. Pidduck. *Thin. Solid. Films.*, 222:78, 1992.

[75] A.J. Pidduck, D.J. Robbins, and A.G. Cullis. Microscopy of semiconductor materials. *Inst. Phys. Conf. Series*, 1993.

[76] J. Pollmann, P. Kruger, and A. Mazur. *J. Vac. Sci. & Technol.*, B5:4, 1987.

[77] S. Ramalingam, D. Maroudas, E. S. Aydil, and S. P. Walch. Abstraction of hydrogen by sih_3 from hydrogen terminated si(001)-(2×1) surfaces. *Surf. Sci.*, 418:L8–L13, 1998.

[78] D. J. Robbins and I. M. Toung. *Appl. Phys. Lett*, 50:1575, 1987.

[79] D.J. Robbins, L. Glasper, A.G. Cullis, and W.Y. Leong. A model for heterogenous growth of $si_{1-x}ge_x$ films from hydrides. *J. App. Phys.*, 69:3729, 1991.

[80] N.M. Russel and W.G. Breiland. A surface kinetics model for the growth of $si_{1-x}ge_x$ films from sih_4/geh_4 mixtures. *J. Appl. Phys.*, 73:3525–3530, 1993.

[81] N.M. Russel and J. G. Ekerdt. Kinetis of hydrogen desorption form germanium covered si(100). *Surf. Sci.*, 369:51–68, 1996.

[82] K. Sakamoto, H. Matsuhata, K. Miki, and T. Sakamoto. Adsorption and desorption of atomic hydrogen on si(100) and its effects on si mbe. *J. Cryst. Growth*, 157:295–299, 1995.

[83] T. Sakamoto, T. Kawamura, and G. Hashiguchi. Observation of alternating reconstructions of silicon (001) 2×1 and 1×2 using reflection high energy electron diffraction during molecular beam epitaxy. *Appl. Phys. Lett.*, 48:1612–1614, 1986.

[84] S. F. Shane, K. W. Kolasinski, and R. N. Zare. Internal state distribution of h_2 desorbed from mono- and dihydride species on si(100). *J. Chem. Phys.*, 97:3704–3709, 1992.

[85] J.W. Sharp and G. Eres. Kinetics of hydrogen desorption in surface limited thin film growth of sige alloys. *Appl. Phys. Lett.*, 62:2807–2809, 1993.

[86] J.W. Sharp and G. Eres. Kinetics of hydrogen desorption from si(100) and si(111) surfaces following chemisorption of disilane and trisilane. *Surf. Sci.*, 320:169–173, 1994.

[87] K. Sinniah, M.G. Sherman, L.B. Lewis, W.H. Weinberg, J.T. Yates, and K.C. Janda. New mechanism for hydrogen desoporption from covalent surfaces: The monohydrode phase on si(100). *Phys. Rev. Lett.*, 62:567–570, 1989.

[88] K. Sinniah, M.G. Sherman, L.B. Lewis, W.H. Weinberg, J.T. Yates, and K.C. Janda. Hydrogen desorption kinetics from from the monydride phase on si(100). *J. Chem. Phys.*, 92:5700–5711, 1990.

[89] E. Srinivasen and G. N. PArsoms. Hydrogen abstraction kinetics and cystallisation in low temperature plasma deposition of silicon. *Appl. Phys. Lett.*, 72:456–458, 1998.

[90] J.N. Stranski and L. Krastanov. *Ber. Akad. Wiss. Wien*, 146:797, 1938.

[91] Y. Suda, D. Lubben, T. Motooka, and J. E. Greene. Adsorption and thermal dissociation of disilane (si_2h_6) on si(100) 2×1. *J. Vac. Sci. & Technol.*, A8:61–67, 1990.

[92] M. Suemitsu, K. Kim, H. Nakazawa, and N. Miyamoto. A model for the temperature dependent adsorptionkinetics of sih_4 on si(100). *Appl. Surf. Sci.*, 107:81–84, 1996.

[93] M. Suemitsu, H. Nakazawa, T. Morita, and N. Miyamoto. Observation of hydrogen coverage and temperature dependent adsorption kinetics of disilane on si(100) during si gas source molecular beam epitaxy. *Jpn. J. Appl. Phys.*, 36:L625–L628, 1997.

[94] S.M. Sze. *Physics of Semiconductor Devices*. John Wiley & Sons.

[95] R.M. Tromp, R.J. Hamers, and J.E. Demuth. *Phys. Rev. Lett.*, 55:1303, 1985.

[96] C.G. Van de Walle and R.M. Martin. Theoretical calculations of heterojunction discontinuities in the si/ge system. *Phys. Rev.*, 34(8):5621–5633, 1986.

[97] J.H. van der Merwe. *J. Appl. Phys.*, 134:123, 1962.

[98] A. Vittadini and A. Selloni. Density functional study of h_2 desorption from monohydride and dihydride si(100) surfaces. *Chem. Phys. Lett.*, 235:334–340, 1995.

[99] M. Volmer and A. Weber. *Proc. R. Soc. London Ser.*, 119:271, 1926.

[100] Y. Wang, M.J. Bronikowski, and R.J. Hamers. An atomically resolved scanning tunnelling microscopy study of the thermal decomposition of disilane on si(001). *Surf. Sci.*, 311:64, 1994.

[101] K. Werner, Butzke S., Radelaar S., and P. Balk. Determination of the sticking coefficient of disilane on si(001) using the first refection high energy electron diffraction oscillation period. *J. Cryst. Growth.*, 136:322–327, 1994.

[102] K. Werner, Butzke S., Radelaar S., and P. Balk. Evidence for non-hydrogen desorption limited growth of si from disilane at very low temperatures in gas source molecular beam epitaxy. *J. Cryst. Growth.*, 136:338–343, 1994.

[103] M.L. Wise, B.G. Koehler, P. Gupta, P.A Coon, and S.M. George. Comparison of hydrogen desoprtion kinetics from si(111)7×7 and si(100)2×1. *Surf. Sci.*, 258:166, 1991.

[104] C. J. Wu and E. A. Carter. Adsorption of hydrogen atoms on the si(100)2×1 surface: implicatinos of the h_2 desorption mechanisms. *Chem. Phys. Lett.*, 185:172–178, 1991.

[105] Y. M. Wu and R. M. Nix. Adsorption of hydrogen and disilane on si(100) and si-ge surfaces. *Surf. Sci.*, 306:59–68, 1994.

[106] Y.M. Wu, J. Baker, P. Hamilton, and R.M. Nix. Mirirs studies of the growth of si and si-ge alloys from molecular precursors. *Surf. Sci.*, 295:133–142, 1993.

[107] L.Q Xia, M.E. Jones, N. Maity, and J.R. Engstrom. Dissociation and pyrolysis of si2h6 on si surfaces: The influence of surface structure and adlayer composition. *J. Chem. Phys.*, 103:1691, 1995.

[108] L.Q Xia, M.E. Jones, N. Maity, and J.R. Engstrom. Dissociation and pyrolysis of si2h6 on si surfaces: The influence of surface structure and adlayer composition. *J. Vac. Sci. & Technol.*, A 13:2651–2664, 1995.

[109] Y. Yasuda, Y. Koide, A. Furukawa, N. Ohshima, and S. Zaima. Relationship between growth processesand strain relaxation in $si_{1-x}ge_x$ films grown on (100) si (2×1) surfaces by gas source molecular beam epitaxy. *J. Appl. Phys.*, 73:2288, 1993.

[110] M.T. Yin and M.L. Cohen. *Phys.Rev.*, B24:2303, 1981.

[111] P.C. Zalm, F.A. van de Walle, D.J. Gravesteijn, and A.A. van Gorkum. Ge segregation st si/$si_{1-x}ge_x$ interfaces grown by molecular beam eptaxy. *Appl. Phys. Lett.*, 55:2520–2522, 1989.

[112] F. C. Zhang, J. Singh, and P. K. Bhattacharya. Surface phenomena and kinetics of $si_{1-x}ge_x$/si growth by molecular beam epitaxy using si_2h_6 and ge/geh_4. *J. Vac. Sci. & Technol.*, B 14:2378–2380, 1996.